Jets, tidal disruption and lenses

Plan and reviews

Plan

1. Jets: AGNs and close binary systems
2. Tidal distruption of stars by SMBHs
3. Spectral lines and lensing

Reviews

- astro-ph/0611521 **High-Energy Aspects of Astrophysical Jets**
- astro-ph/0306429 **Extreme blazars**
- astro-ph/0312545 **AGN Unification: An Update**
- astro-ph/0212065 **Fluorescent iron lines as a probe of astrophysical black hole systems**
- arXiv: 1104.0006 **AGN jets**
- astro-ph/0406319 **Astrophysical Jets and Outflows**
- arXiv: 2003.06322 Relativistic Jets of Blazars
- **arXiv: 1707.07134 AGNs of different types**

Jets in AGNs and close binaries

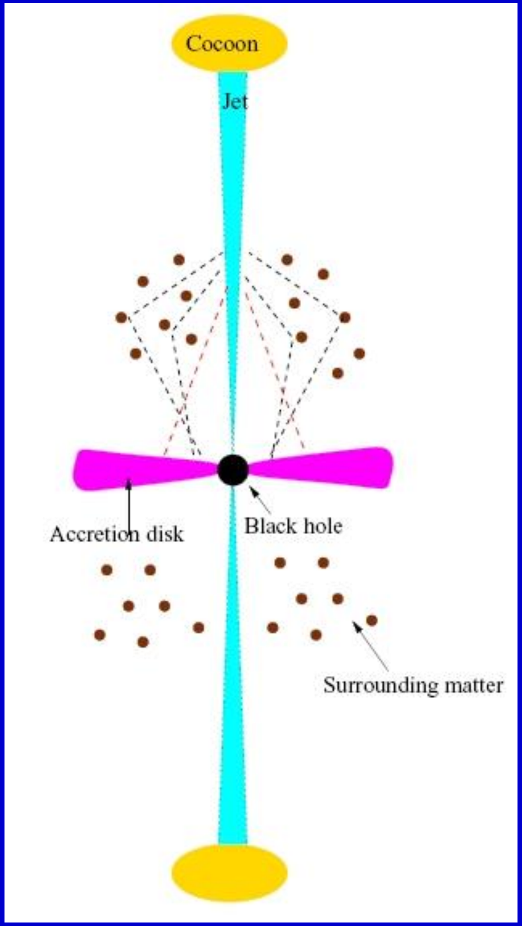

AGN: $M_{BH}=10^8\text{-}10^9\ M_0$
$L<\sim L_{Edd}\sim 10^{42}\text{-}10^{47}$ erg/s
< few Mpc
$\Gamma\sim 5\text{-}50$
$\Delta t\sim$ hours-years

CBS: $M_{BH}\sim 10\ M_0$
$L<\sim L_{Edd}\sim 10^{37}\text{-}10^{40}$ erg/s
~ pc
$\Gamma\sim 1\text{-}10$
$\Delta t\sim$ days

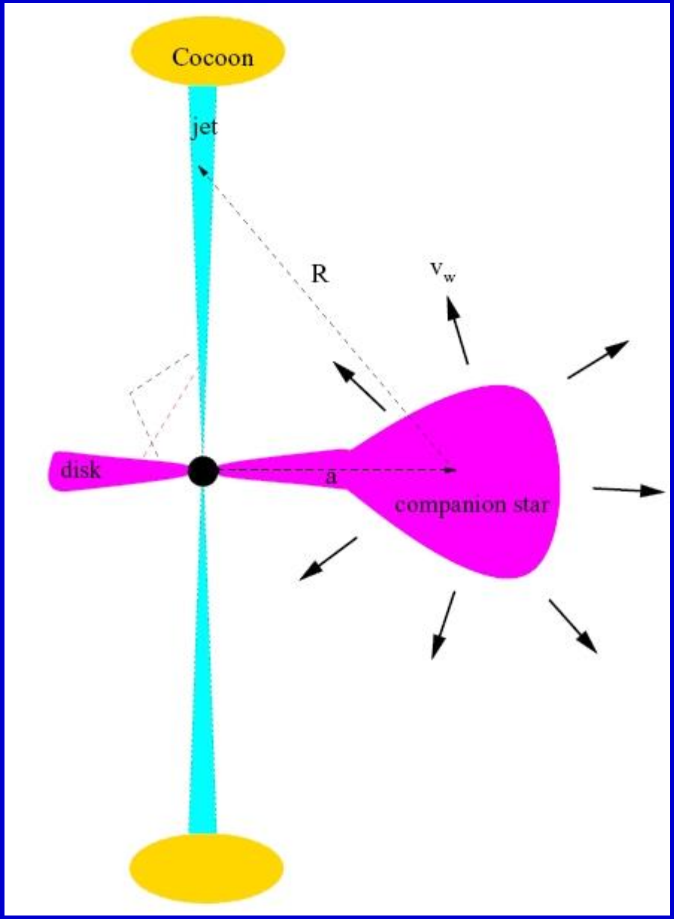

see astro-ph/0611521

All jets in one plot

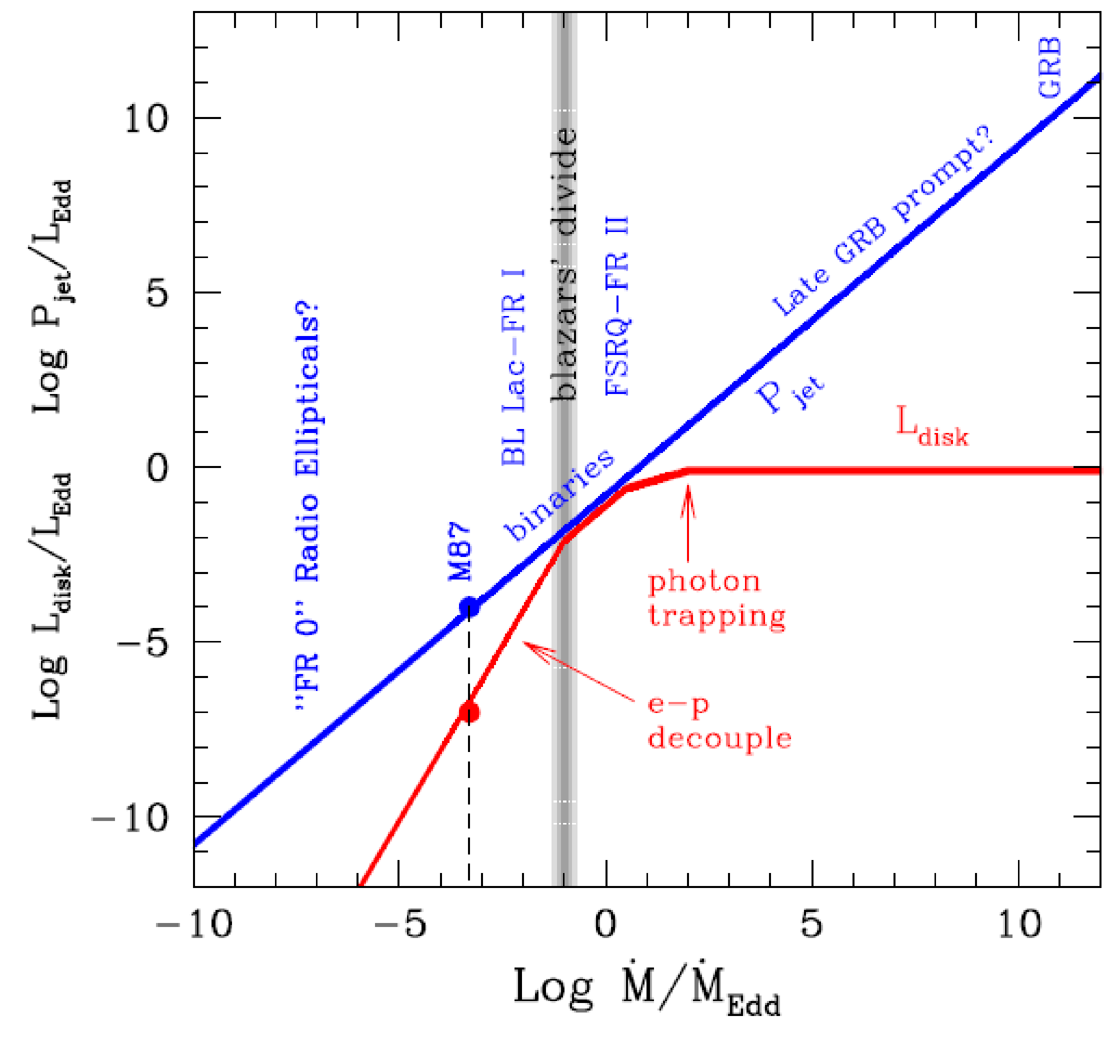

A schematic plot for different jets.

It is assumed that the jet power always scales linearly with Mdot, while accretion rates below a critical value produce radiatively in efficient accretion disks.

1104.0006

Close-by and far-away jets

1% of SMBH are active. 10% out of them launch relativistic jets.
Jets are not magnetically dominated.

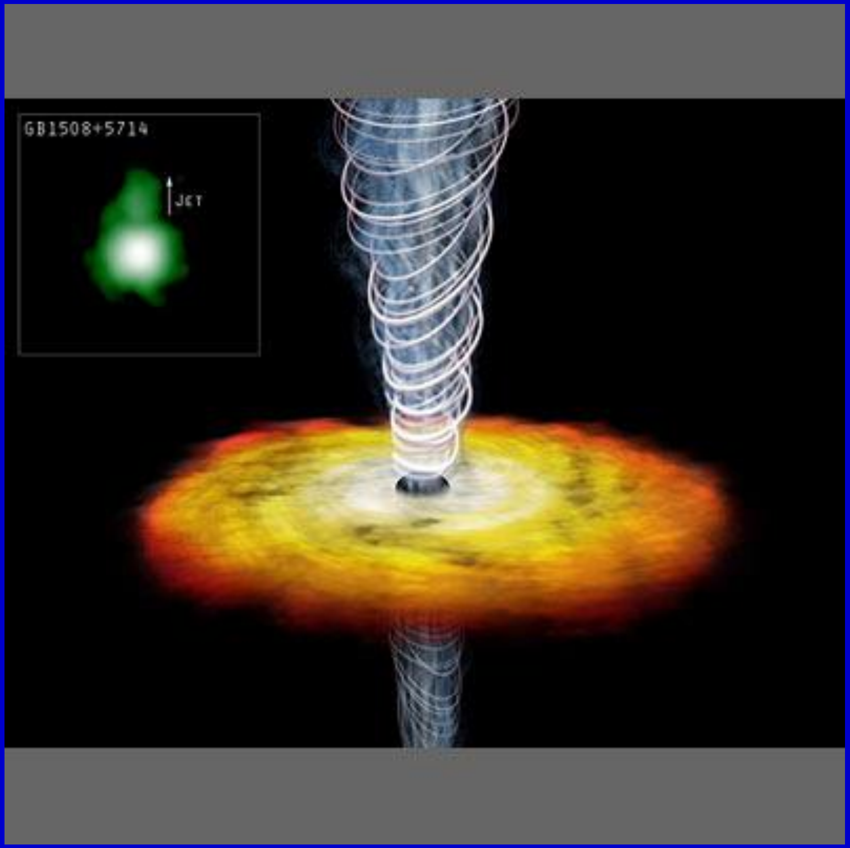

GB1508+5714 z=4.30

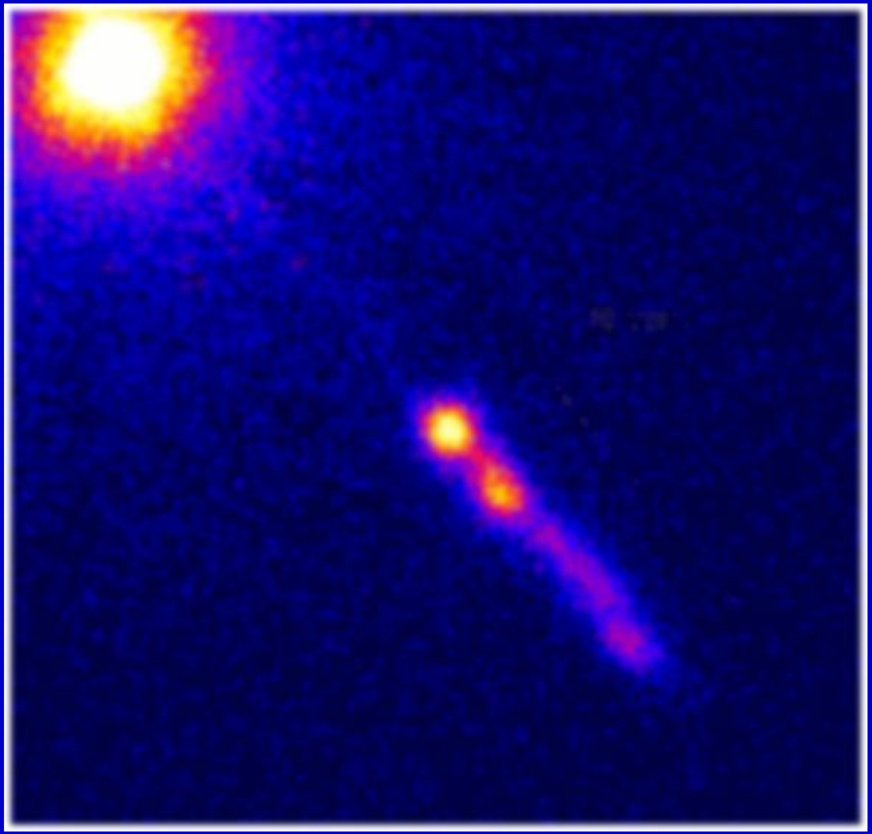

3C273

See a review in 1104.0006

Classification of AGN radio jets

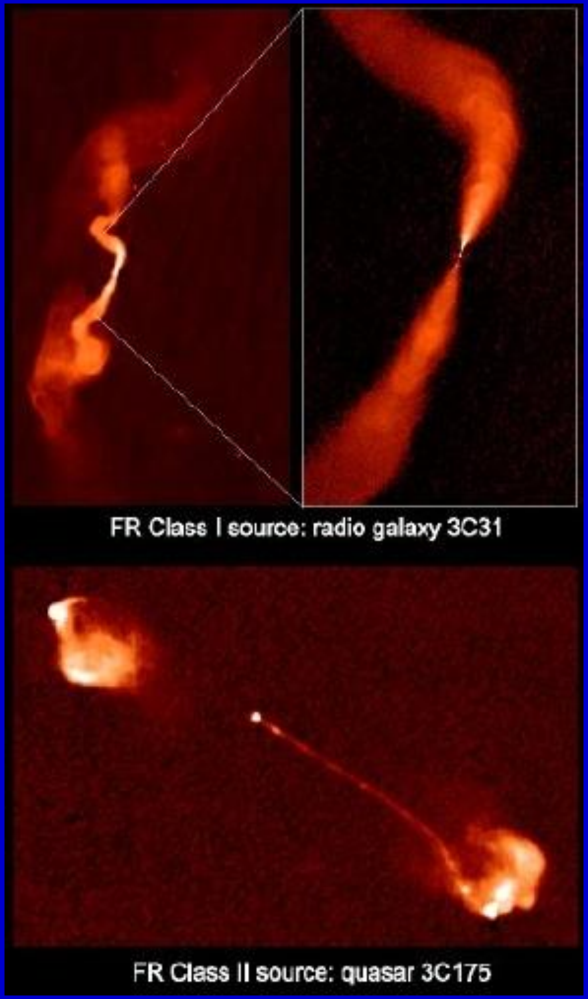

astro-ph/0406319

FR I. Two-sided jets.
Jets dominate in the emission.
Usually are found in rich clusters.

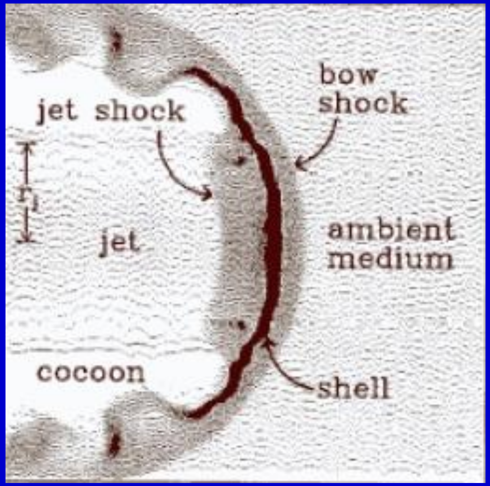

FR II. One-sided jets.
Radio lobes dominate over jets.
Mostly isolated galaxies
or poor groups.

See a review on radio galaxies in arXiv: 1101.0837

Diversity of radio jets

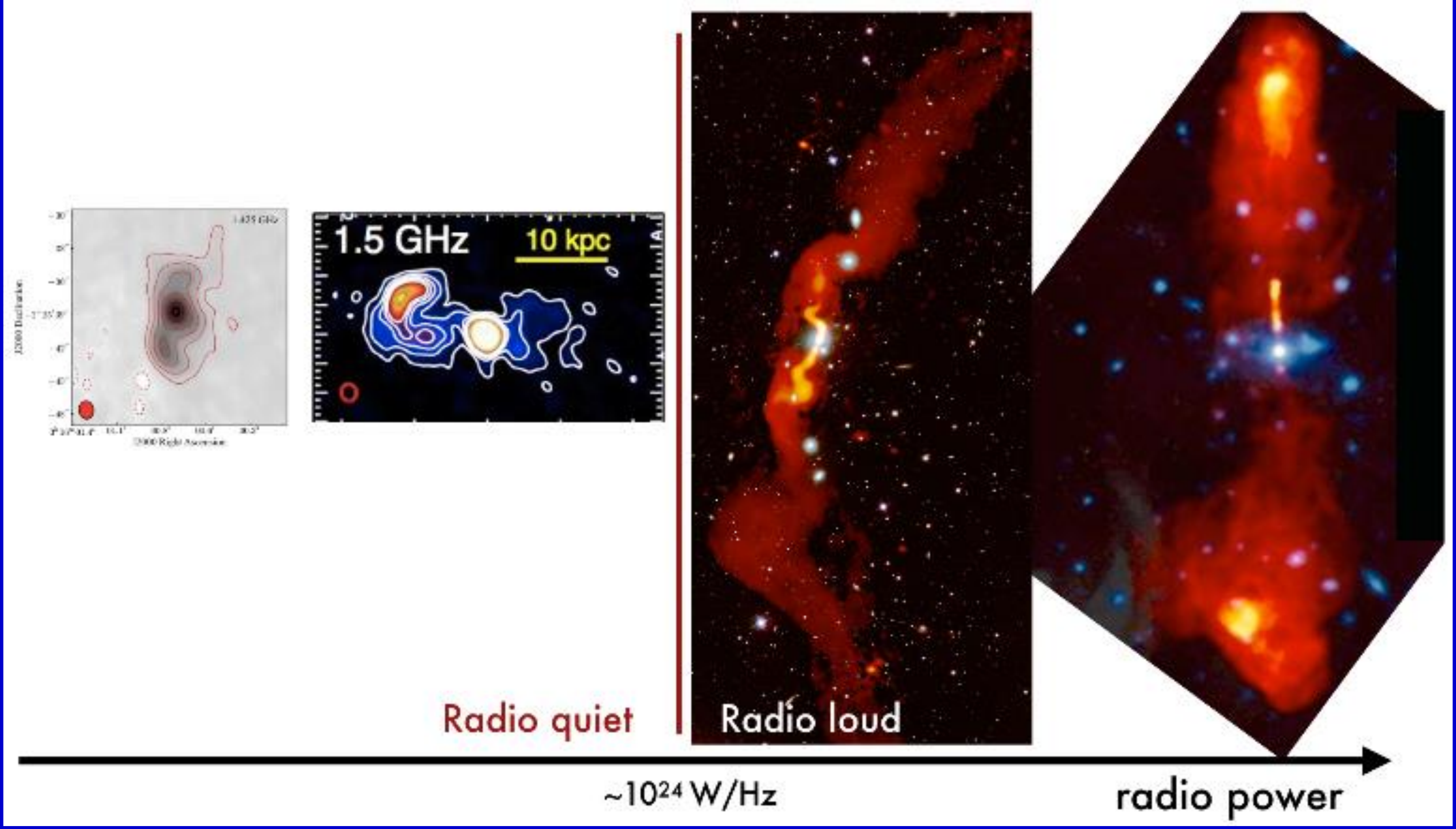

2001.02675

X-ray and radio properties

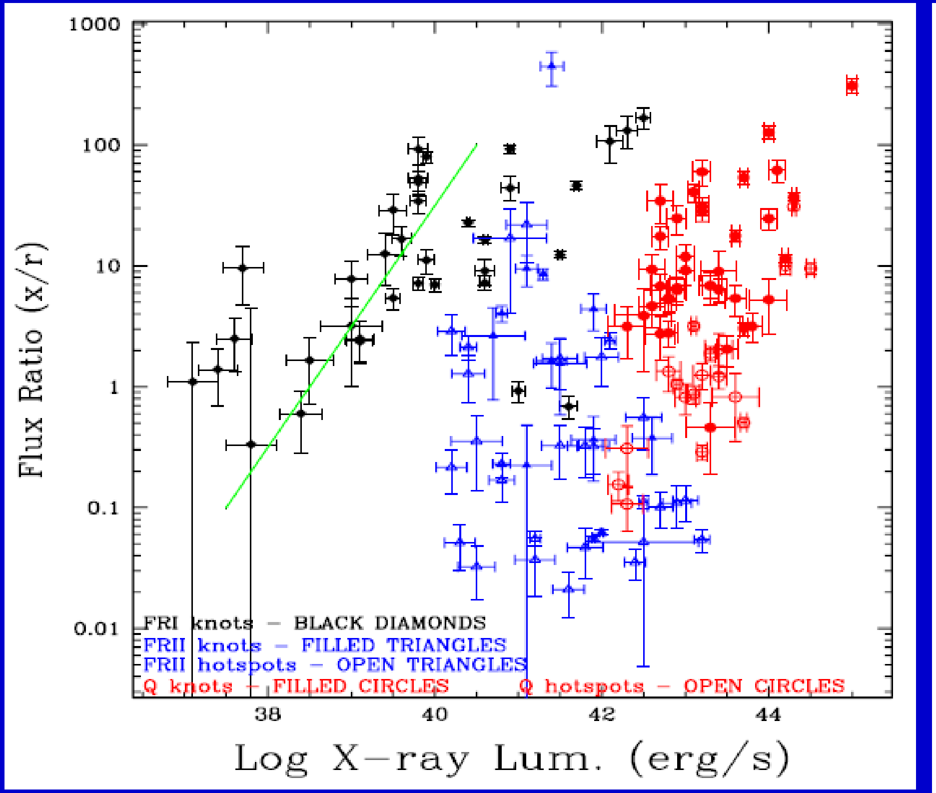

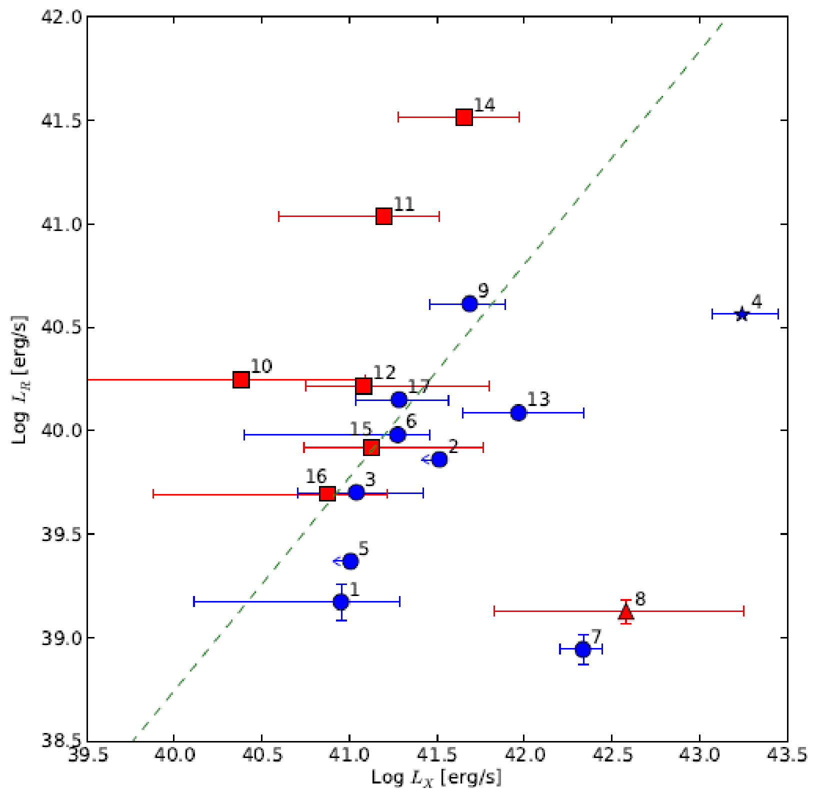

1003.0976

1104.3575

Magnetic field in a jet

Observations of M87 tell us that the magnetic field in the jet is mostly parallel to the jet axis, but in the emission regions ("knots") it becomes perpendicular (see astro-ph/0406319).

The same structure is observed in several jets with radio lobes.

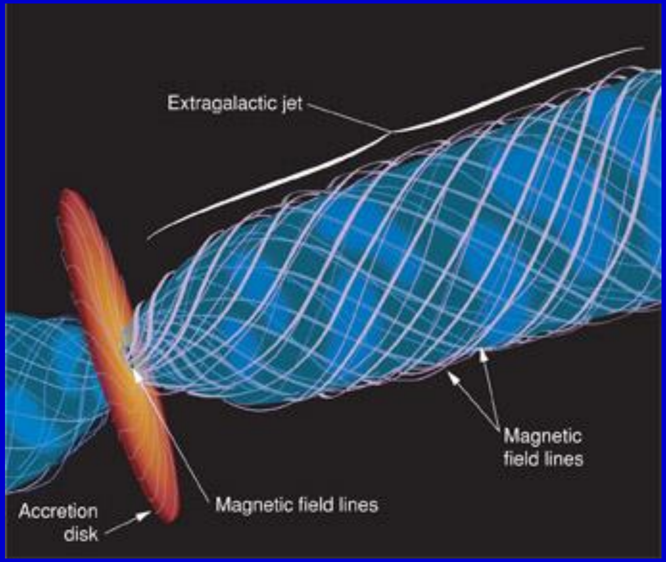

New RadioAstron data give some new insights.

Magnetic field in the jet

Due to modern high resolution observations new important results on the magnetic field in jets are obtained.

ALMA 0.01 pc scale

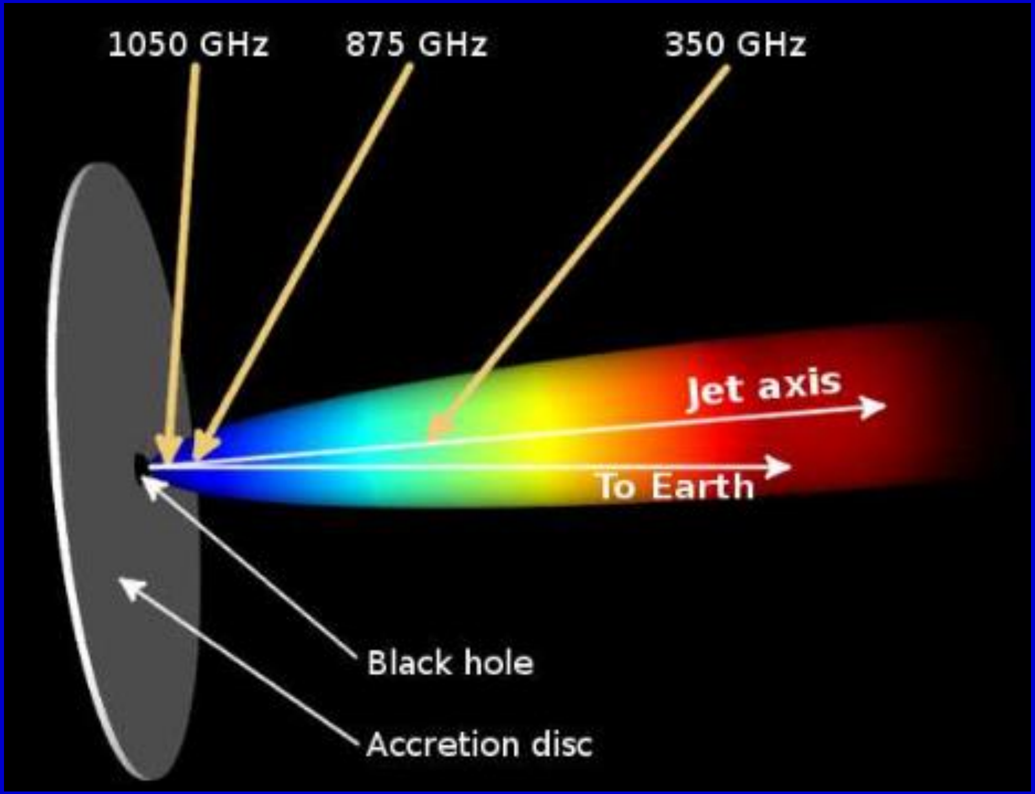

Magnetic fields of at least tens of Gauss (and possibly considerably higher) on scales of the order of light days (0.01 pc) from the black hole.

1604.01898

3C84 jet

Jet followed down to >~100 R_{sh}
BH mass ~2 10^9

Jet is already cylindrical at few 100 R_{sh}
Jet from the disc, not from ergosphere?

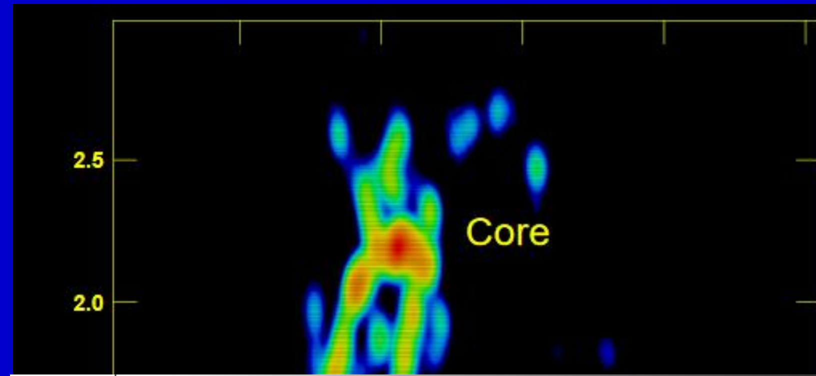

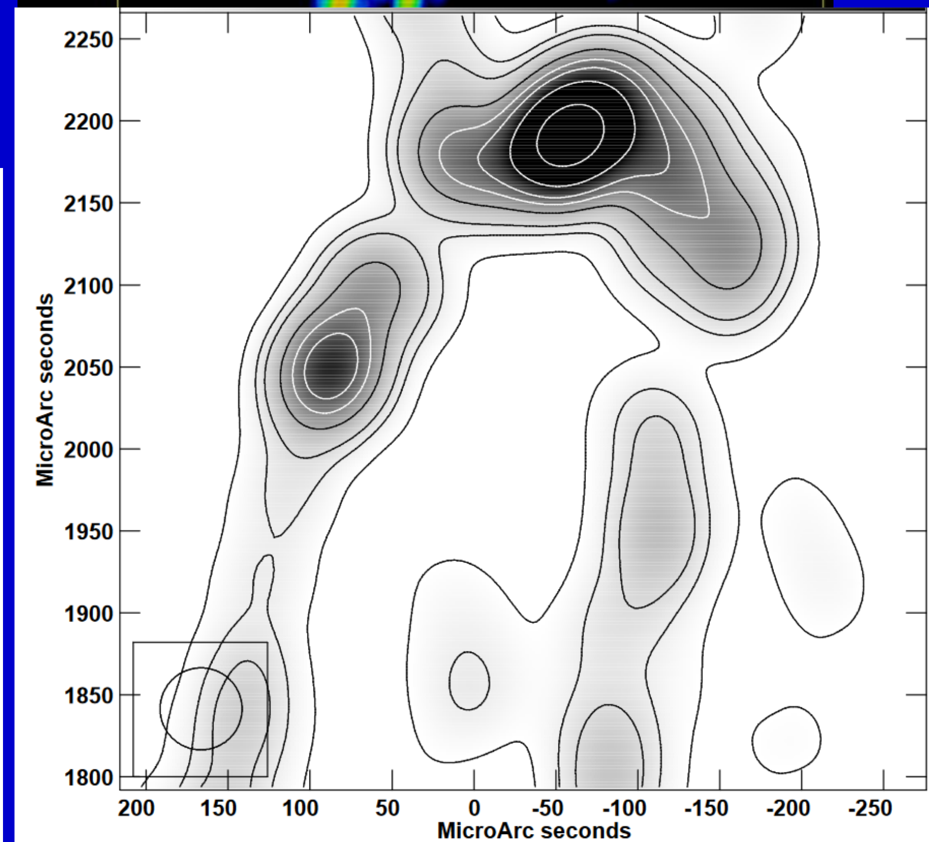

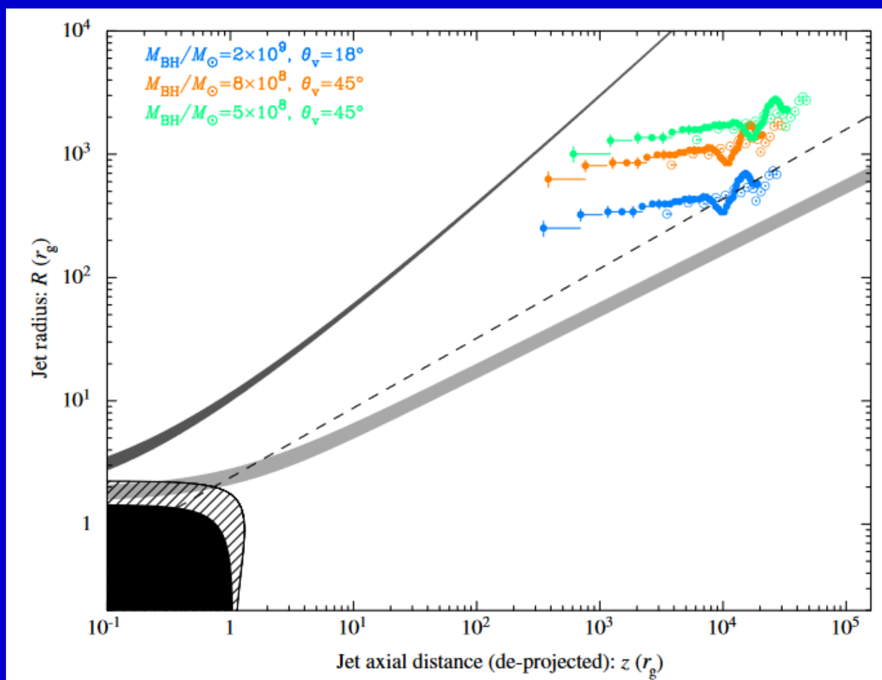

1804.02198

Blobs in jets

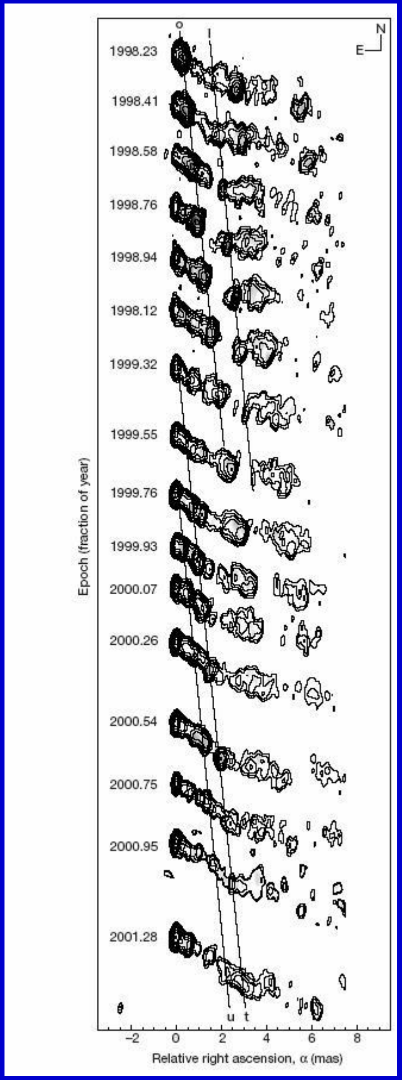

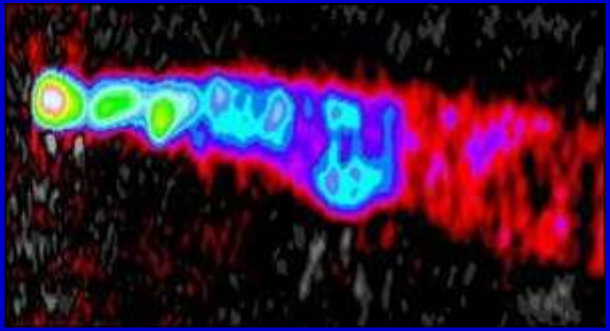

It is believed that bright features in AGN jets can be results of the Kelvin-Helmholtz instability. This instability leads to a spiral structure formation in a jet. (see, for example, astro-ph/0103379)

3C 120

However, in the case of 3C 120 the blobs appearence is due to processes in the disc. Dips in X-rays (related to the disc) appear before blobs ejection (Marscher et al. 2002).

Marscher, A.P., et al., NATURE Vol 417 p. 625

Blazars

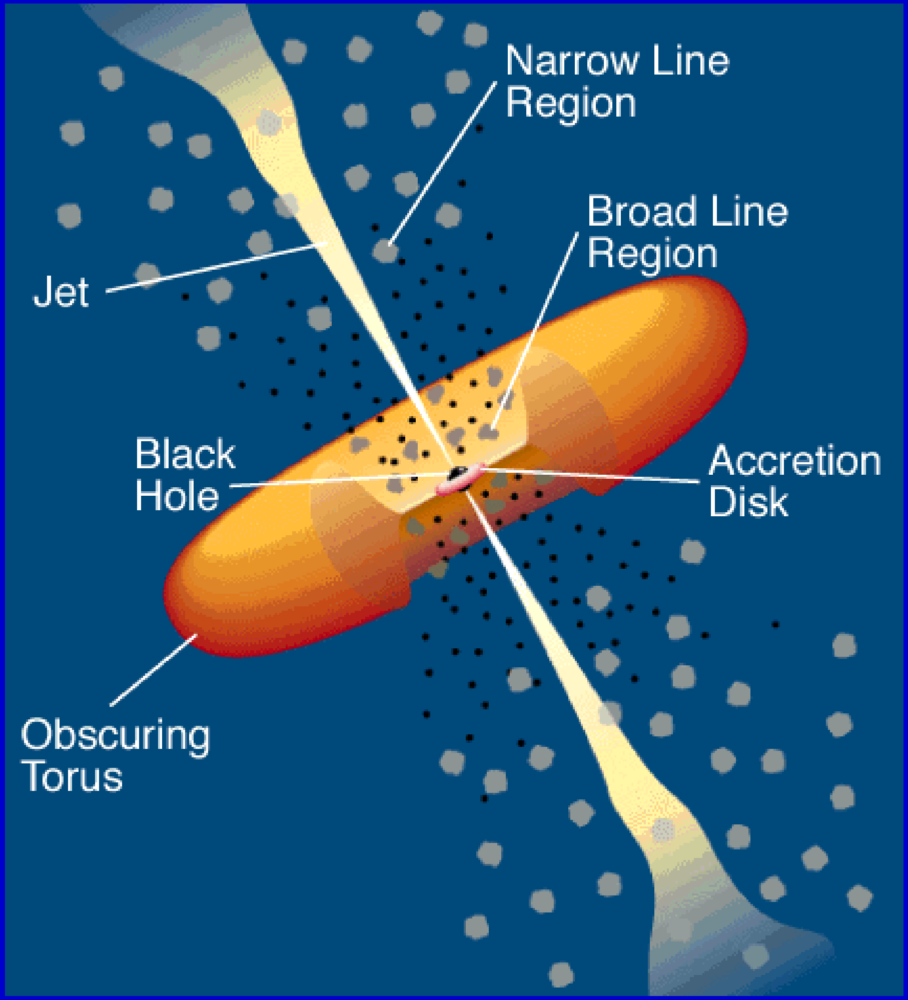

If a jet is pointing towards us, then we see a *blazar*.

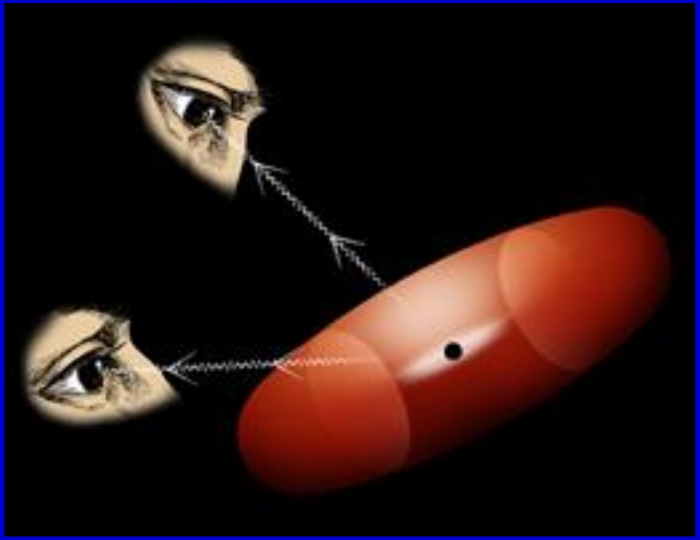

A review on blazar jets 2003.06322

Blazars at very high energies

Blazars are powerful gamma-ray sources. The most powerful of them have equivalent isotropic luminosity 10^{49} erg/s.

Collimation $\theta^2/2 \sim 10^{-2} - 10^{-3}$. θ – jet opening angle.
EGRET detected 66 (+27) sources of this type.
More results have been obtained after the launch of GLAST.

Many sources have been detected in the TeV range by ground-based gamma-ray telescopes. All of them, except M87, are BL Lacs at $z<0.2$ (more precisely, to high-frequency-peaked BL Lac – HBL).

Observations show that often (but not always) after a gamma-ray bursts few weeks or months later a burst happens also in the radio band.

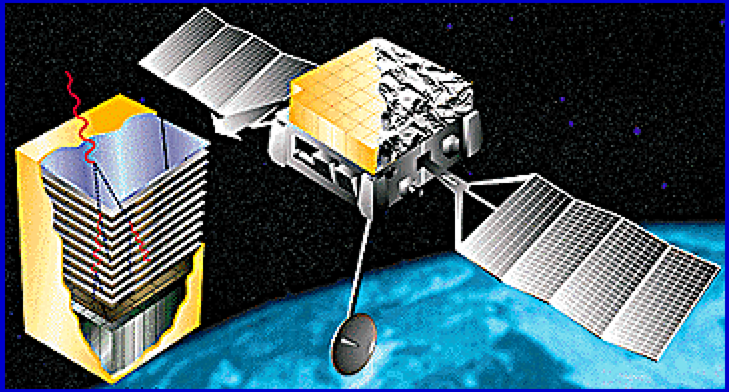

Fermi

see astro-ph/0611521, but notice rapid progress

Blazar spectra

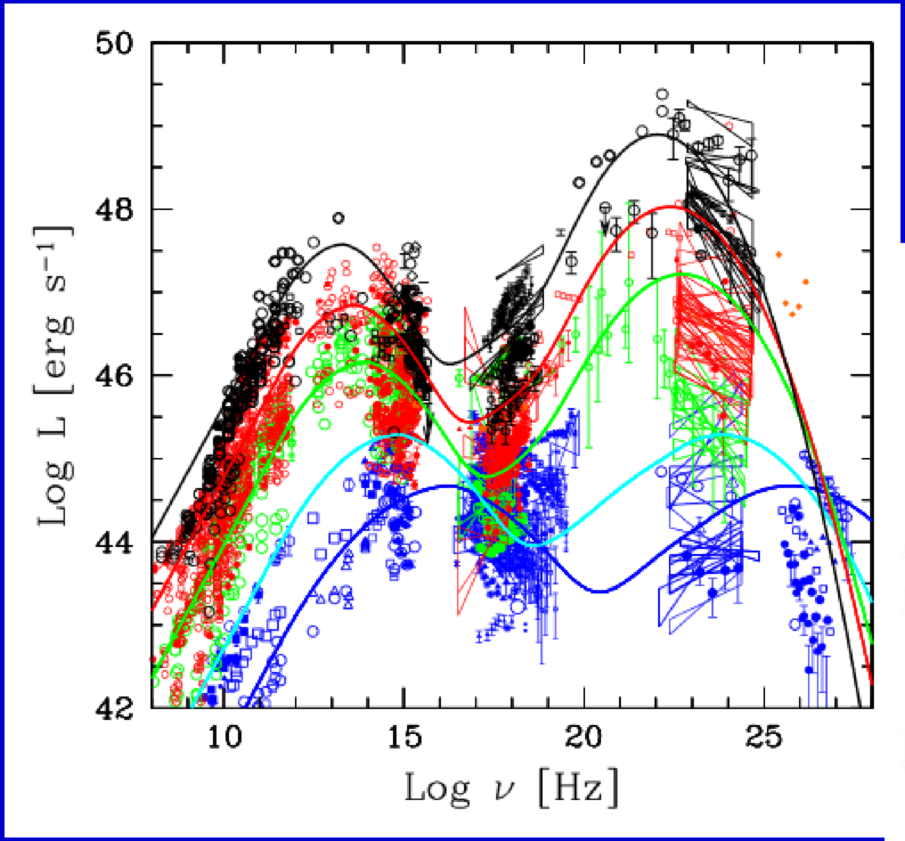

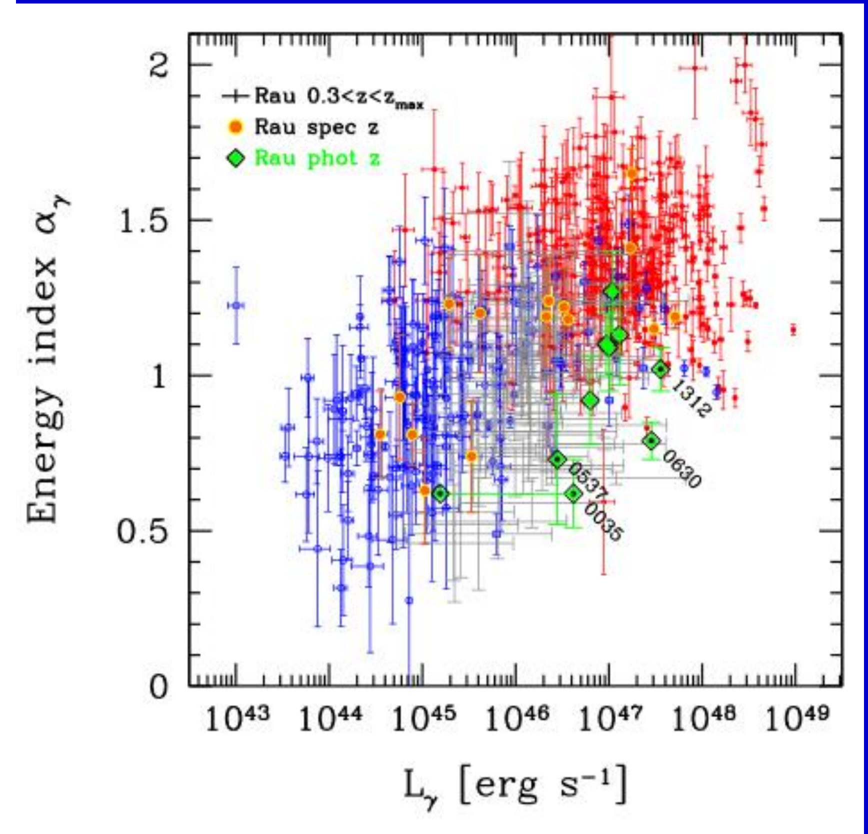

1309.4772

Microquasars

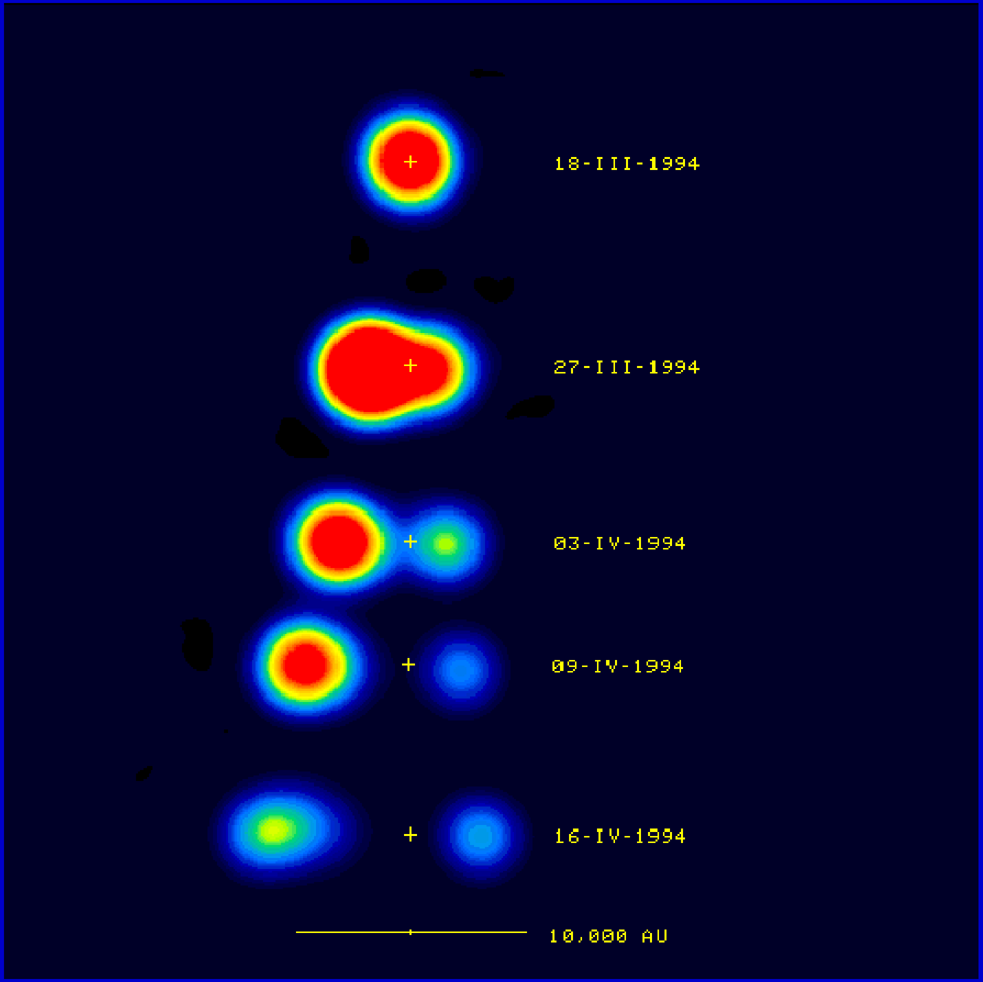

GRS 1915

The correlation between X-ray and synchrotron (i.e. between disc and jet emission) is observed.

Microquasars jets in radio

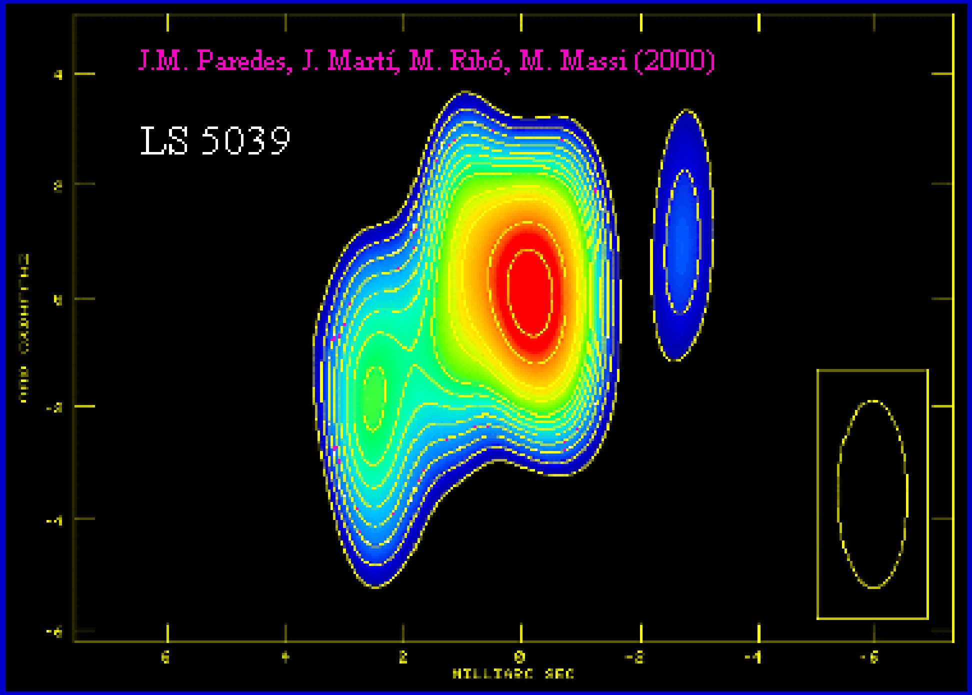

LS 5039/RX J1826.2-1450 –
is a galactic massive X-ray binary.

The jet length is ~1000 a.e.

Probably, the source was observed by EGRET as 3EG J1824-1514.

The role of a donor

An important difference between the microquasars case and AGNs is related to the existence of a donor-star.
Especially, if it is a giant, then the star can inject matter and photons into the jet.

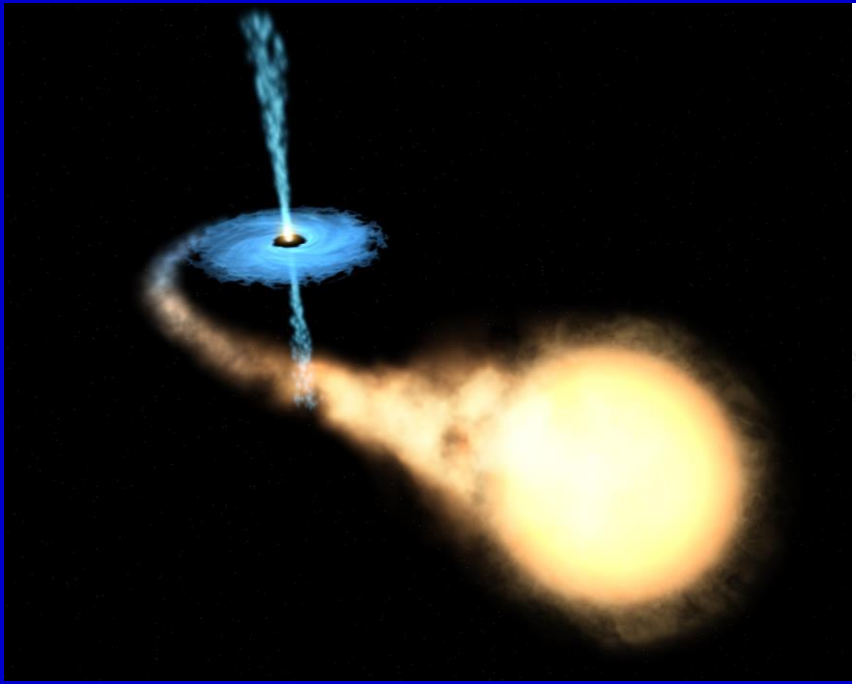

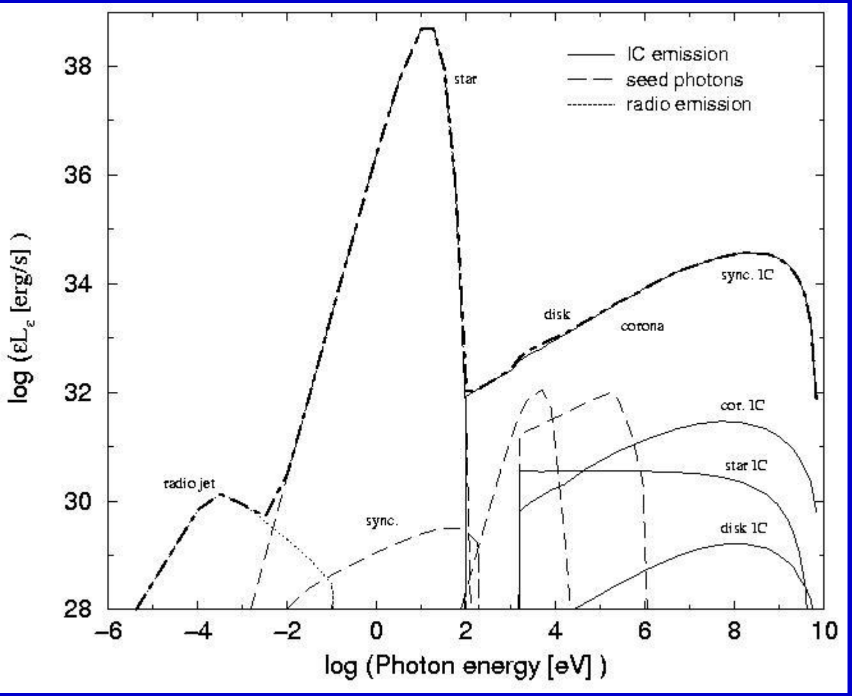

see Paredes astro-ph/0412057

Microquasars in gamma-rays: TeV range

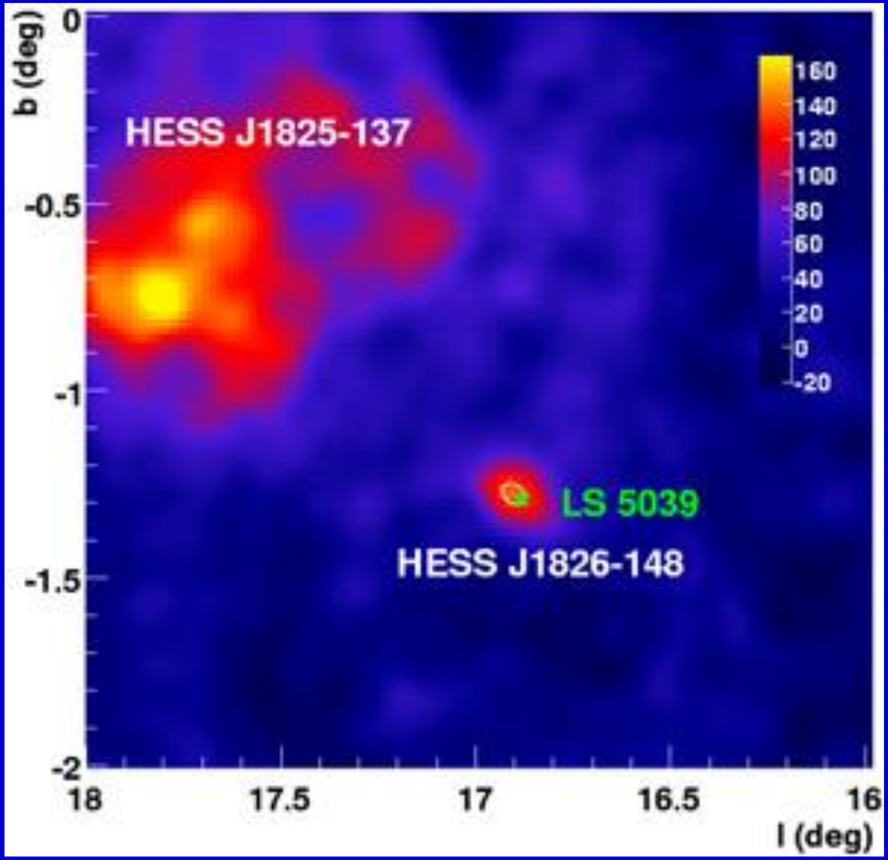

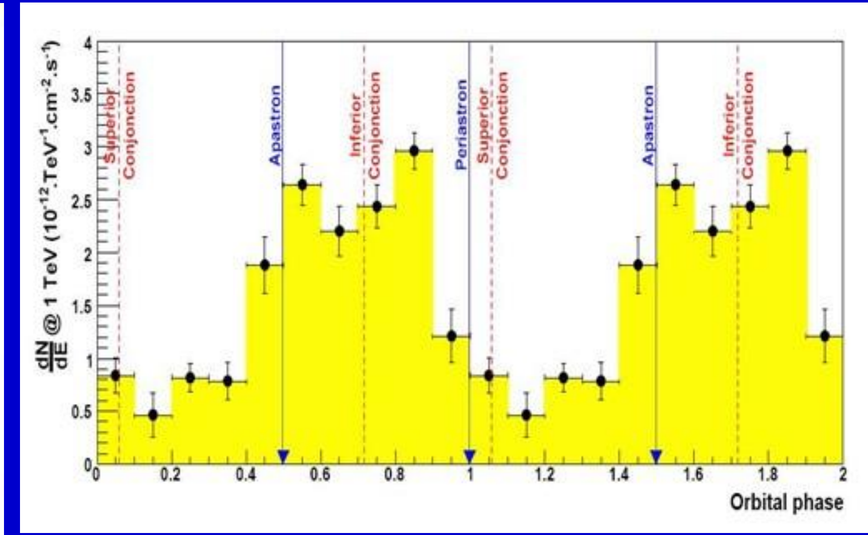

F. Aharonian et al.

TeV emission from Cyg X-1

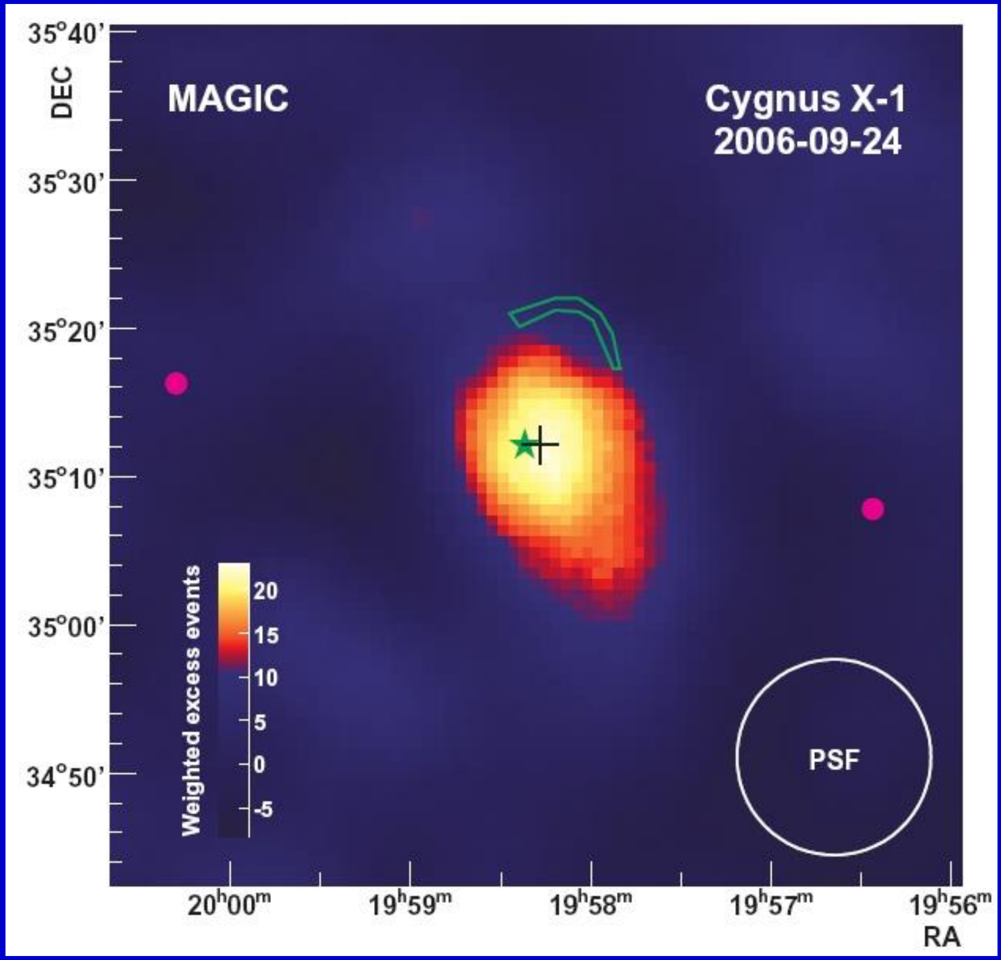

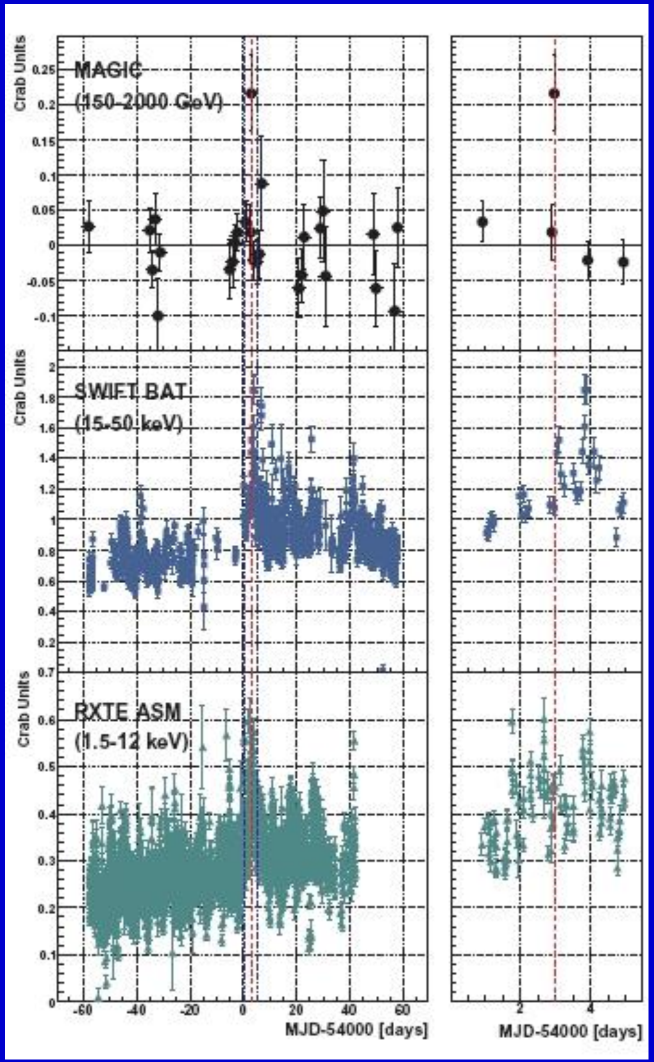

arxiv:0706.1505

See a review on jets in binaries in 1407.3674

Jet models

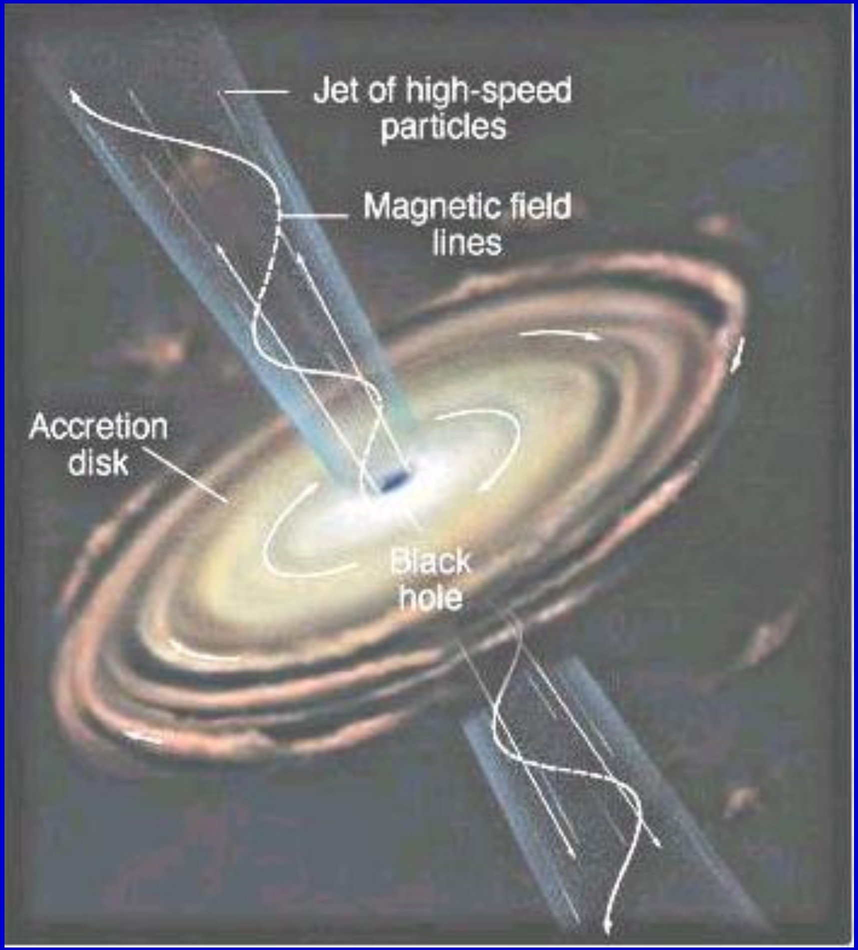

Table 1. Characteristic parameters of relativistic jet sources.

	L_j (erg/s)	Γ	Δt
GRB	10^{47}-10^{50}	$10^2 - 10^3$	millisec - min.
AGN	10^{42}-10^{47}	5 - 50	hours - years
MQ	10^{37}-10^{40}	1 - 10	days
GF	10^{43}-10^{46}	1	seconds

In all models jets are related to discs. Velocity at the base of a jet is about the parabolic (escape) velocity.

(the table is from astro-ph/0611521)

Jet power

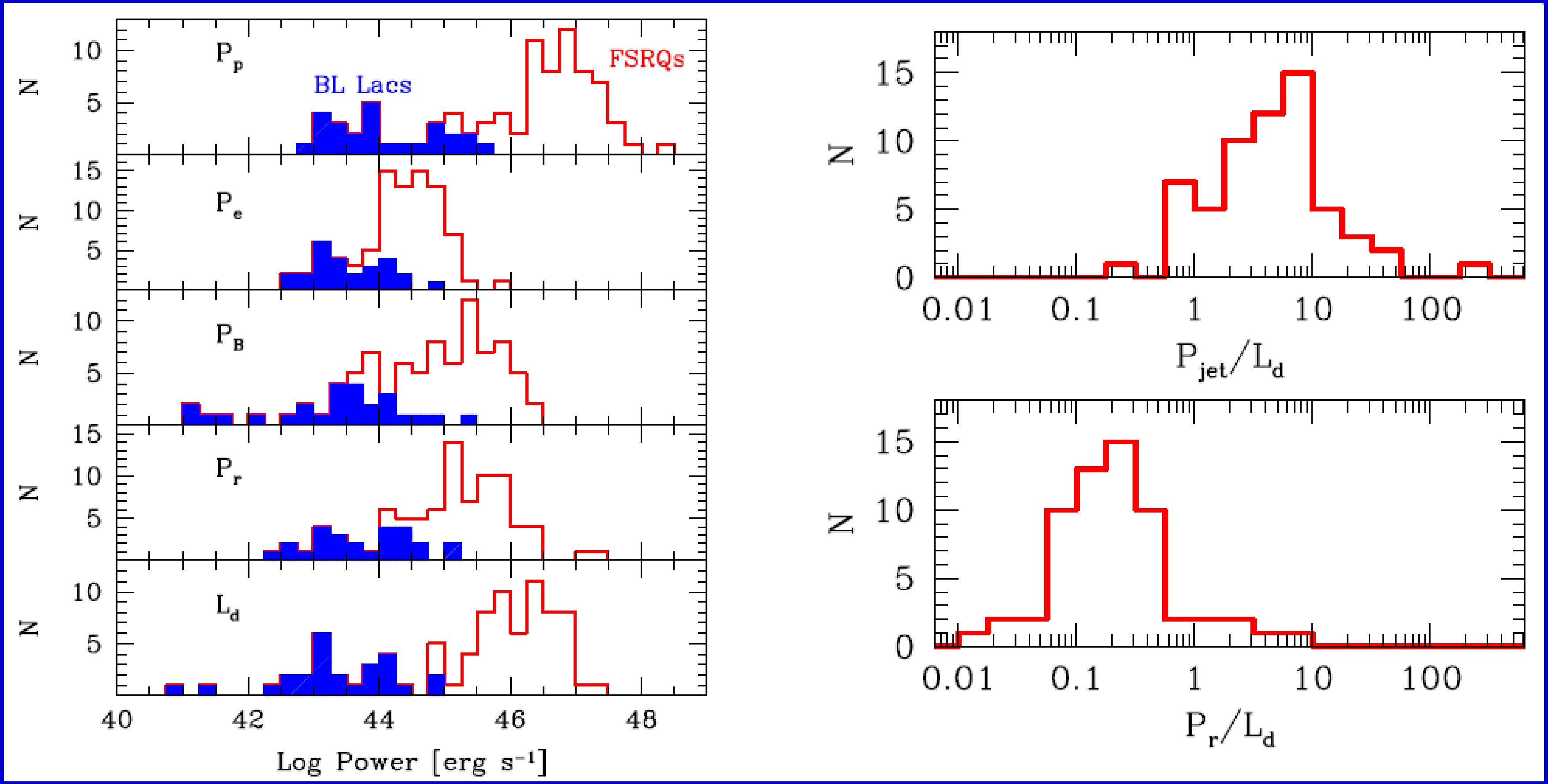

$P_{jet}>2P_r=2L/\Gamma^2$

1104.0006

Jet and disc

L_d – disc luminosity.
$P_{jet}=P_B+P_P+P_e$
In the gray stripes P_{jet} ~ Mdot and
at low accretion rates L_d ~ $Mdot^2$, at large - L_d ~ Mdot.

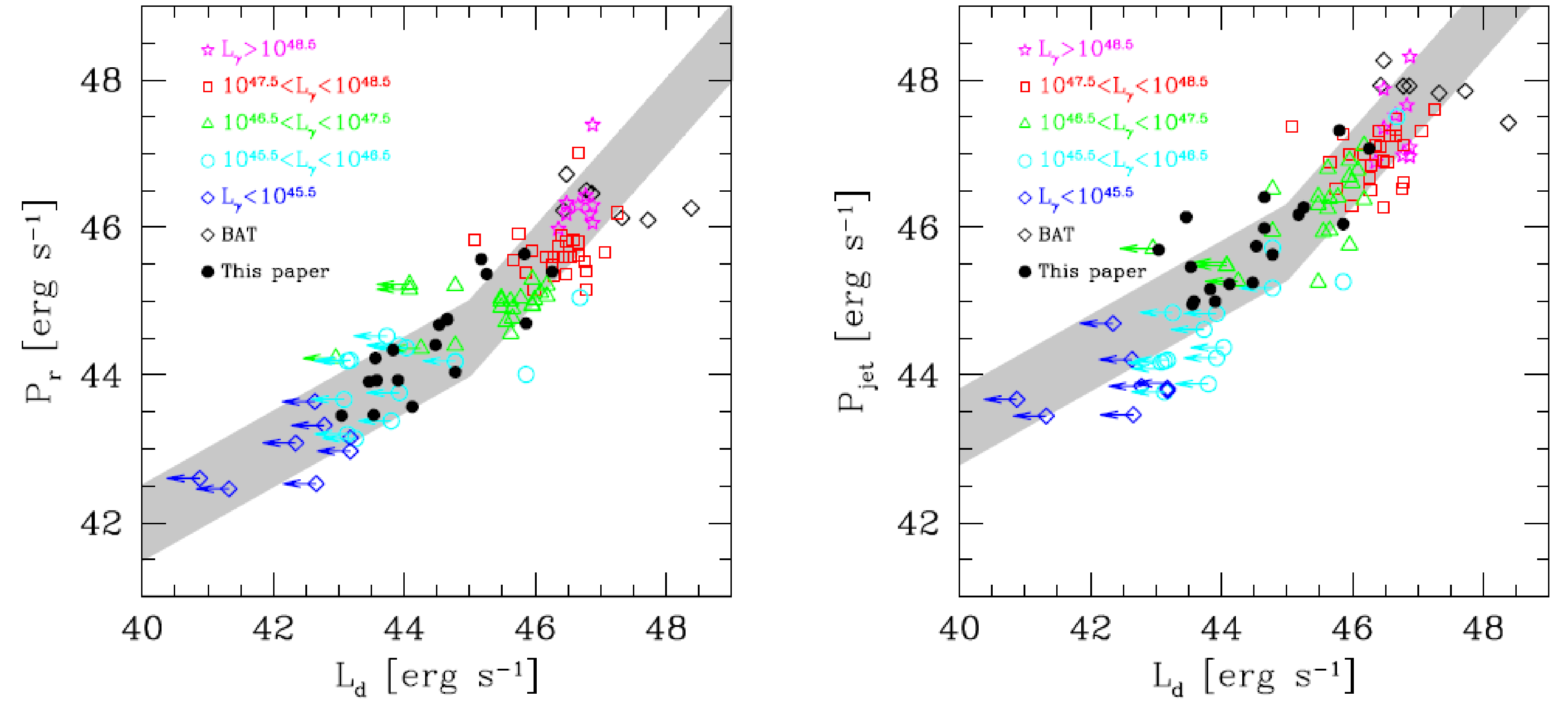

1104.0006

Jets are more powerful than discs

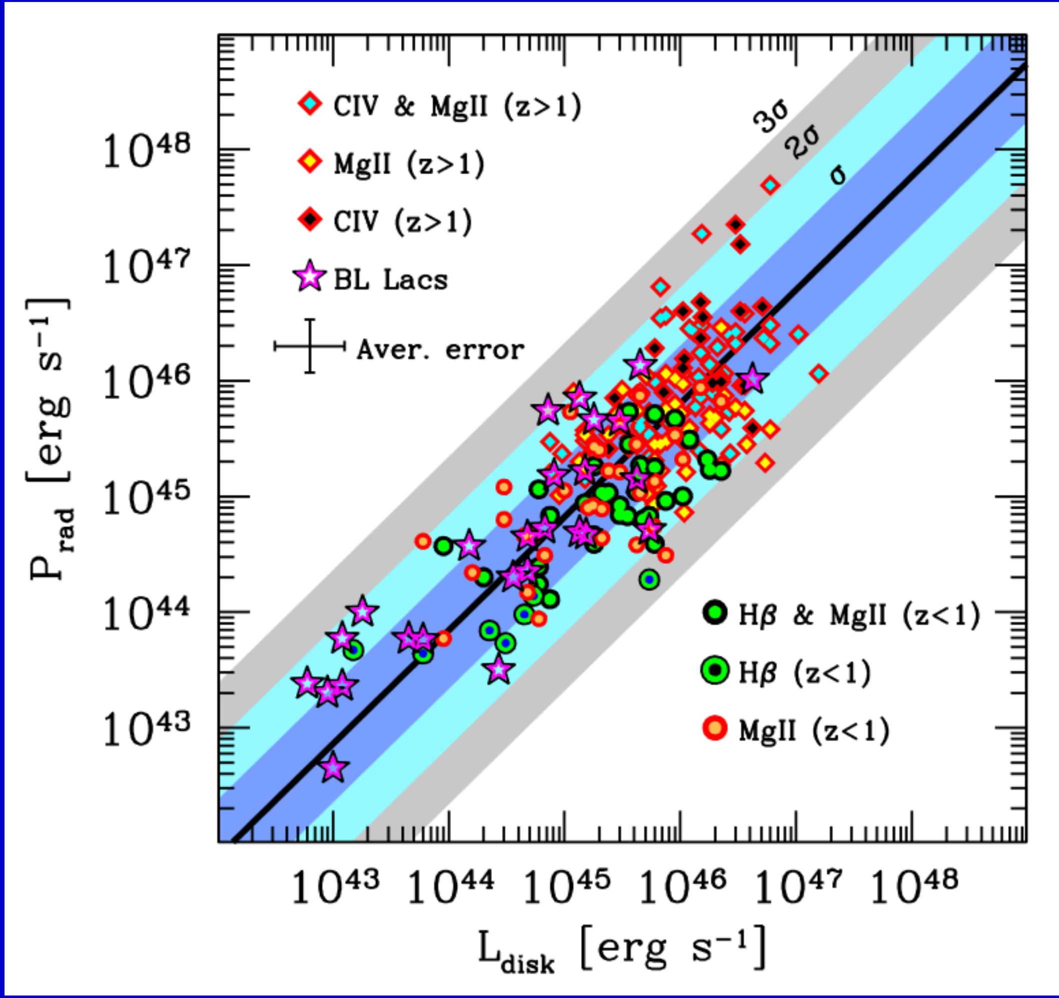

Jets also serve as sites for particle acceleration, see 2003.06587

$$P_{\rm rad} = 2\,f\,\frac{L_{\rm jet}^{\rm bol}}{\Gamma^2}$$

1411.5368

Displaced SMBH in M87

Projected displacement of 6.8+/-0.8 pc
consistent with the jet axis
displaced in the counter-jet direction

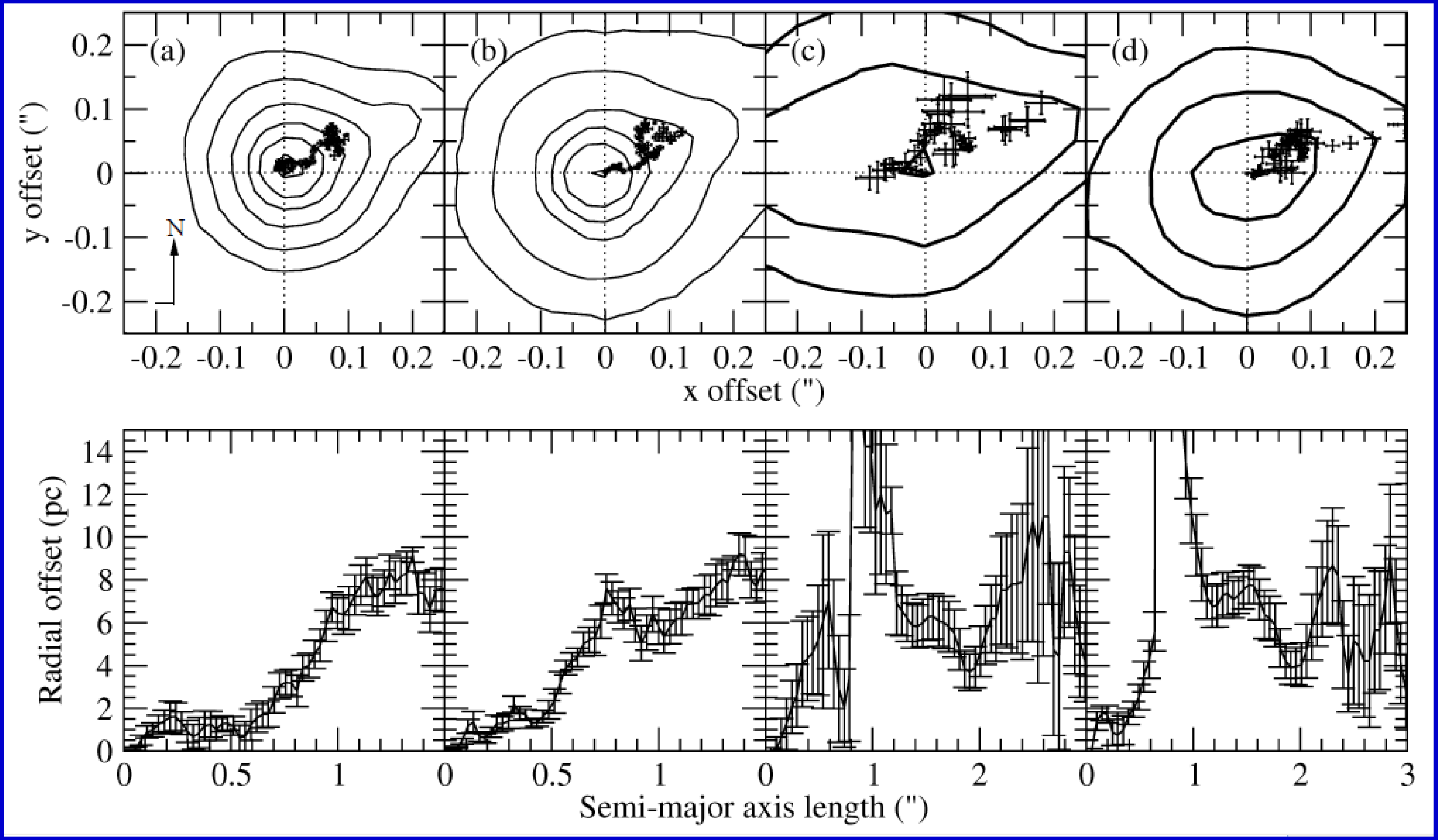

1005.2173

Other explanations are possible

Different accretion regimes in AGNs

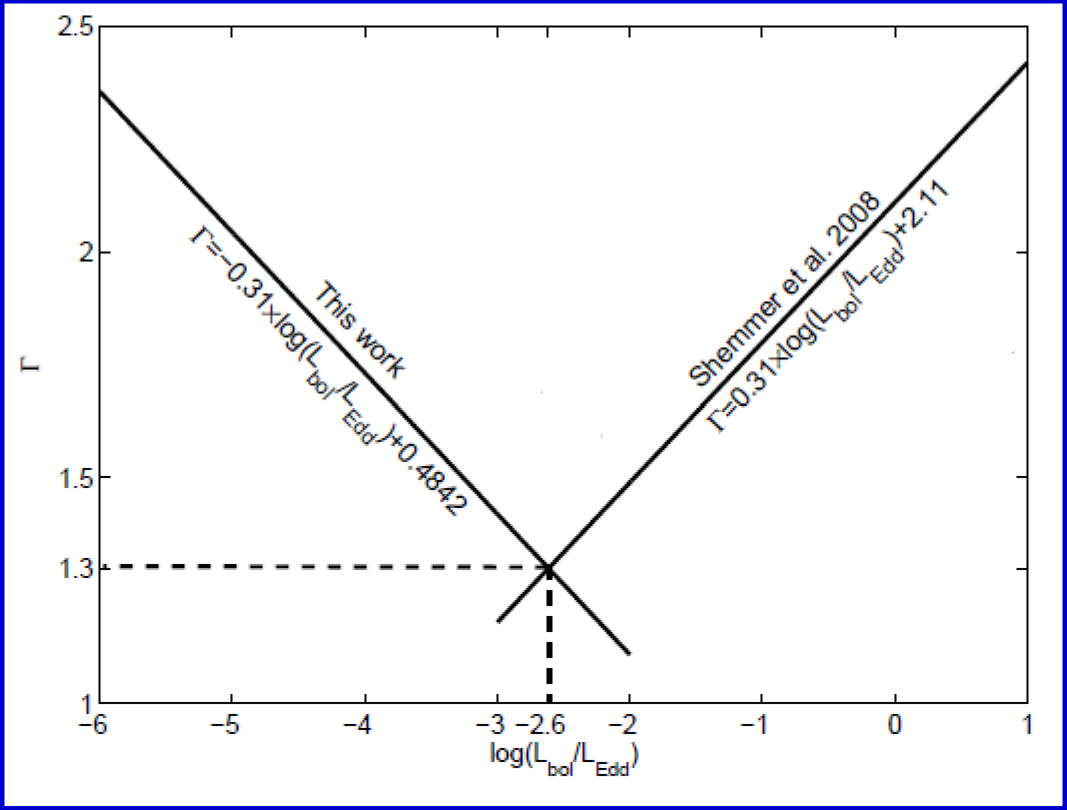

Γ- photon index

Anticorrelation for low-luminosity AGNs (LINERS).

Correlation for luminous AGNs.

In the critical point
the accretion regime
can be changed:
from a standard thin accretion disc
to RIAF (radiatively inefficient
accretion flow).

1104.4891

BH mass determination

Accretion disc contribution is visible in opt-UV.
It allows to estimate the BH mass.
It can be compared with emission lines estimates.
Bars correspond to different lines used.

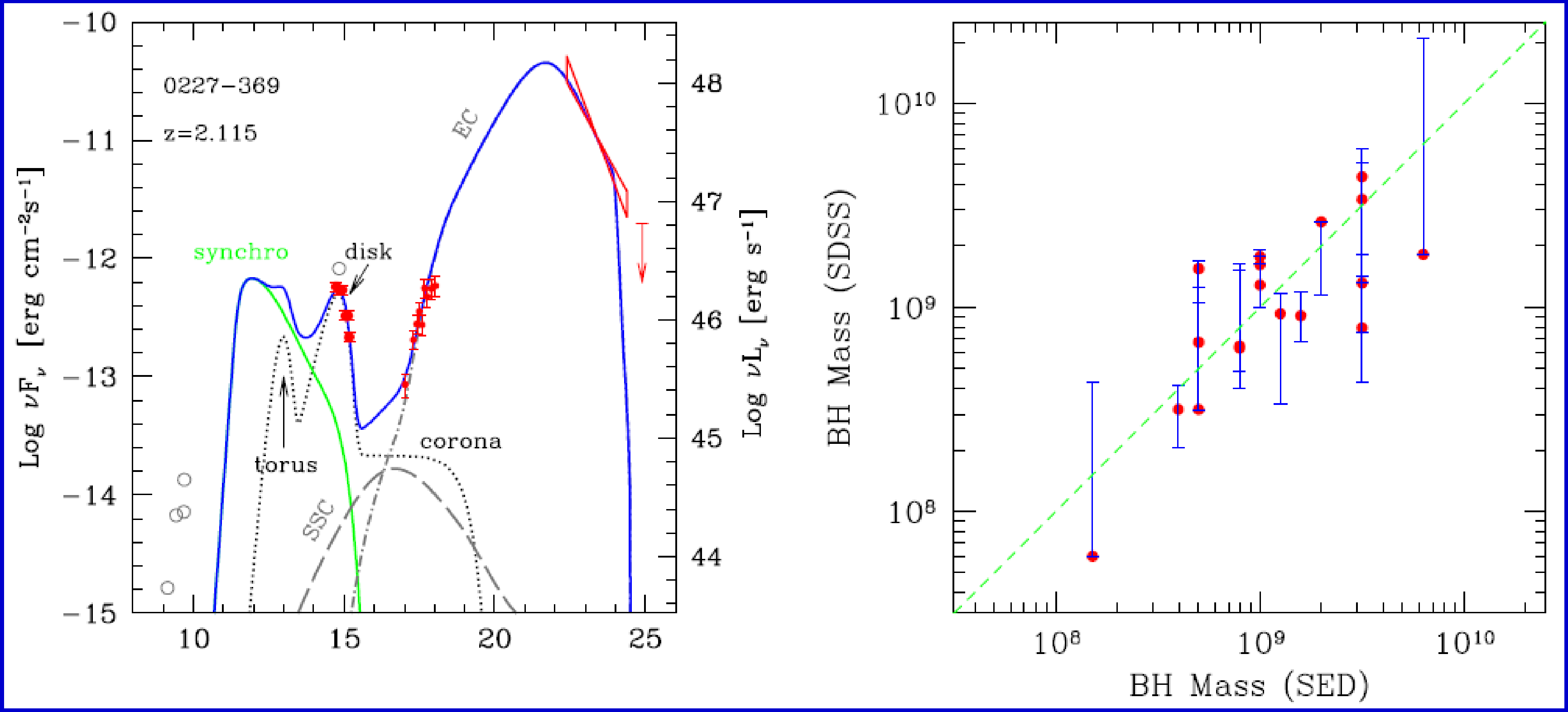

1104.0006

BH mass and jet properties in M87

Table 3. Predicted jet and BH parameters for $M = 6.5 \times 10^9$ $M_\odot$.

σ_M (1)	$\Gamma\theta_j$ (2)	ϕ (3)	a_* (4)	W_j (10^{42} erg/s) (5)
10	0.062	3.2	0.093	1.9
20	0.063	3.3	0.144	4.7

Estimates are in correspondence with the EHT data on the BH mass.

If the mass is assumed to be known,
then the initial magnetization σ_M can be determined.

1904.05665

Tidal disruption

The Hills limit: 3 10^8 solar masses. A BH disrupts stars.

After a disruption in

$$(t_0 - t_D) \sim 1.1 M_8^{1/2} \ \mathrm{yr}$$

happens a burst with the temperature

$$T_{\rm eff} \approx (L_{\rm Edd}/4\pi\sigma R_T^2)^{1/4} = 3.7 \times 10^5 M_8^{1/12} \ \mathrm{K}$$

The maximum accretion rate

$$\dot{M}_{\rm max} \sim 0.14 \, M_8^{1/2} \, M_\odot \ \mathrm{yr}^{-1}$$

This rate corresponds to the moment

$$(t_{\rm max} - t_D) \sim 1.5 \, (t_0 - t_D)$$

Then the rate can be described as

$$\dot{M}(t) = 0.3 \, M_8 \, [(t - t_D)/(t_0 - t_D)]^{-5/3} \, M_\odot$$

For a BH with M <10^7 M_0 the luminosity at maximum is:

$$L_{\rm flare} \geq \eta \dot{M}_{\rm Edd} c^2 > 1.3 \times 10^{45} M_7 \ \mathrm{ergs \ s^{-1}}$$

(astro-ph/0402497)

See a review in 1505.01093

General picture

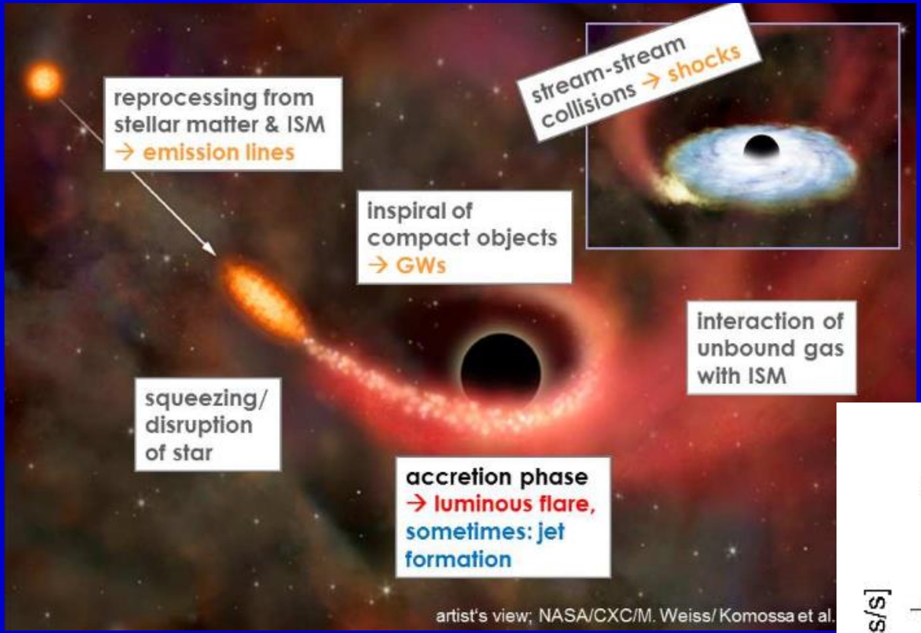

Rate of TDE is ~1/100000 yrs per galaxy (1407.6425).

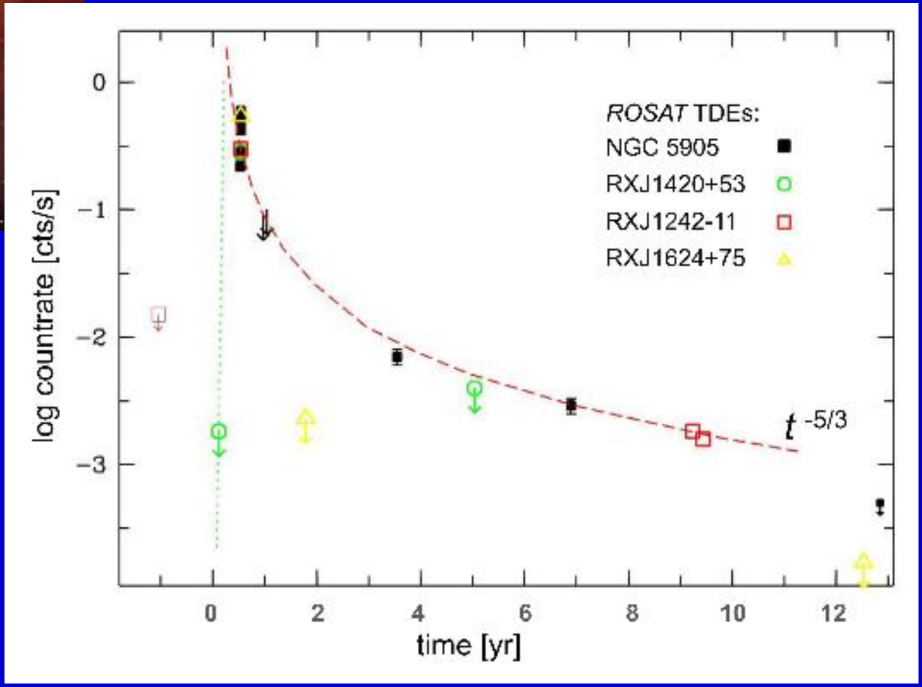

See a review in 1505.01093

Rate of TDE

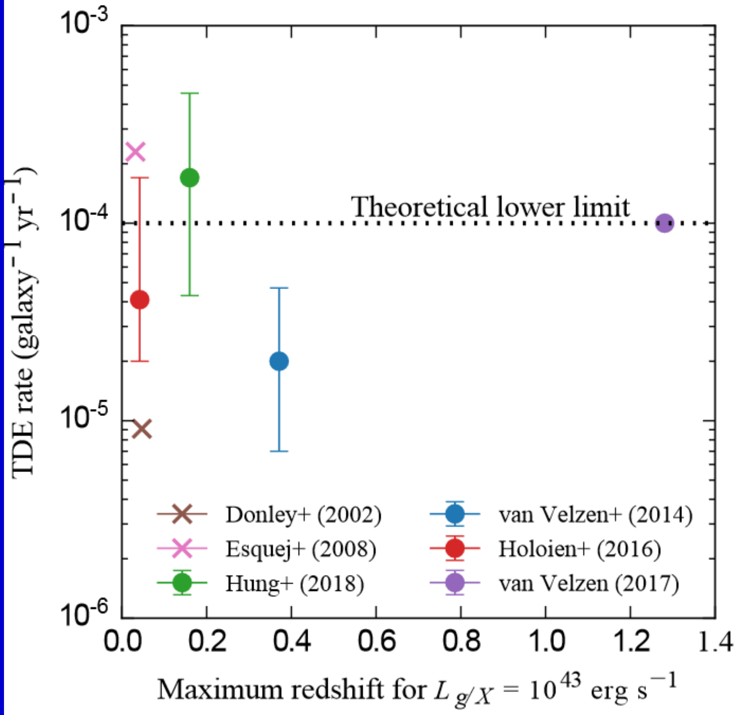

Volumetric TDE rates are dominated by the smallest galaxies that typically host SMBHs.

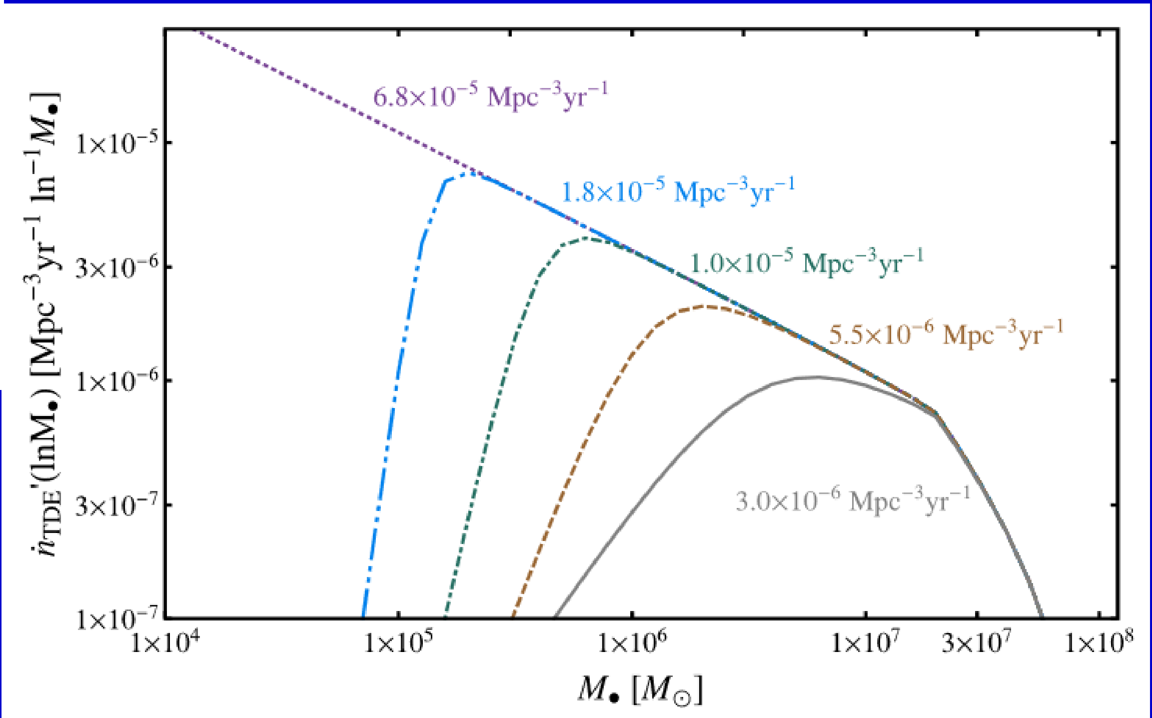

2003.08953

A burst in NGC 5905

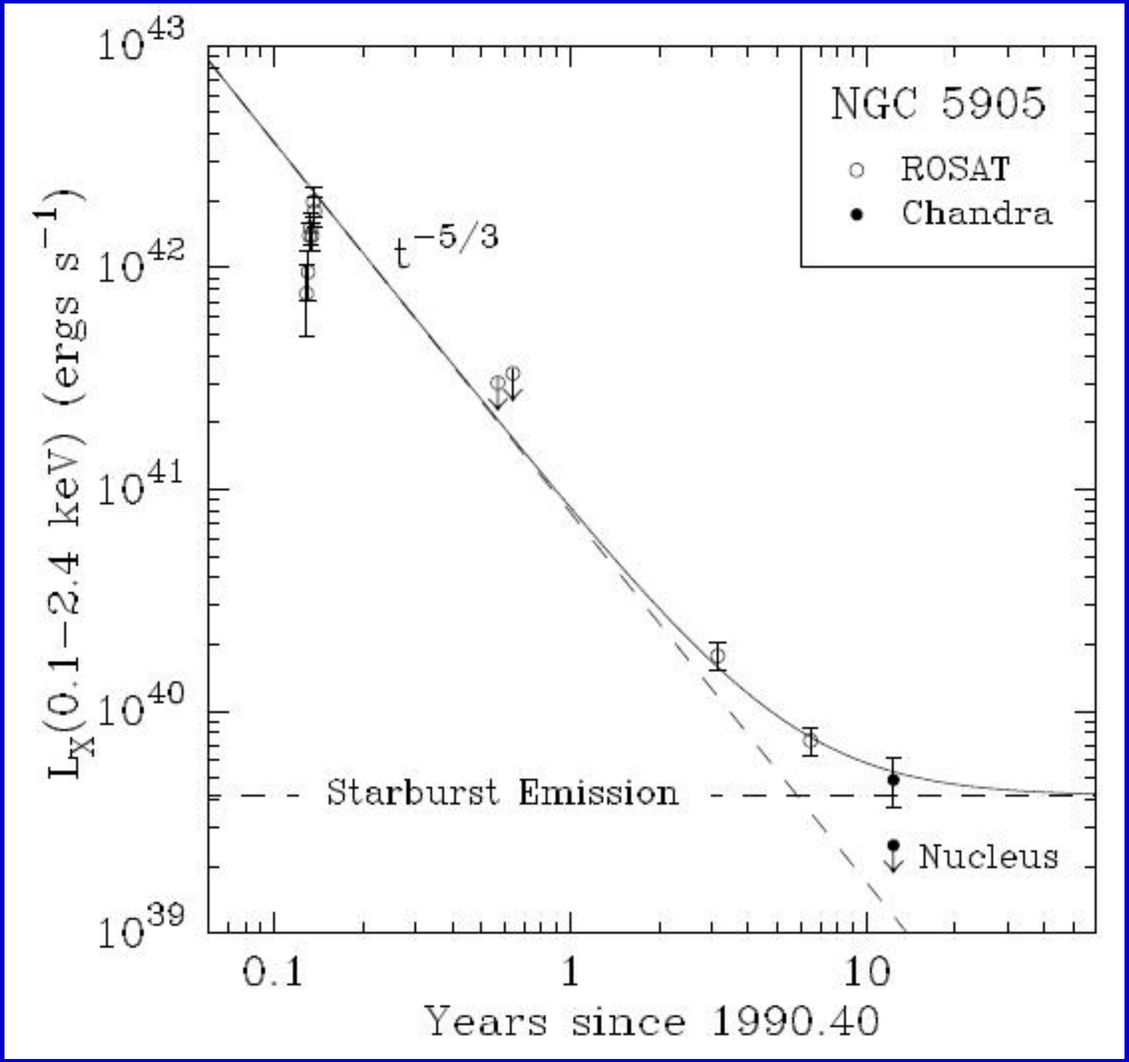

The decay was well described by the relation:

$$(t - t_D)^{-5/3}$$

Two other bursts discovered by ROSAT and observed by HST and Chandra:

RX J1624.9+7554
RX J1242.6-1119A

astro-ph/0402497

High-energy transient Swift J164449.3+573451

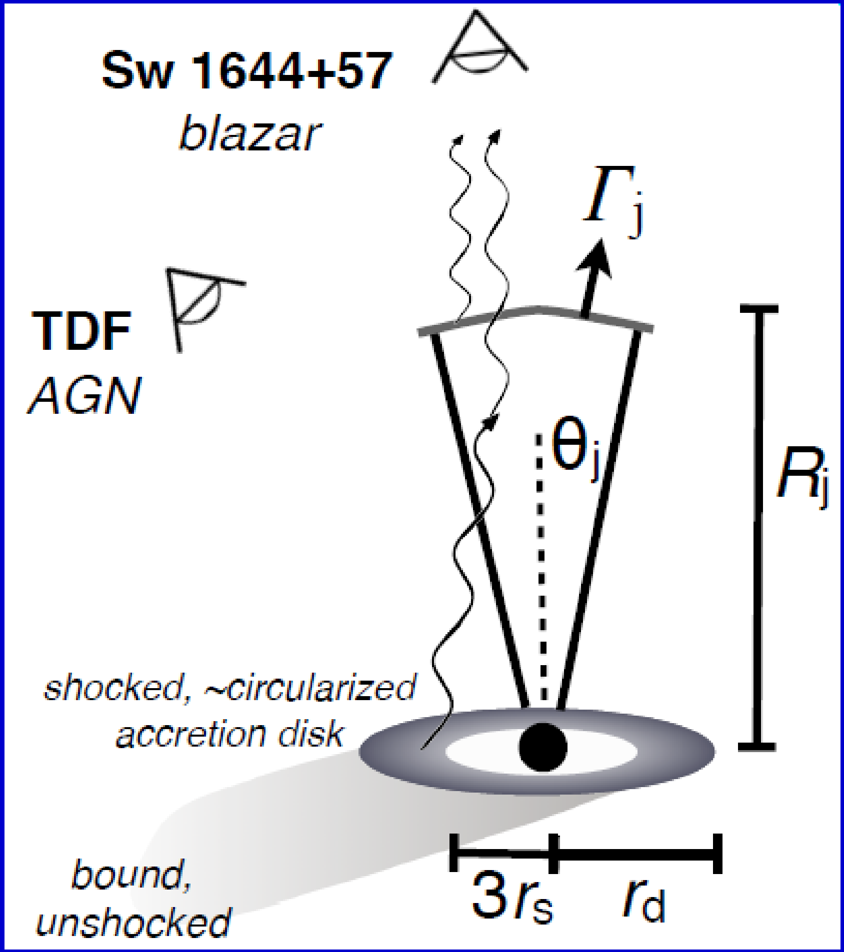

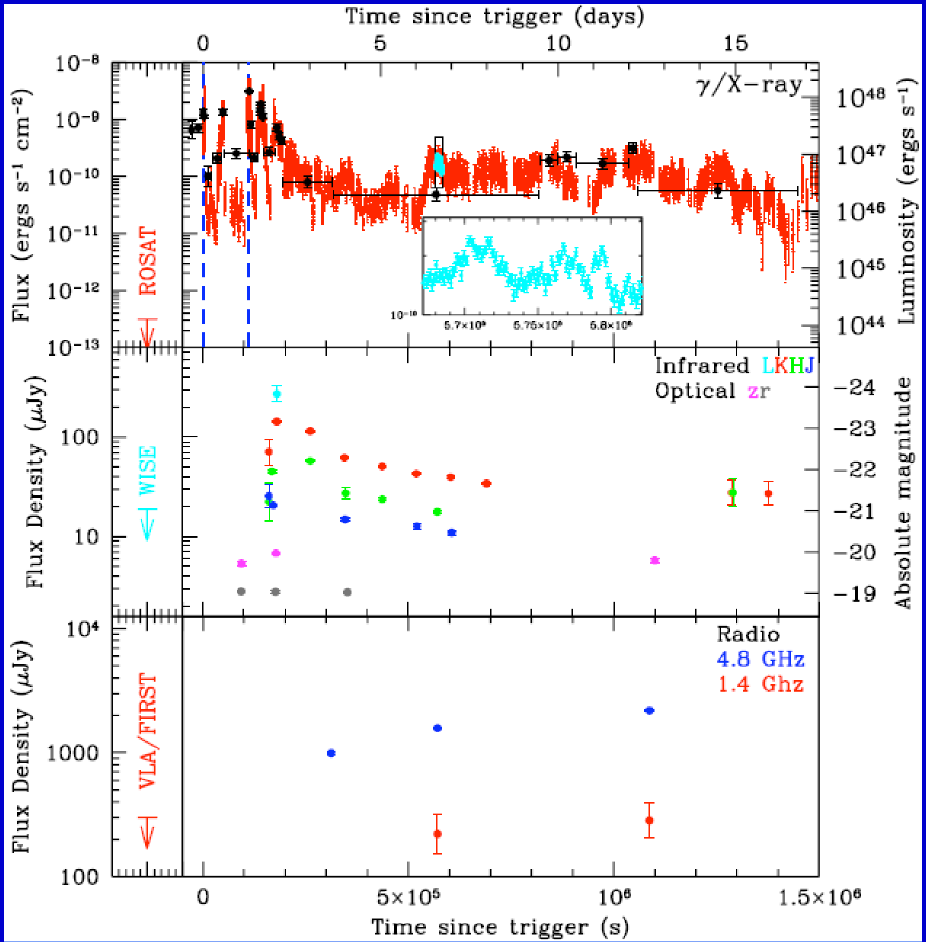

1104.3257

1104.3356

Also known as GRB 110328A

A unique event

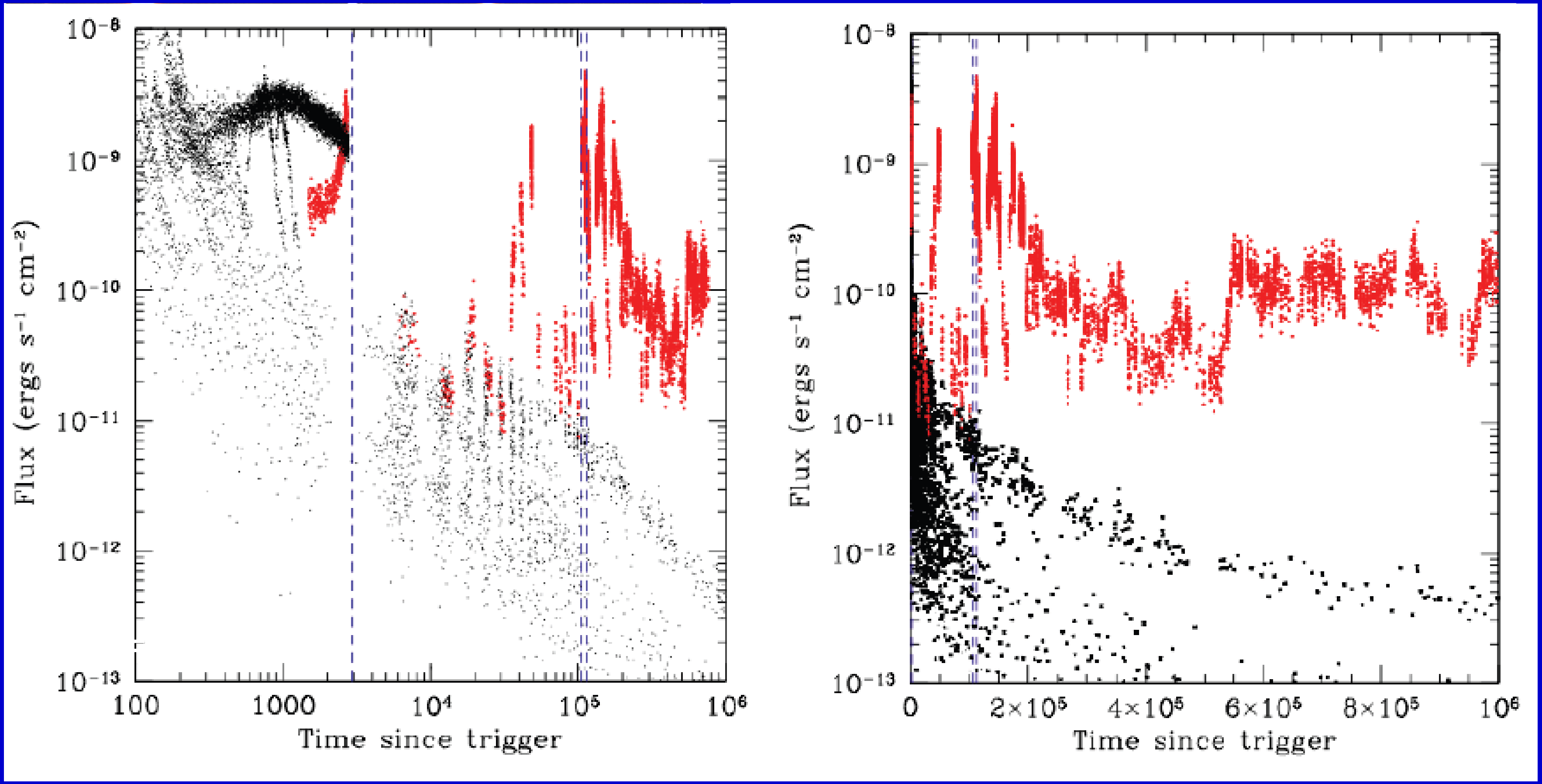

The transient does not looks similar to GRBs, SN or any other type of event

1104.3356

A tidal disruption event

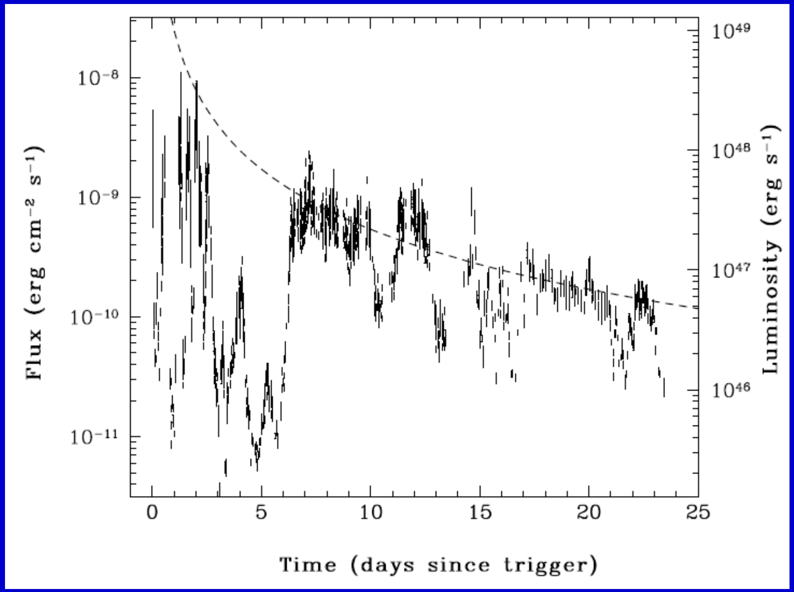

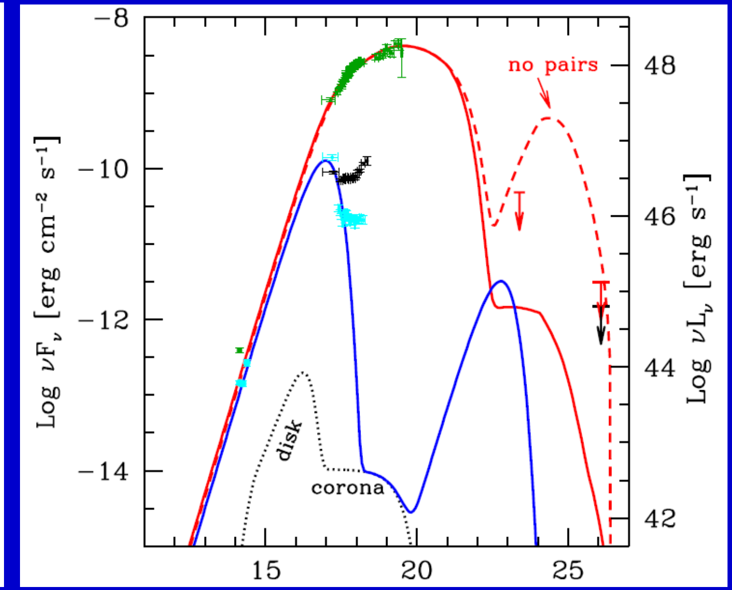

Light curve fits the prediction for a tidal event. The spectrum is blazar-like.

1104.4787

See a review on jets from TDE in 1911.01442.

Name	year	z	X-rays?	
Swift J164449.3+573451	2011/2011	0.3543	non-thermal	On-axis jet
Swift J2058.4+0516	2011/2012	1.1853	non-thermal	On-axis jet
Swift J1112.2-8238	2011/2015	0.89	non-thermal	On-axis jet
Arp 299-B AT1	2005/2018	0.0103	-	Off-axis jet

Optical observations of tidal disruptions

GALEX data

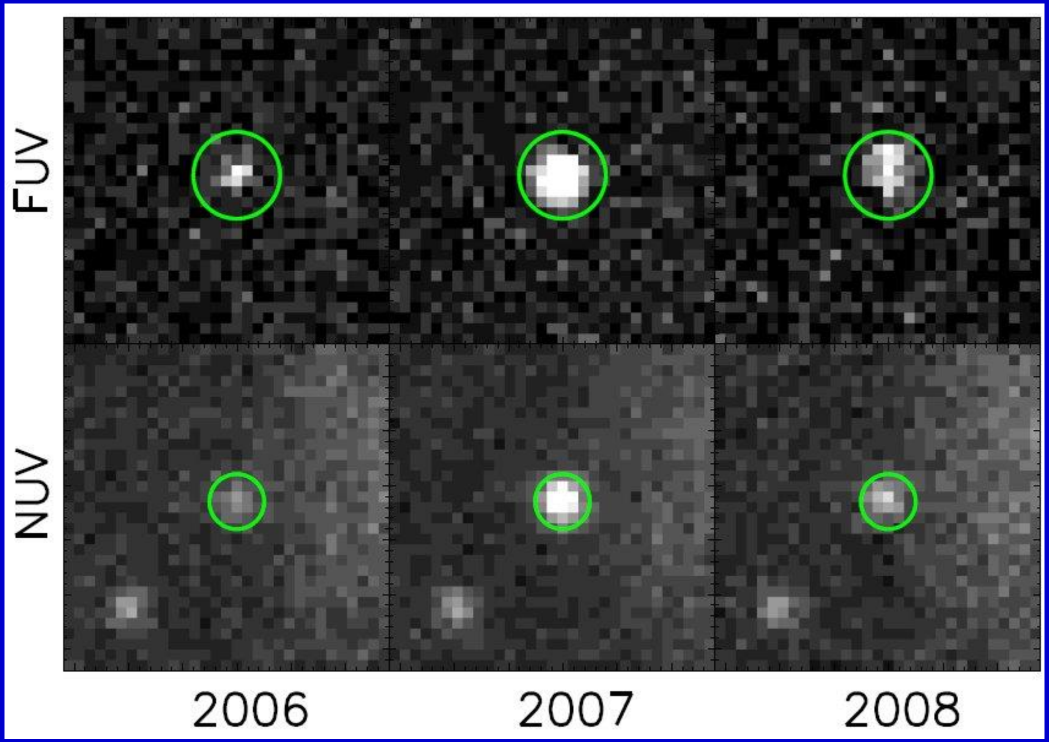

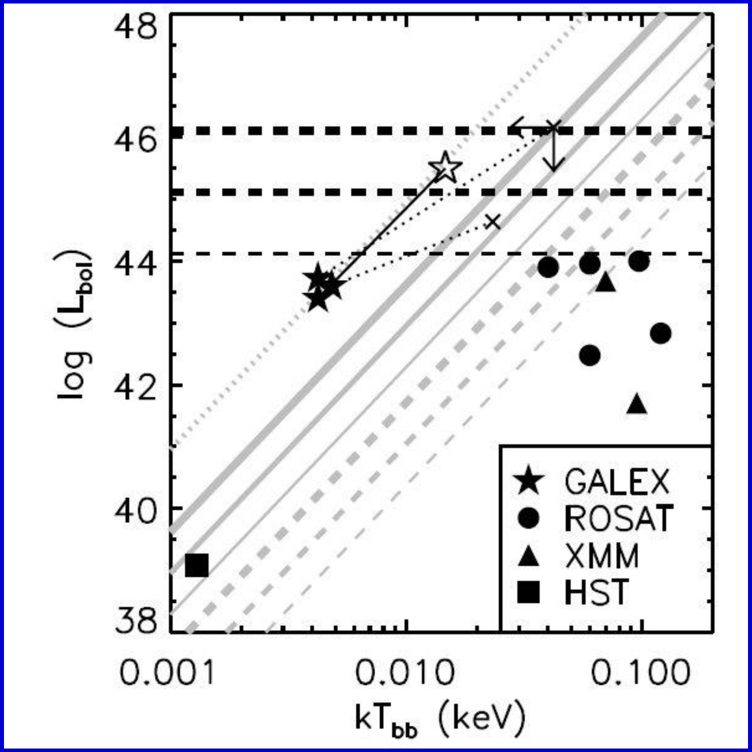

In optics one can observe events far from the horizon.
Surveys like Pan-STARRS
can discover 20-30 events per year.

arxiv:0904.1596

Two more examples of optical flares due to tidal disruption events

SDSS data

Atypical flares

Rate estimates:
~10^{-5} per year per galaxy
or slightly more

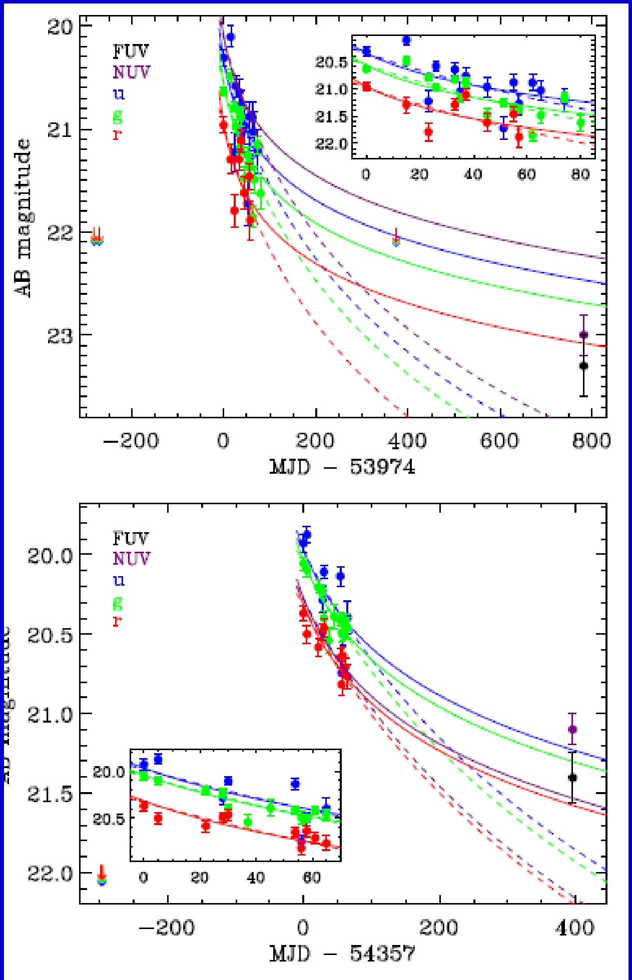

1009.1627

Dashed lines: -5/3
Solid lines: -5/9

The first radio discovery

CNSS J001947.3+00352
VLA search for transients
No X-rays detected

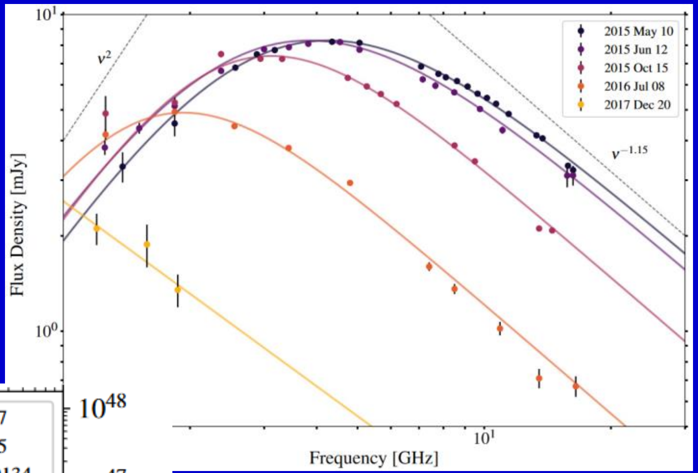

Spectral evolution

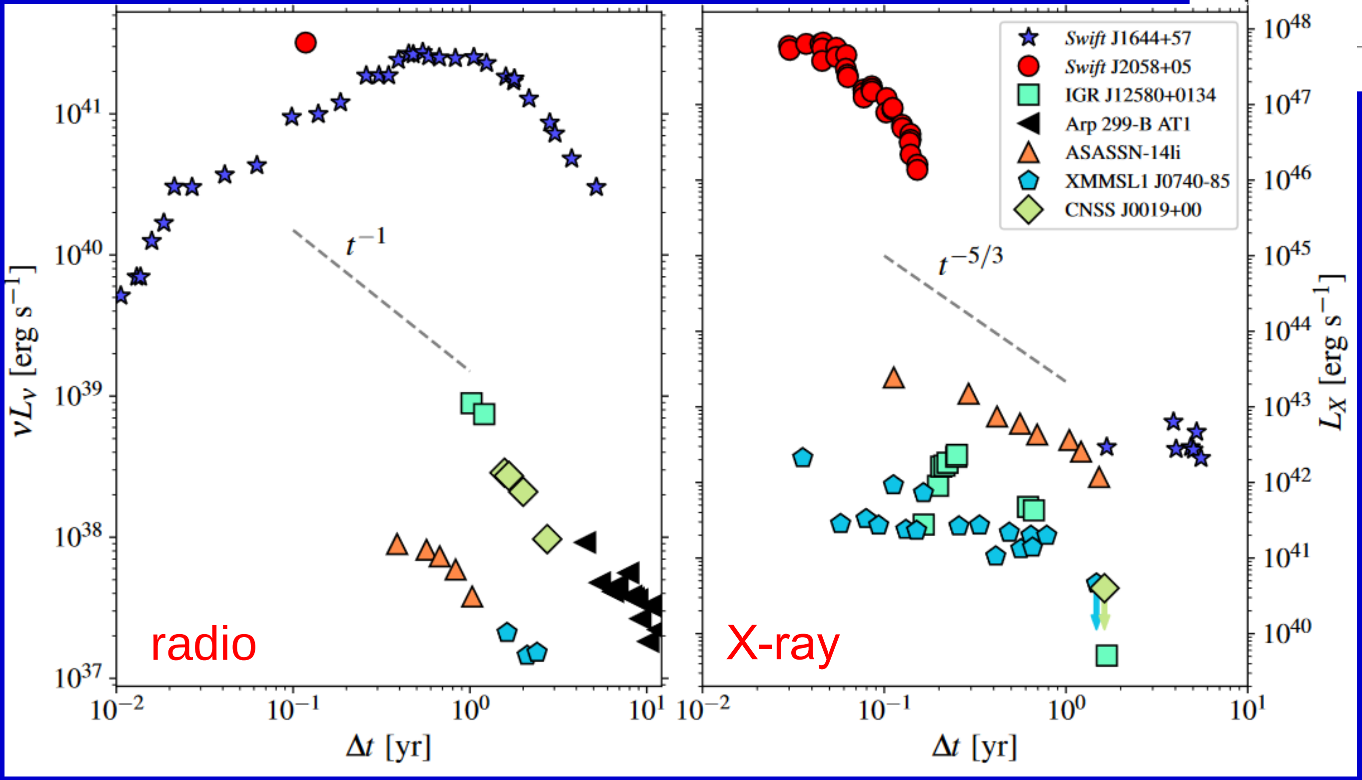

Comparison with all TDE with detected radio emission.

Age obtained by extrapolation of expansion.

Further observations are necessary to certify that this is indeed a TDE.

1910.11912

Theoretical models

- X-rays. 1105.2060
- Radio. 1104.4105

Flows of hot X-ray emitting gas have been identified after one of tidal disruption events. 1510.06348

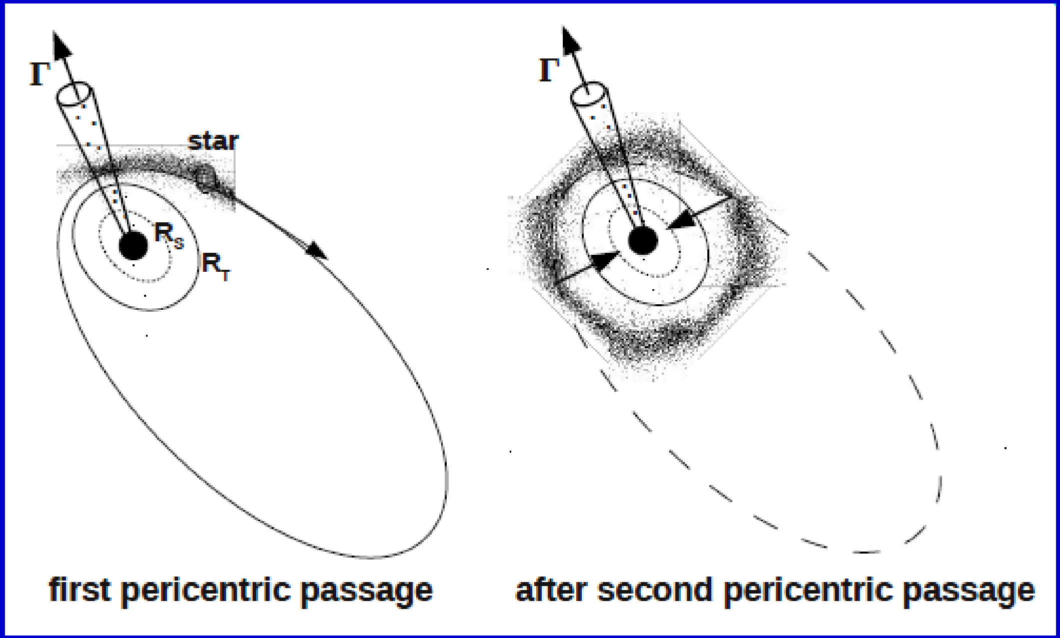

1104.2528

Stellar masses

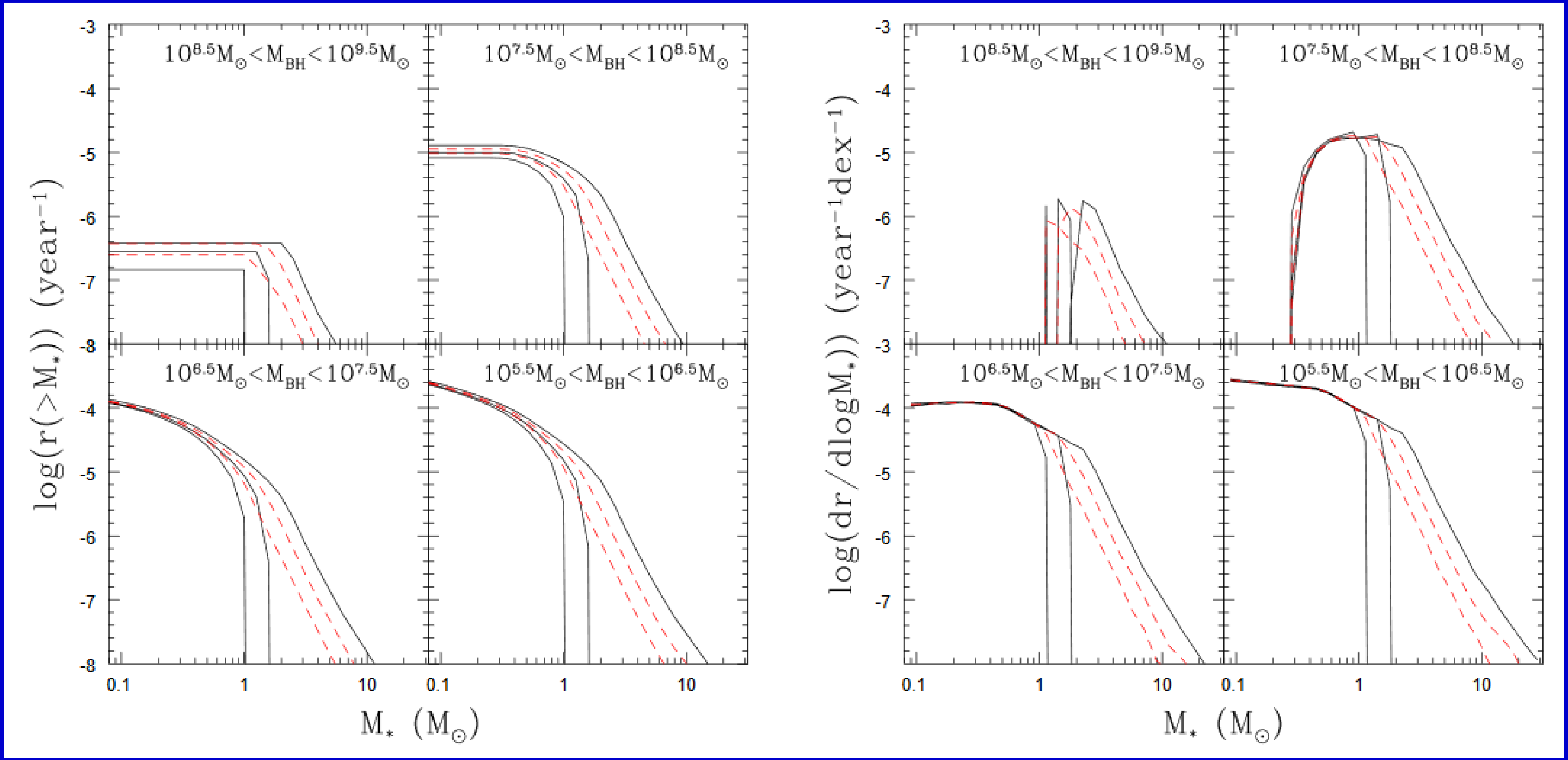

For not too massive BHs the main contribution is due to M-dwarfs (0.3Msolar).
For massive BHs contribution from massive and evolved stars grows.

1601.06787

Role of stellar spin

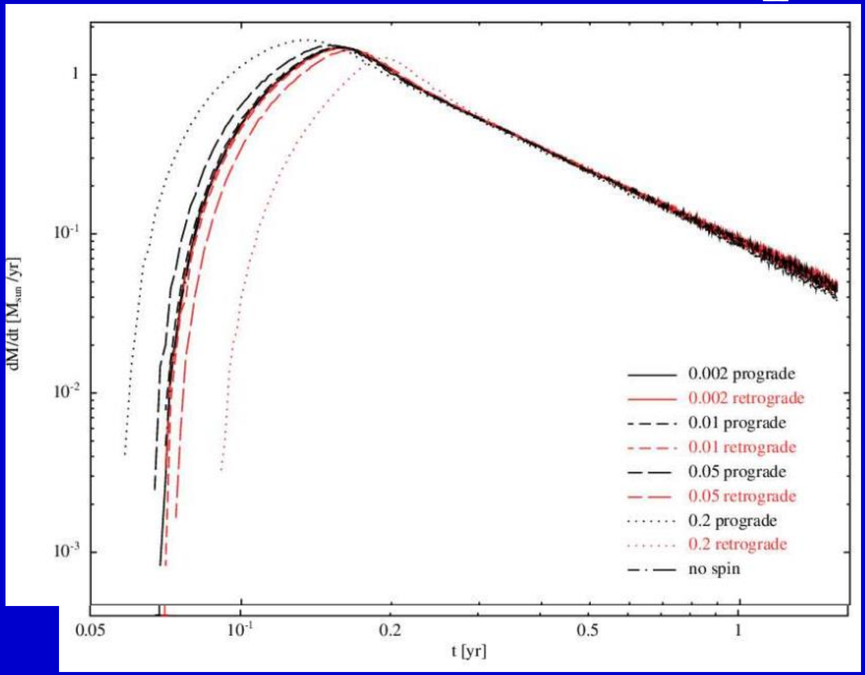

1901.03717

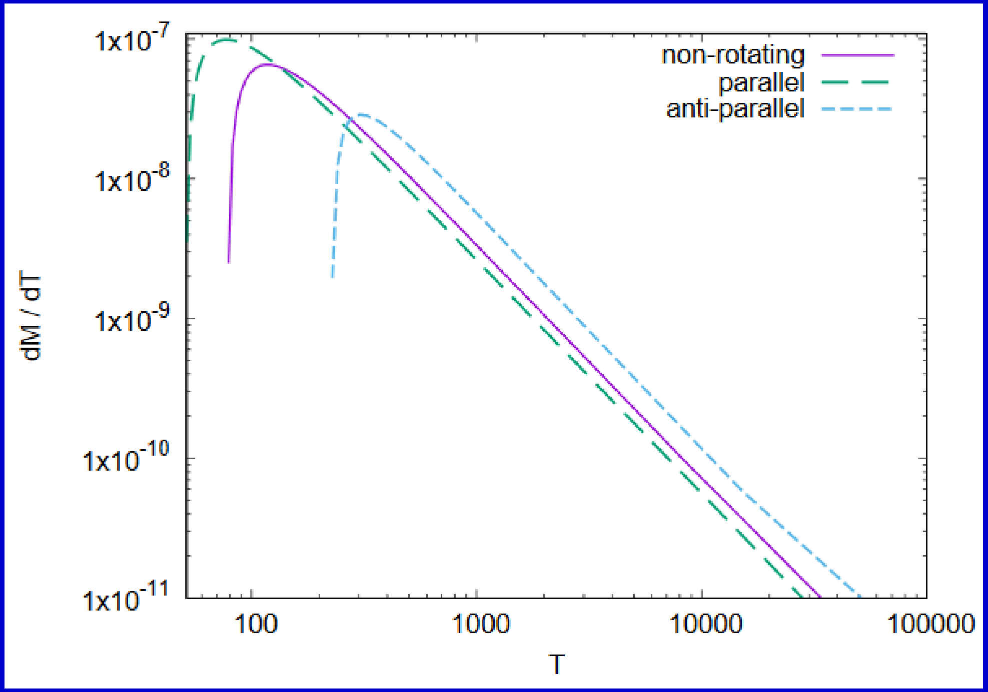

1901.05644

Role of BH spin

For deep encounters rotating BHs accretion rate and mass of the disc can be reduced.

$r_{\rm tid} \equiv r_\star (M/m_\star)^{1/3}$ $M = 10^6\ {\rm M}_\odot$ $m_\star = {\rm M}_\odot,\ r_\star = {\rm R}_\odot$

$\beta \equiv r_{\rm tid}/r_{\rm p}$ r_p - periapsis $e = 1$ $a^\star \equiv Jc/GM^2$

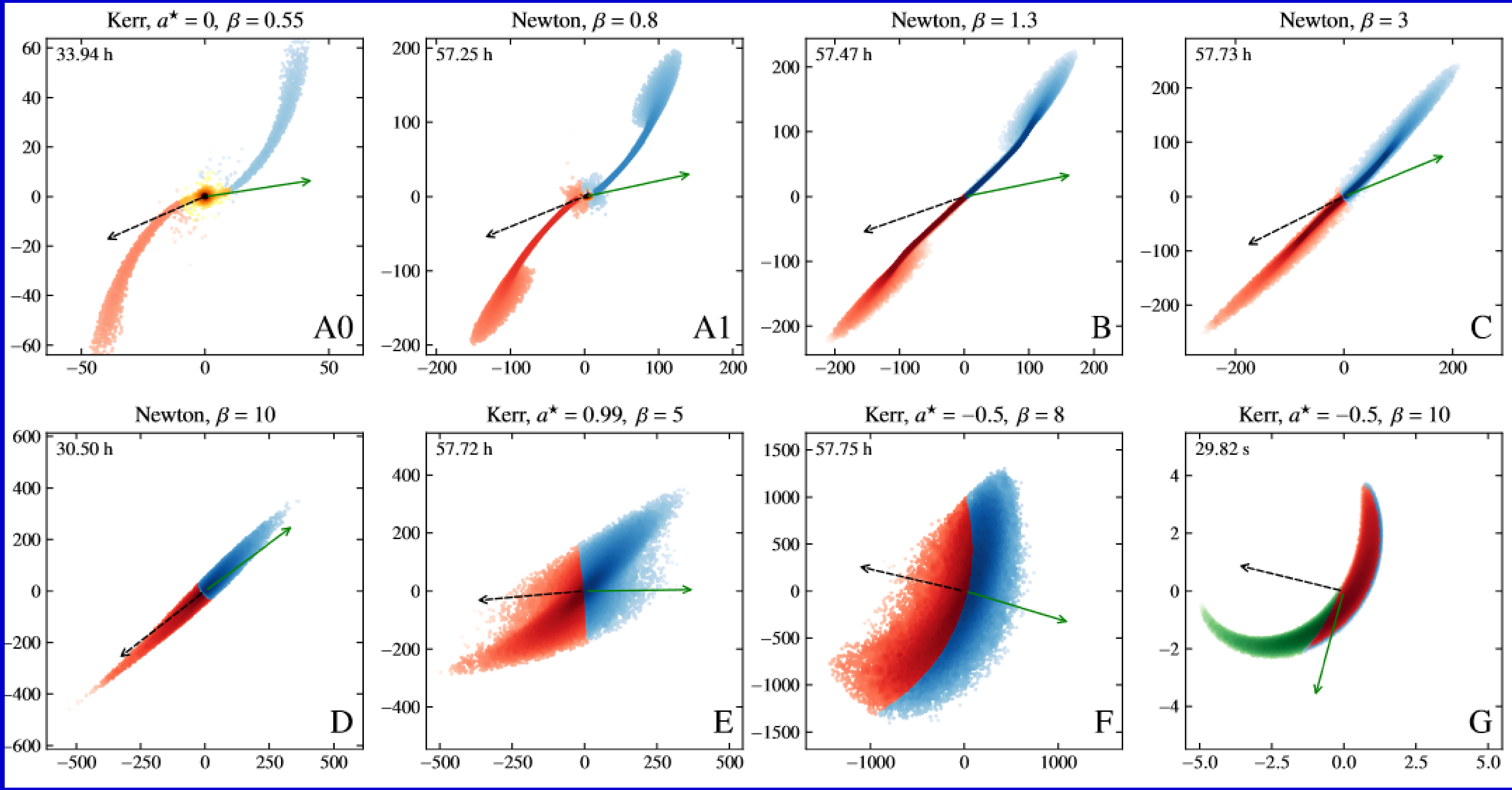

1903.09147

Detailed structure is important

The authors used MESA to model stellar structure before tidal disturbances.

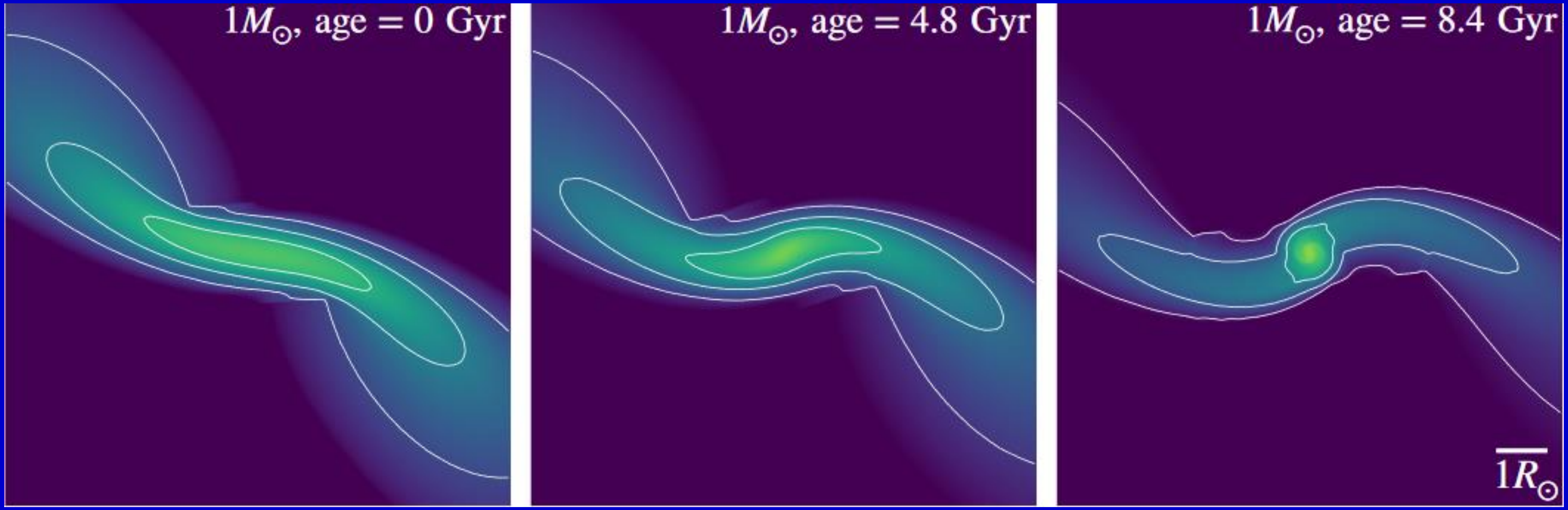

Interaction with a 1 000 000 solar mass BH.

1907.04859

….and again details and MESA

For realistic stellar structure the accretion rate is different from that for polytropic models.

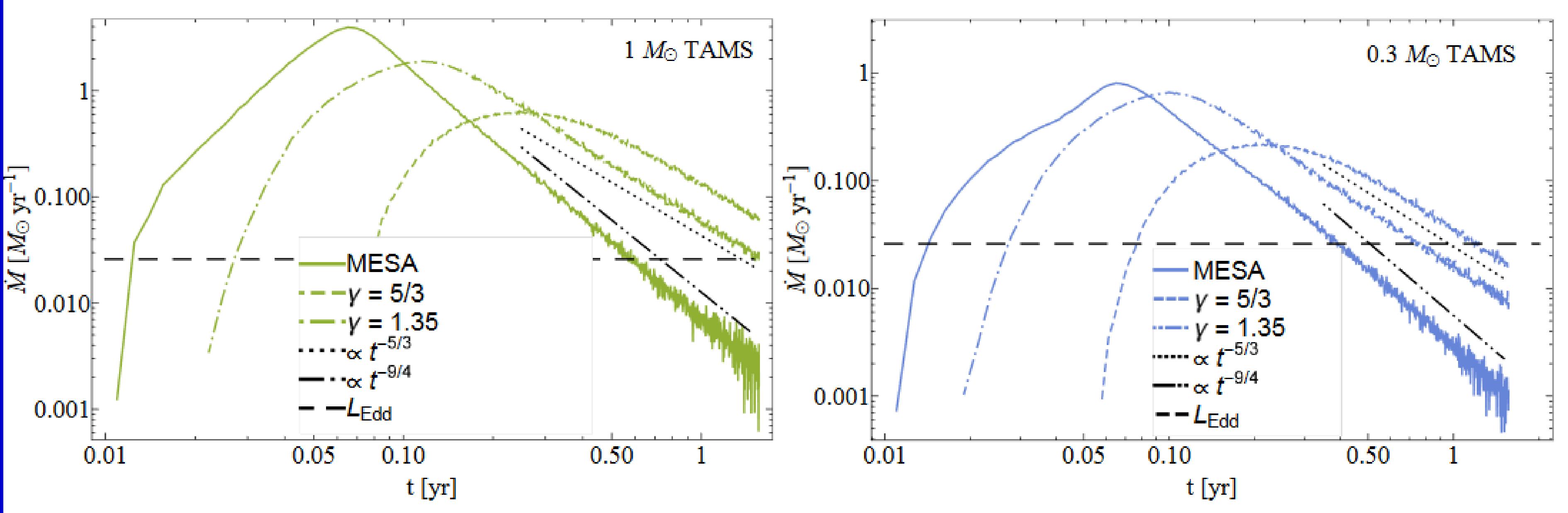

TAMS - terminal-age main sequence

1907.05895

TDE and binary SMBHs

It has been predicted that after a TDE in a system of close SMBH binary there might be particular drops in the light curve. Such phenomena was observed.

SDSS J120136.02+300305.5
XMM-Newton observations

Masses ~10^7 and 10^6 solar masses,
orbital separation ~10^{-3} pc
Eccentricity ~0.3

TDEs in supermassive BH binaries were recently modeled in 1802.07850.

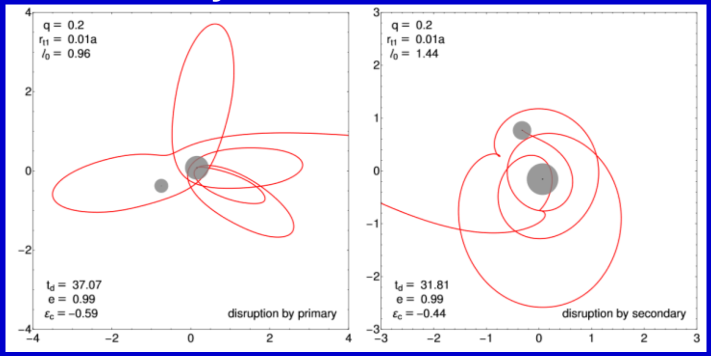

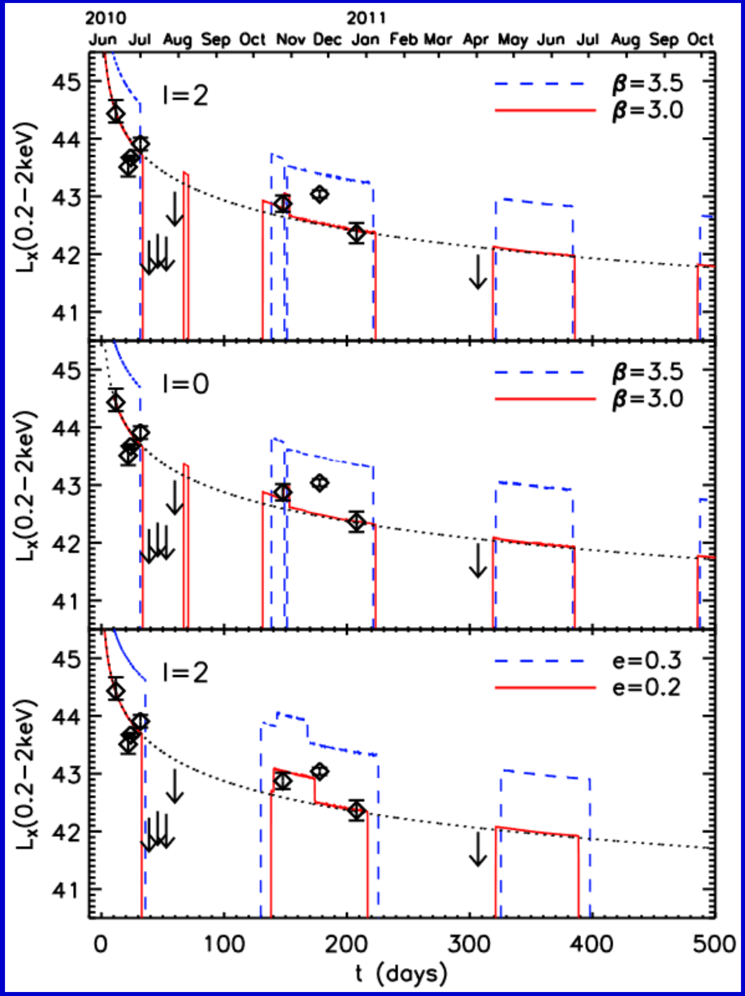

1404.4933

See a review on binary SMBHs and TDEs in 1909.12849

How binarity influences TDE

- Lidov-Kozai influence on the star
- Dynamical influence on the debris

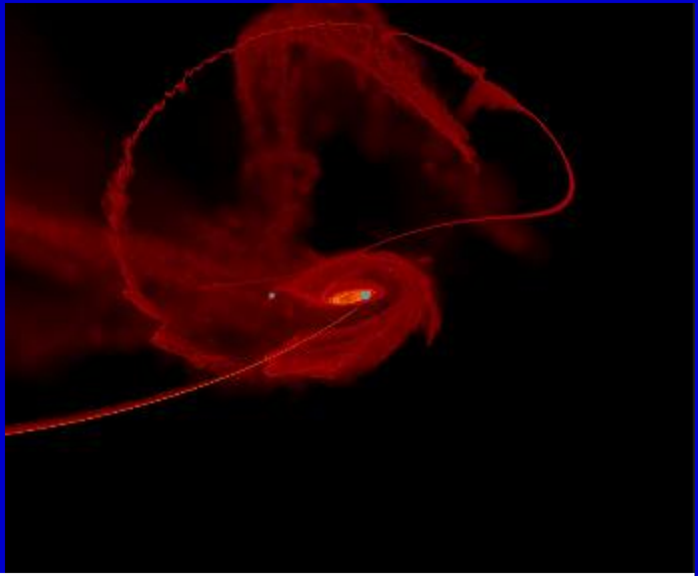

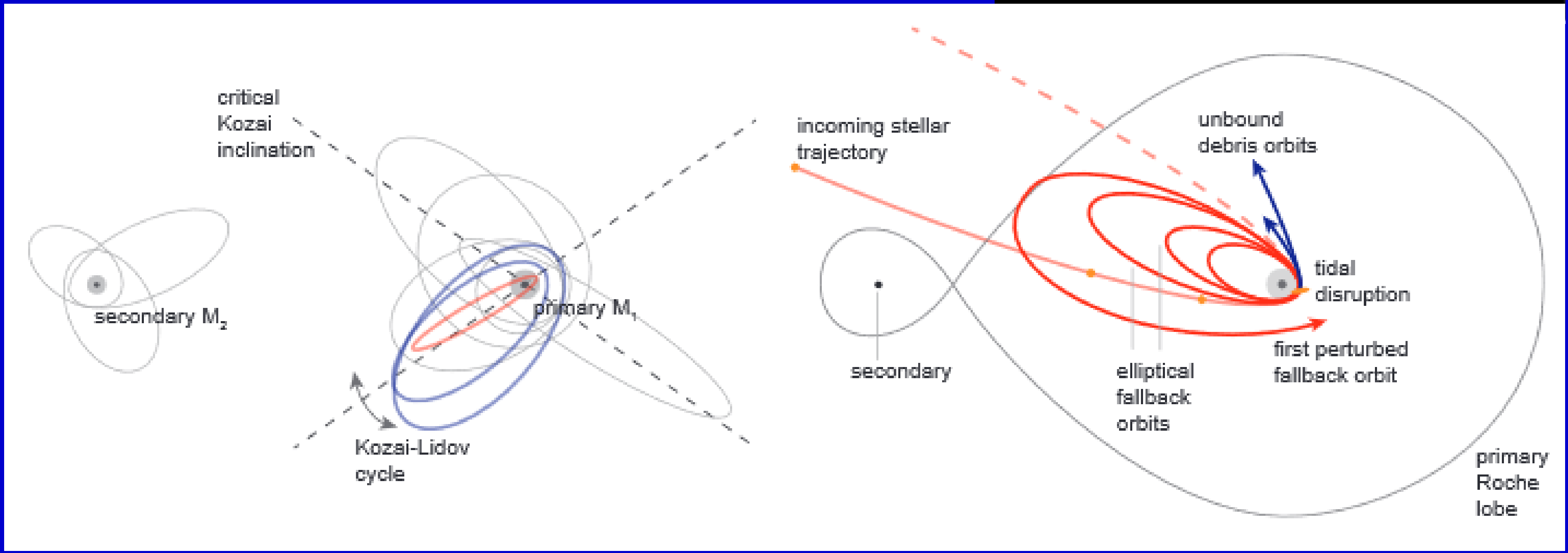

1909.12849

Mass determination from TDE

12 optically/UV selected TDE host galaxies

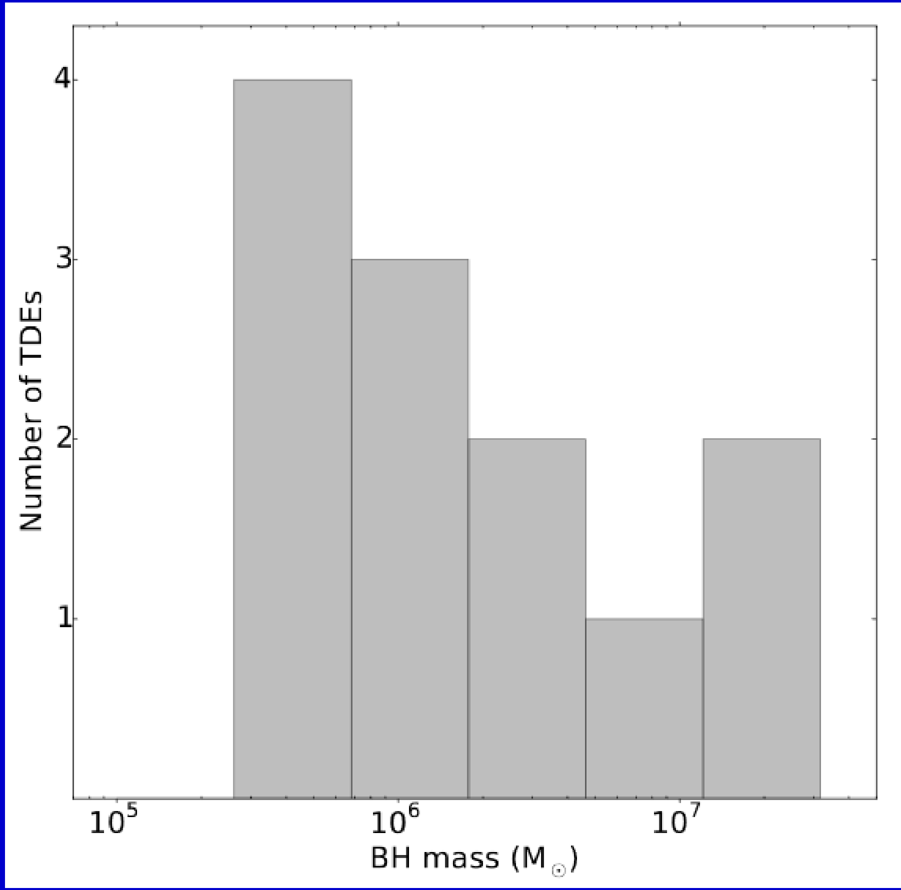

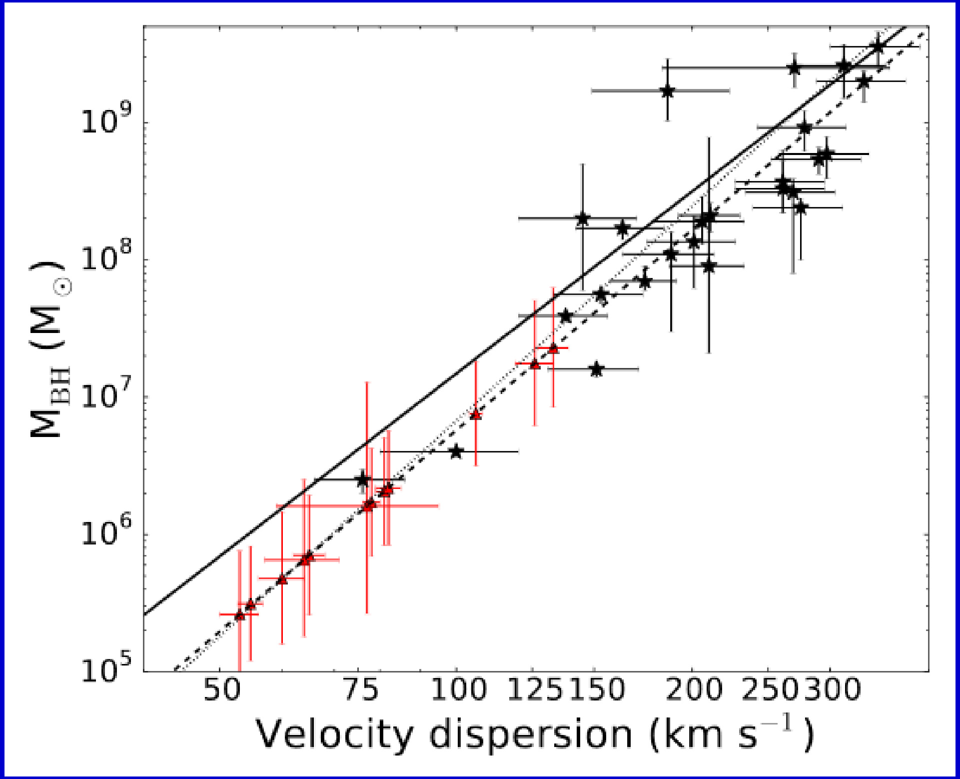

Red- new data, lines – best fits, black – Ferrarese, Ford (2005).

1706.08965

Squeezars

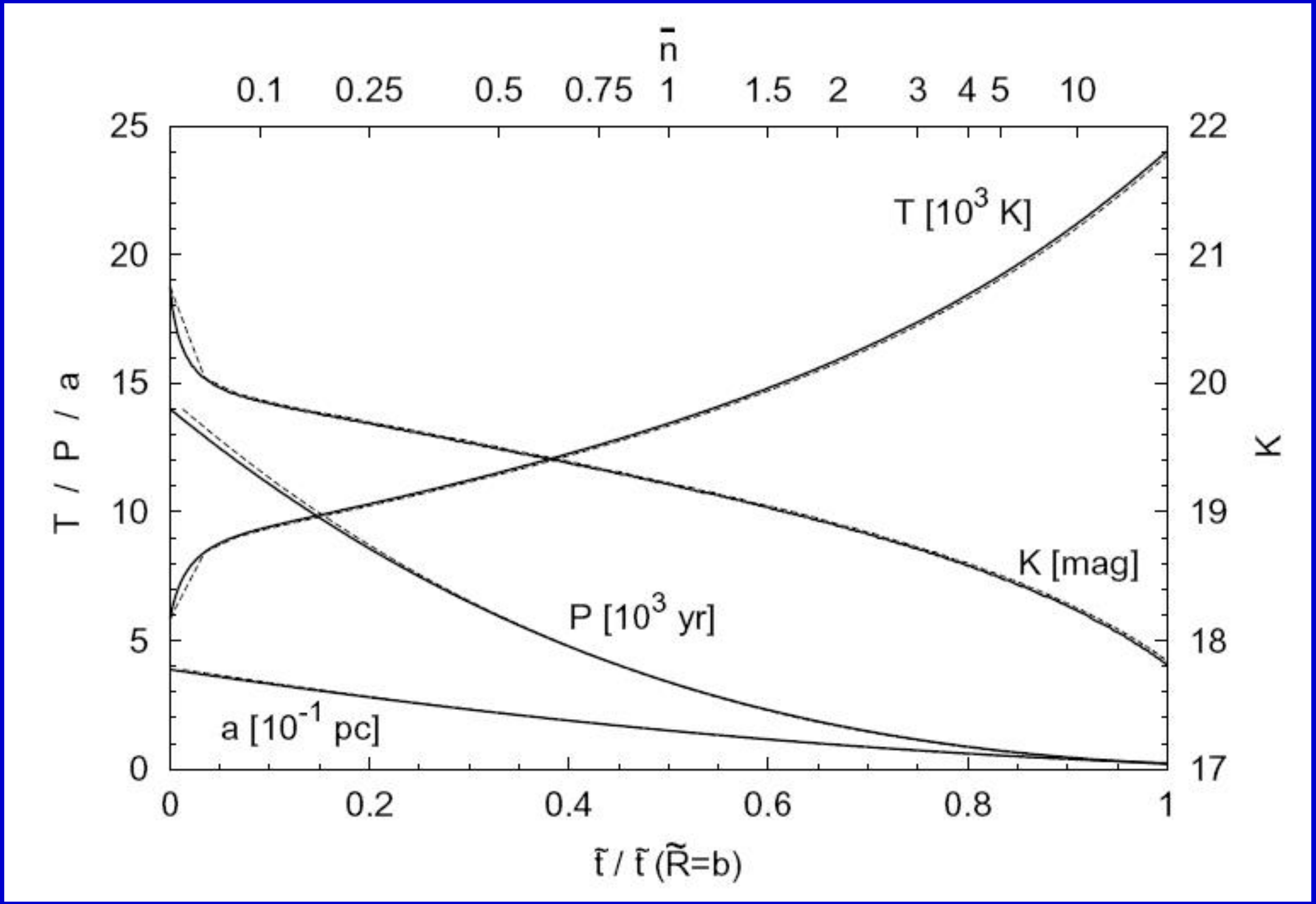

The rate of formation is lower than the rate of tidal disruption events, but the observable time is longer.

Graphs are plotted for a solar-type star orbiting the BH in the center of our Galaxy.

astro-ph/0305061

Структура диска вокруг сверхмассивной черной дыры

Наблюдение микролинзирования позволяет выявлять структуру аккреционного диска. Кроме этого, наблюдалась линзированная линия железа. Удалось «увидеть» корону диска.

1204.4480

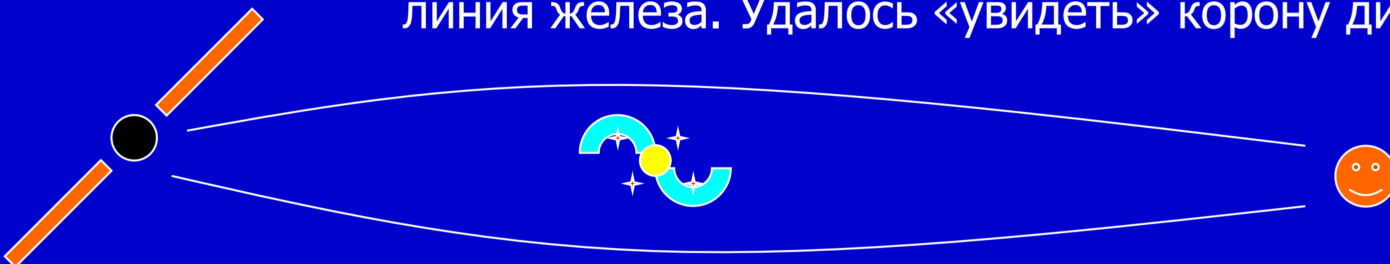

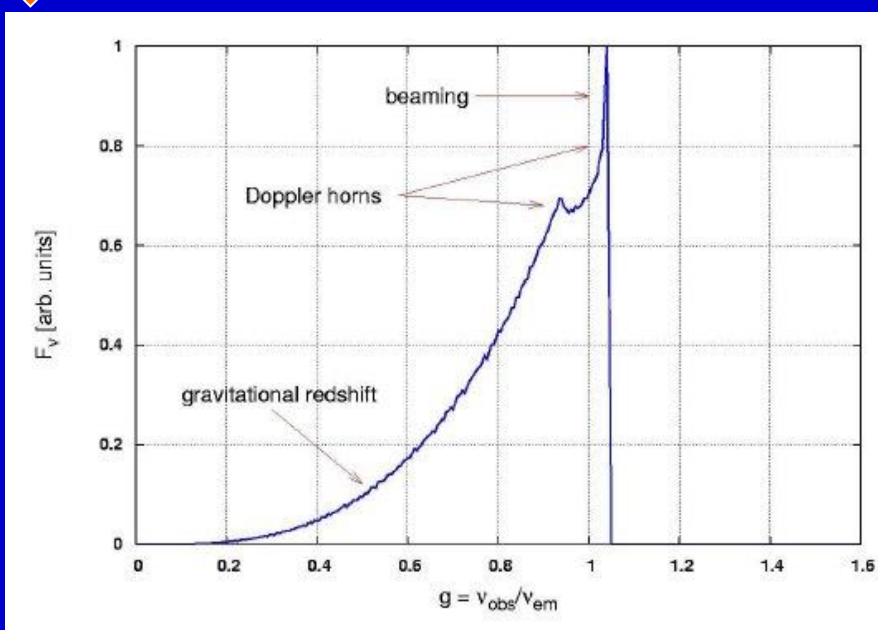

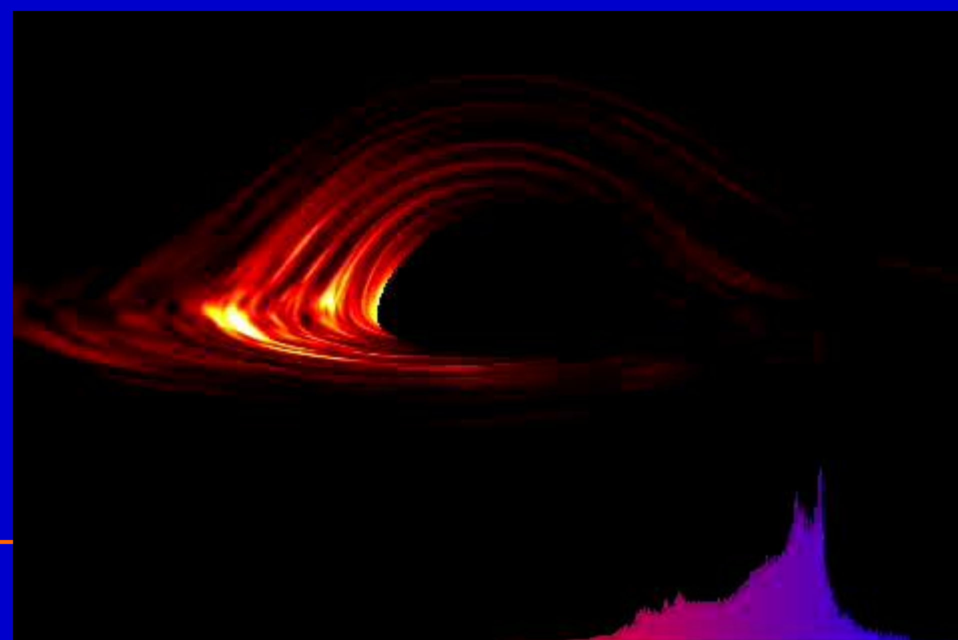

Disc structure from microlensing

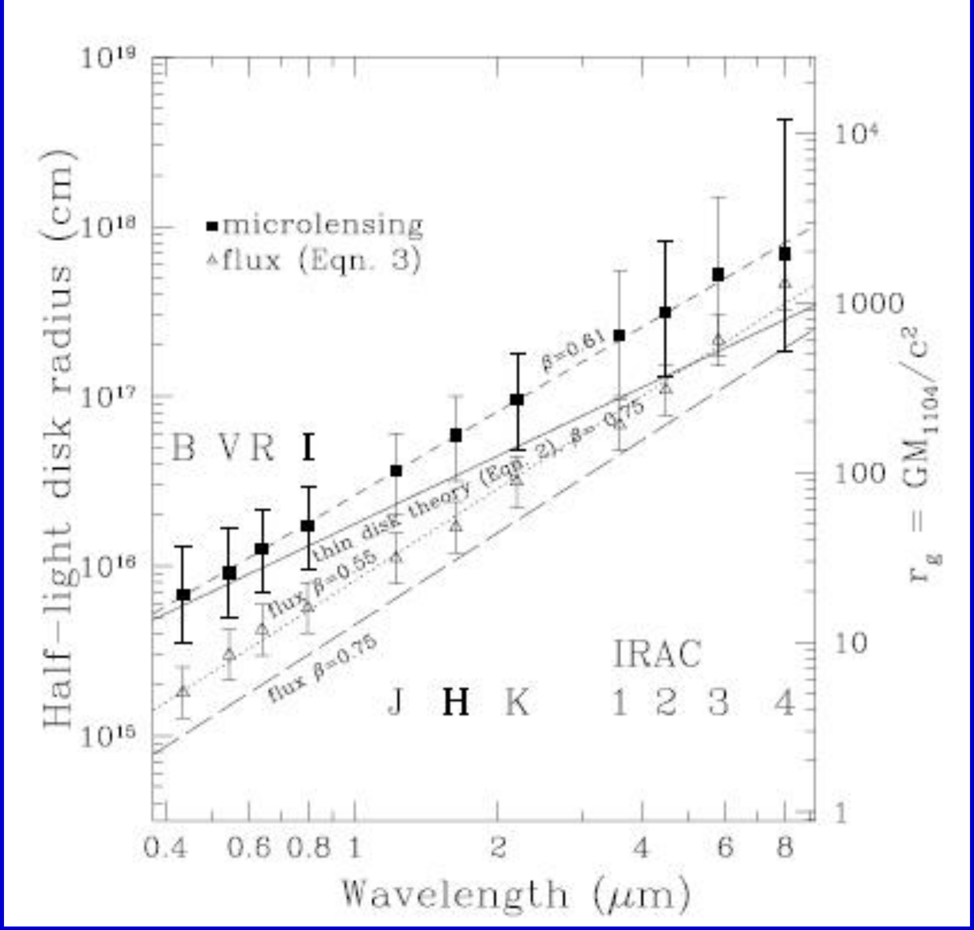

Using the data on microlensing at wavelengths 0.4-8 microns it was possible to derive the size of the disc in the quasar HE1104-1805 at different wavelengths.

arXiv:0707.0003 Shawn Poindexter et al.
«The Spatial Structure of An Accretion Disk»

Disc size – BH mass

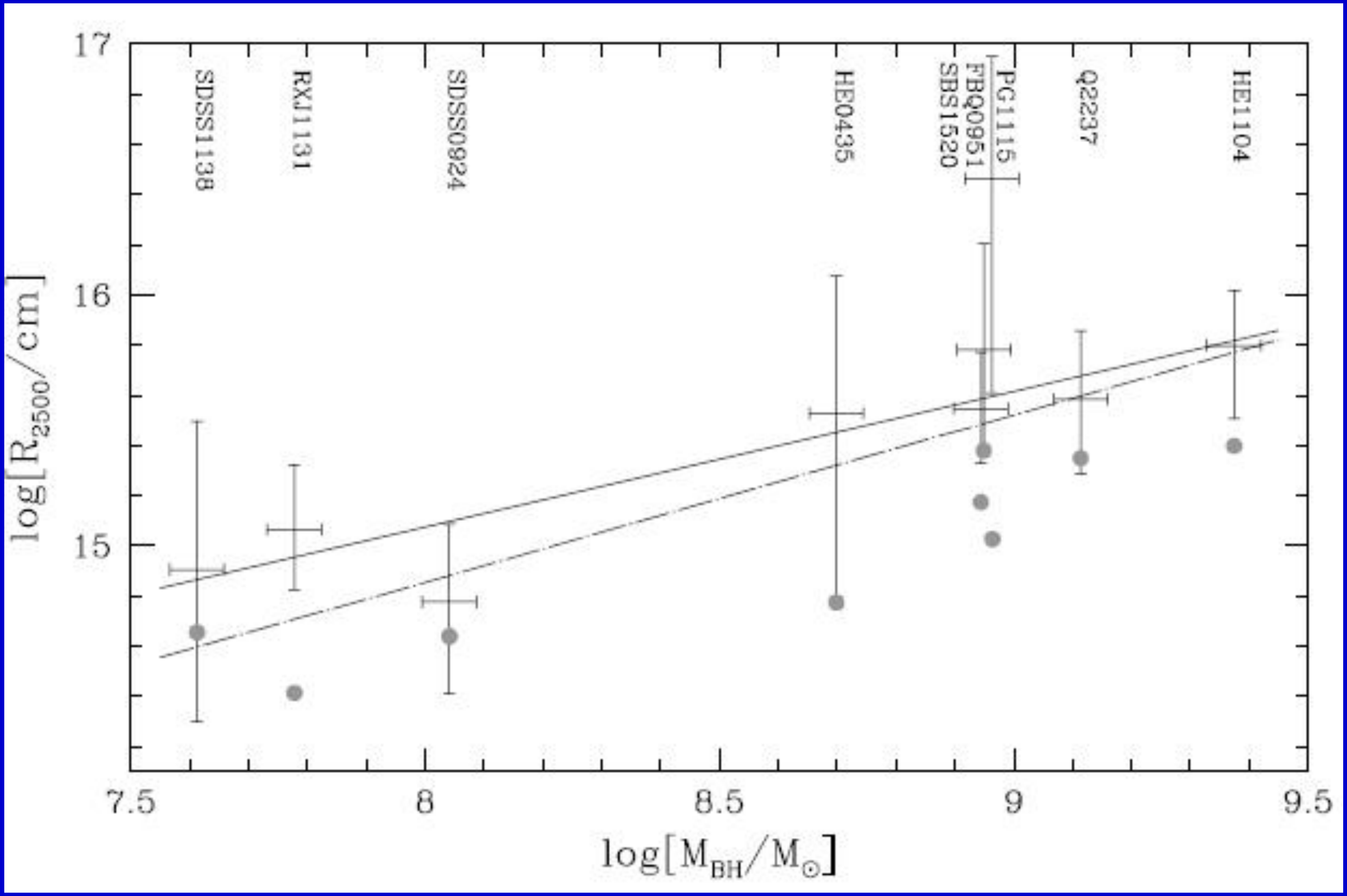

Disc size can be determined from microlensing.

arXiv:0707.0305 Christopher W. Morgan et al.
«The Quasar Accretion Disk Size - Black Hole Mass Relation»

More data

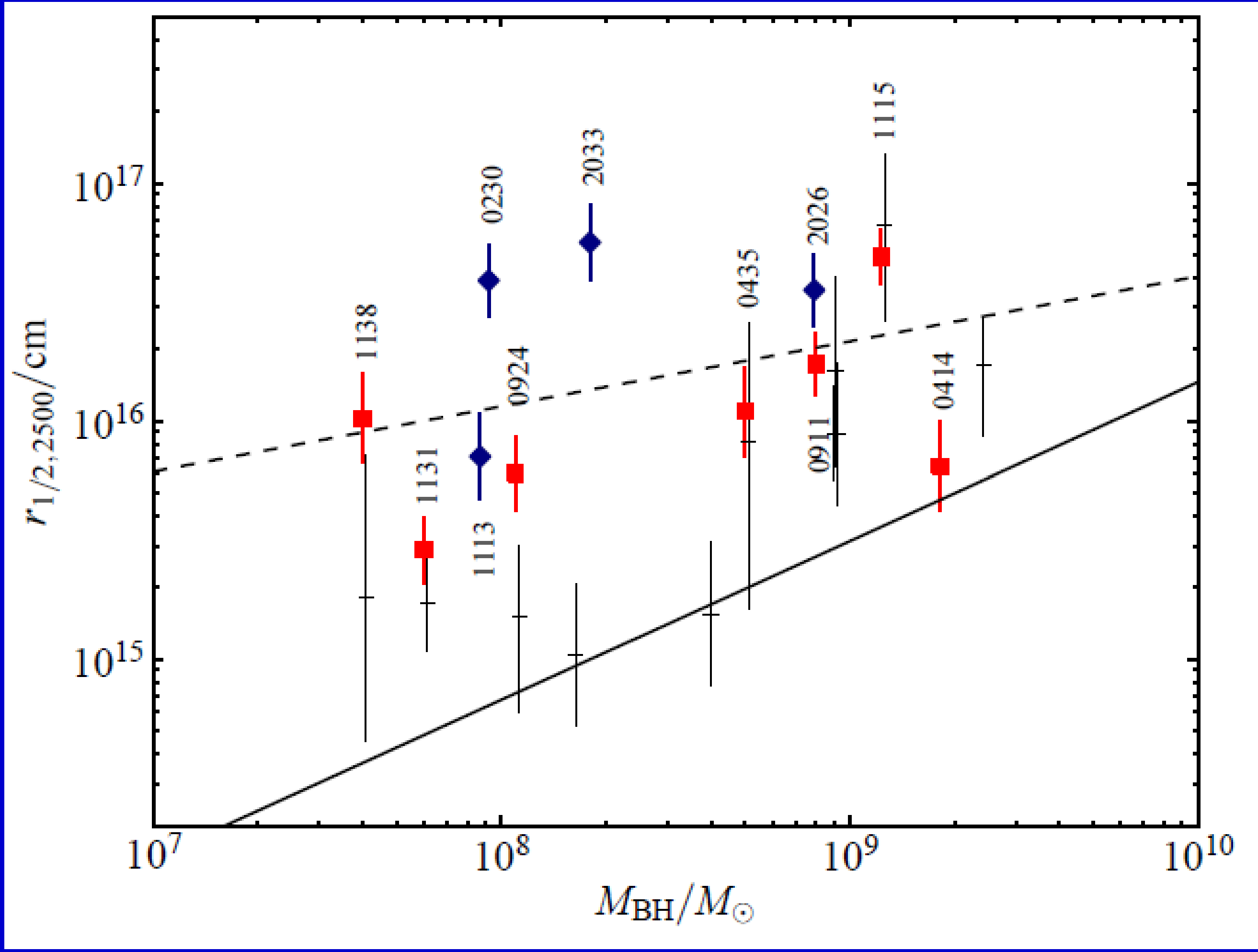

IR and optics.

Chromatic microlensing:
blue light from
the inner regions
is more strongly
microlensed than
red light from farther out

Solid line is
the prediction
of the thin disk model.

1007.1665

Standard disc properties

$$T_{\rm eff}(r) = \left(\frac{3G^2M_{\rm BH}^2 m_p f_{\rm Edd}}{2c\sigma_B\sigma_T\eta r^3}\right)^{1/4} g(r_{\rm in}/r)^{1/4}.$$

Standard disc model

$$r_{1/2} = 2.44\left[\frac{45G^2M_{\rm BH}^2 m_p f_{\rm Edd}\lambda^4}{4\pi^5 h_P c^3\sigma_T\eta}\right]^{1/3}\sqrt{\cos i}$$
$$= 1.68\times10^{16}{\rm cm}\left(\frac{M_{\rm BH}}{10^9M_\odot}\right)^{2/3}\left(\frac{f_{\rm Edd}}{\eta}\right)^{1/3}\left(\frac{\lambda}{\mu{\rm m}}\right)^{4/3}$$

$r_{1/2} \sim \lambda^{4/3}$

1007.1665

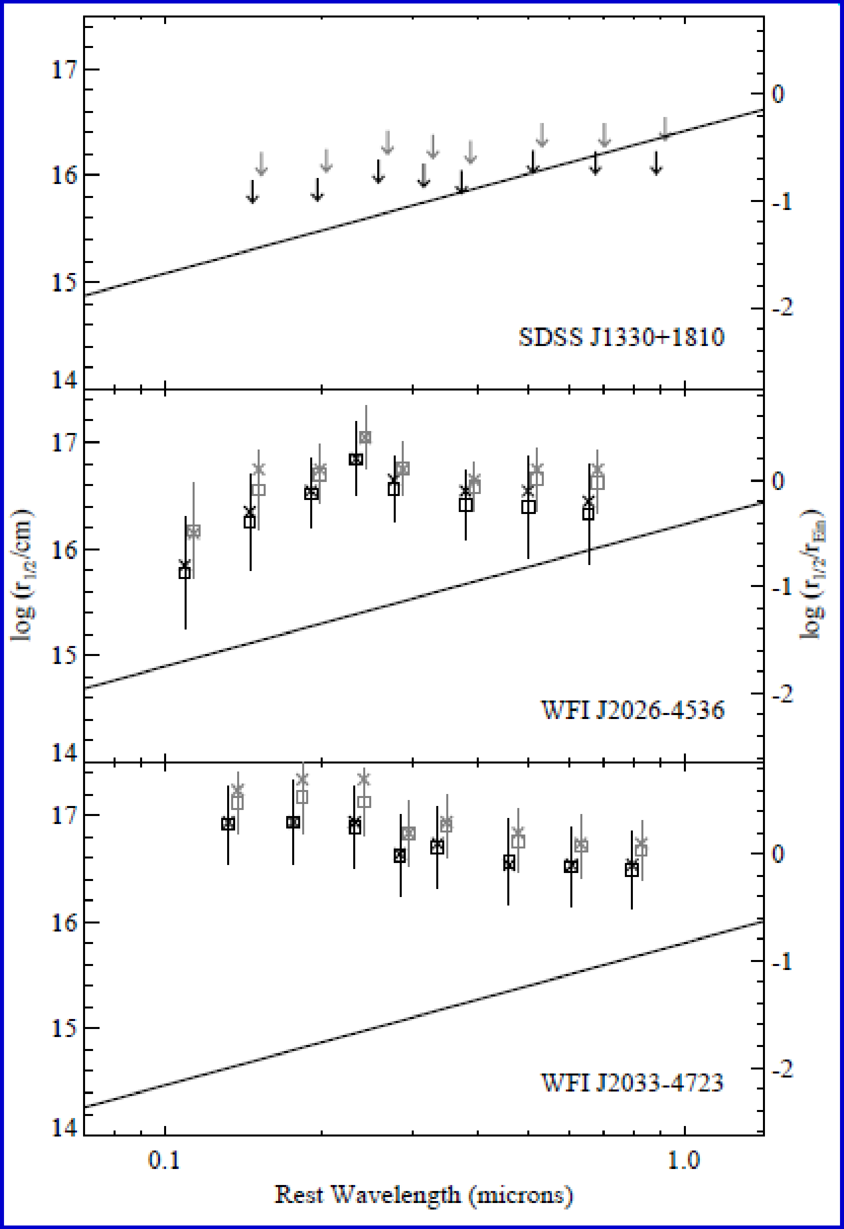

SDSS J1330+1810
WFI J2026-4536
WFI J2033-4723
log (r_{1/2}/cm)
log (r_{1/2}/r_{Ein})
Rest Wavelength (microns)
0.1
1.0

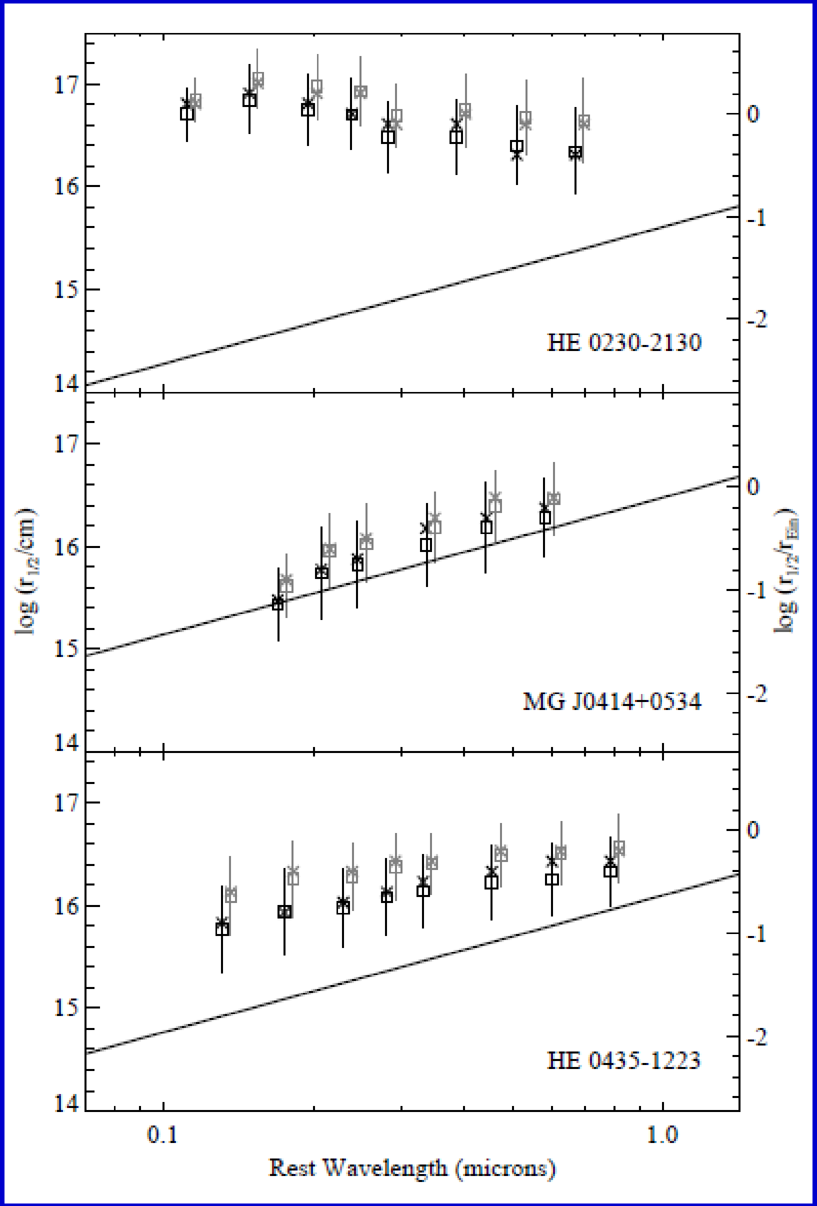

HE 0230-2130
MG J0414+0534
HE 0435-1223
log (r_{1/2}/cm)
log (r_{1/2}/r_{Ein})
Rest Wavelength (microns)
0.1
1.0

1007.1665

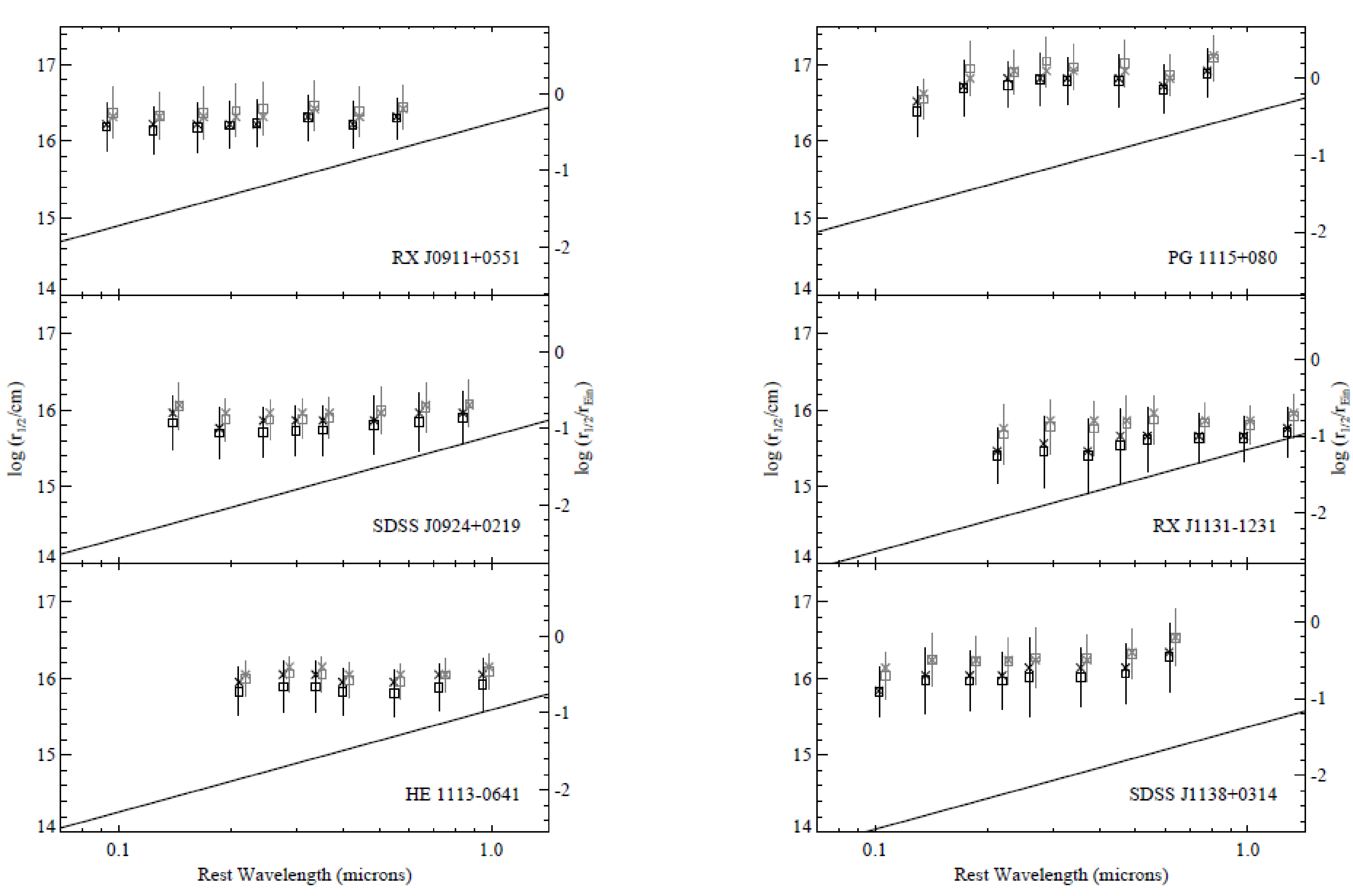
RX J0911+0551
PG 1115+080
SDSS J0924+0219
RX J1131-1231
HE 1113-0641
SDSS J1138+0314
log ($r_{1/2}$/cm)
log ($r_{1/2}/r_{Ein}$)
Rest Wavelength (microns)
0.1
1.0

1007.1665

Super-Eddington discs

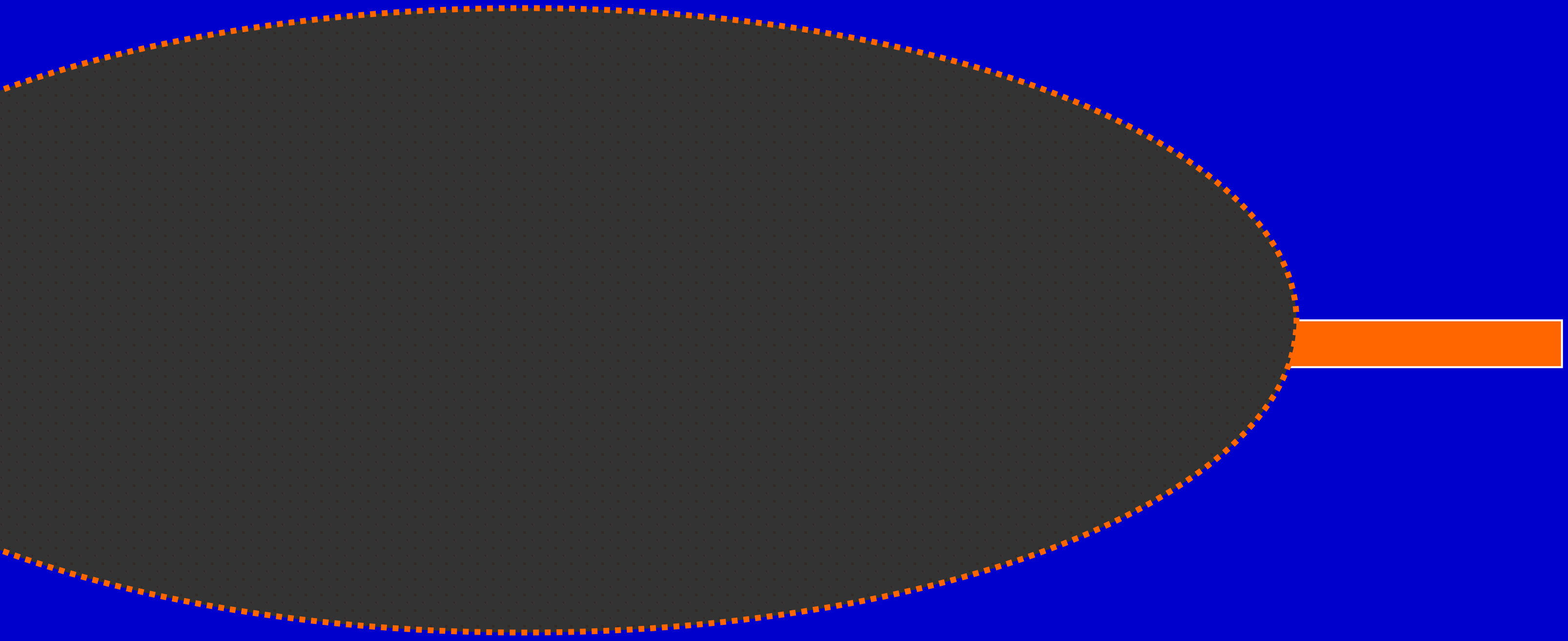

Super-Eddington accretion leads to formation of an optically-thick envelope scattering the radiation formed in the disc.
This makes the apparent disc size larger and practically independent of wavelength

1208.1678

Disc reverberation mapping

super-Eddington AGN
Mrk 142 (PG1022+519)
z= 0.045

Accretion disk RM uses time lags between the continuum at different wavelengths to probe the size and temperature of the accretion disk.

High energy photons from a central corona irradiate the accretion disk, driving variability at longer wavelengths.
The hotter, inner disk will respond to variability in the irradiating photons before the cooler, outer disk.
This then leads to correlated continuum light curves with longer wavelengths lagging shorter wavelengths.

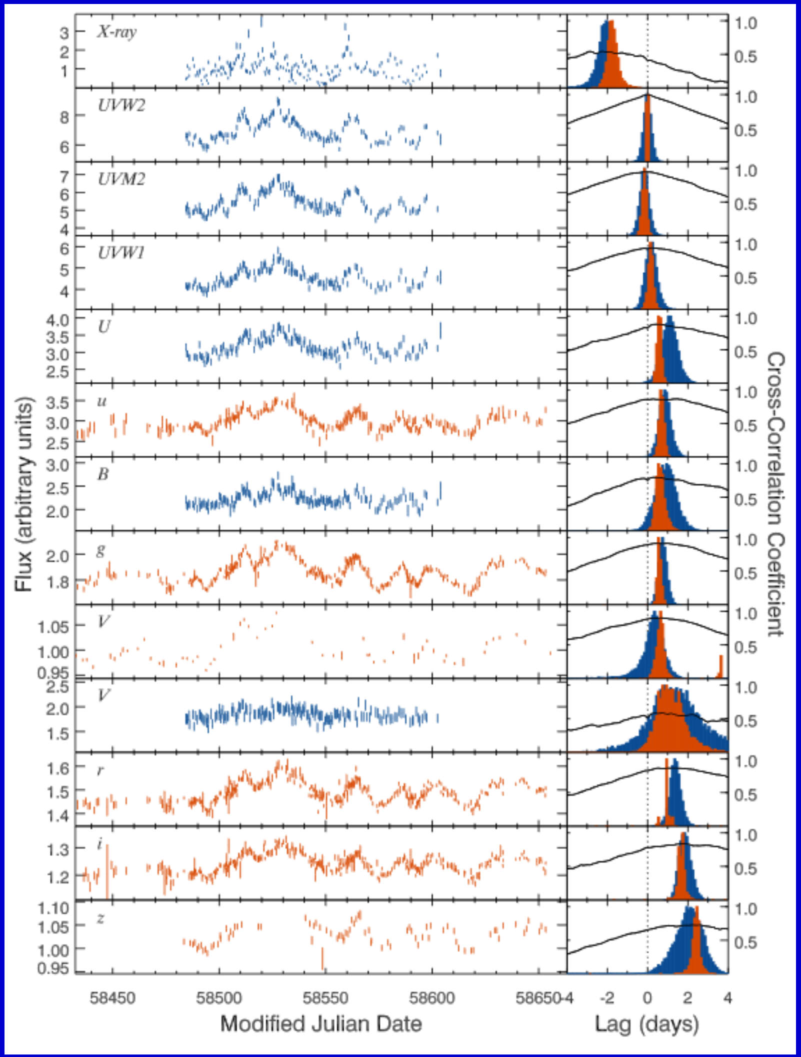

2005.03685

Right: correlation with UVW2

Discs observed by VLTI

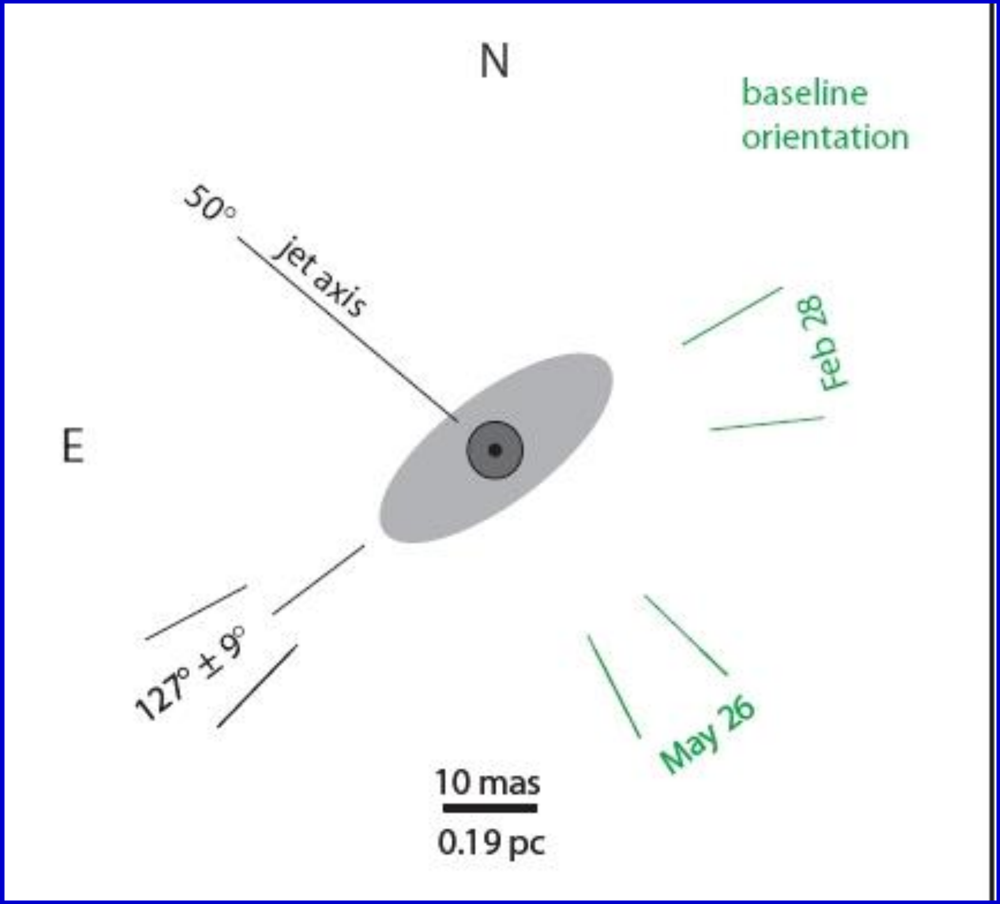

The structure of the disc in Cen A was studied in IR for scales <1 pc.

The data is consistent with a geometrically thin disc with diameter 0.6 pc.

Observations on VLTI.

arXiv:0707.0177 K. Meisenheimer et al.
«Resolving the innermost parsec of Centaurus A at mid-infrared wavelengths»

Discs around black holes: a look from aside

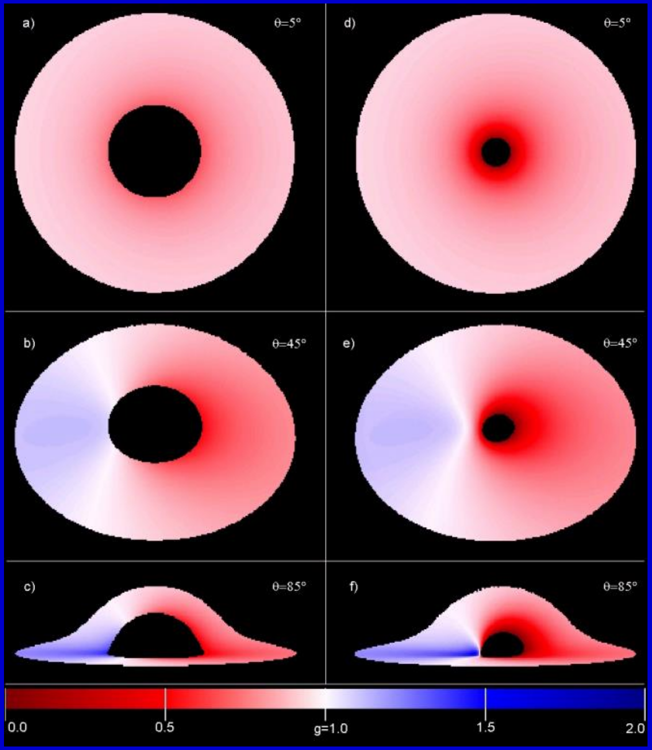

Discs observed from infinity.
Left: non-rotating BH,
Right: rotating.

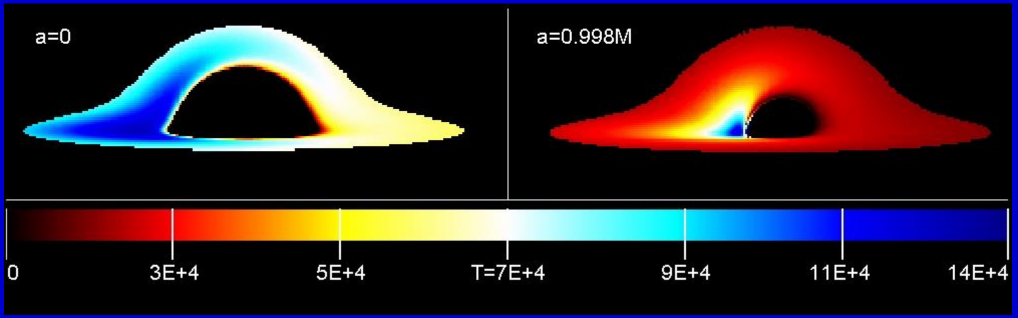

Disc temperature

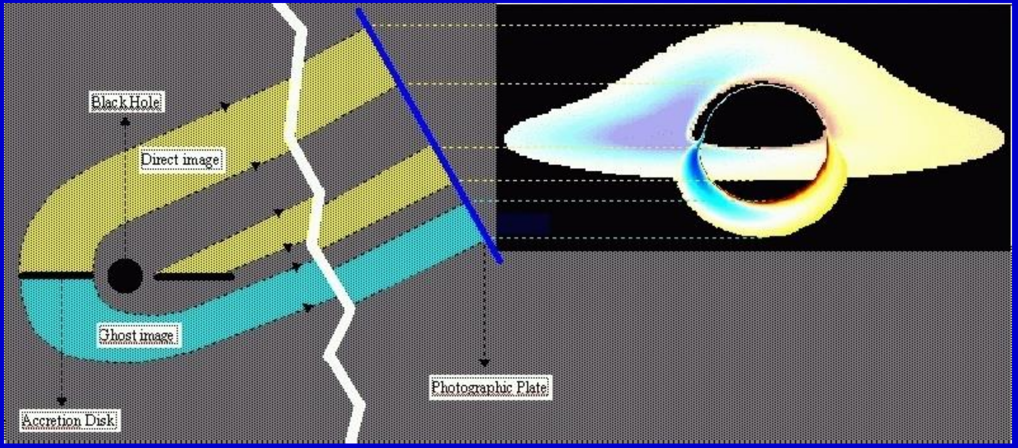

http://web.pd.astro.it/calvani/

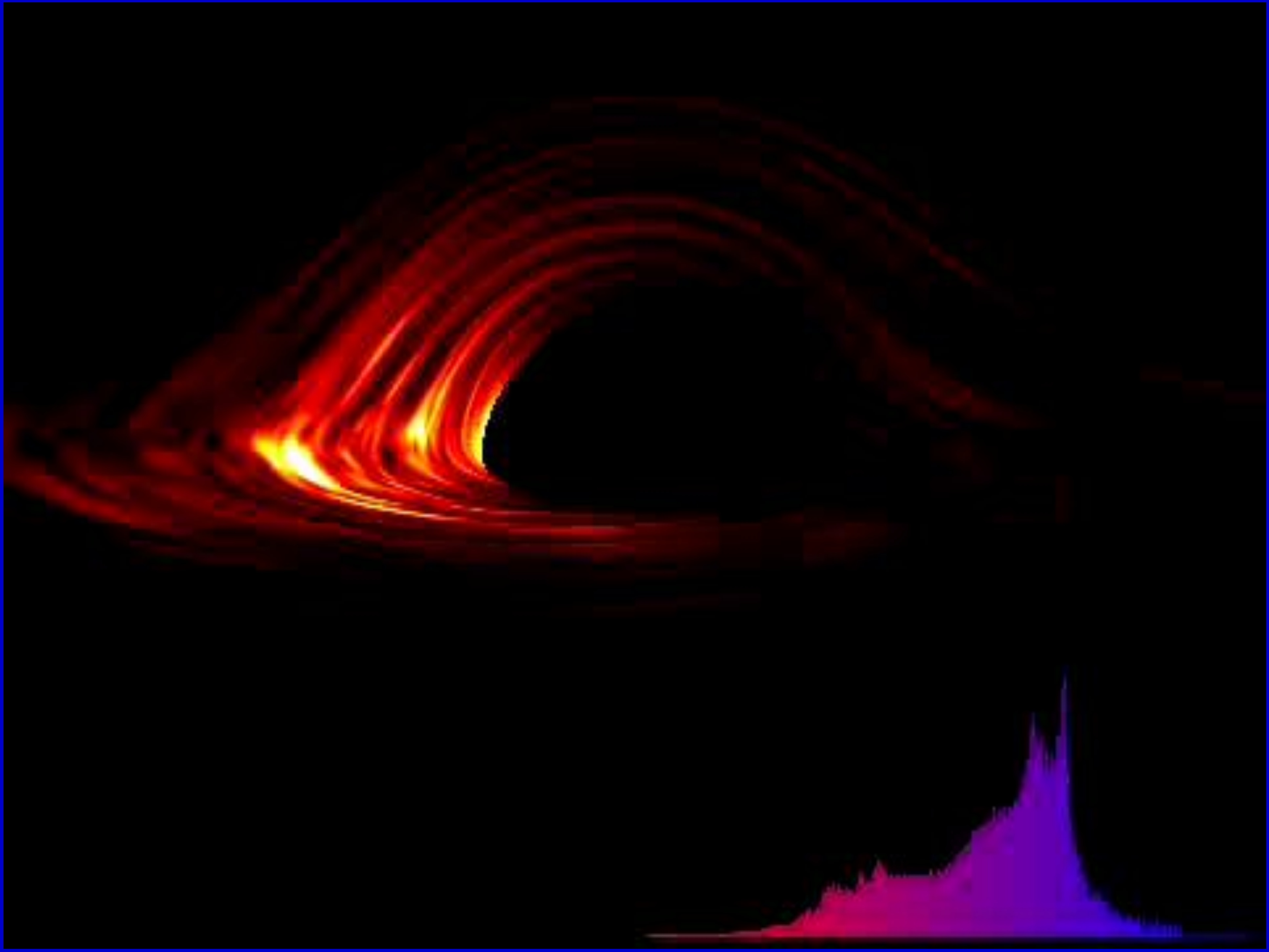

from gr-qc/0506078

Discs from Interstellar movie

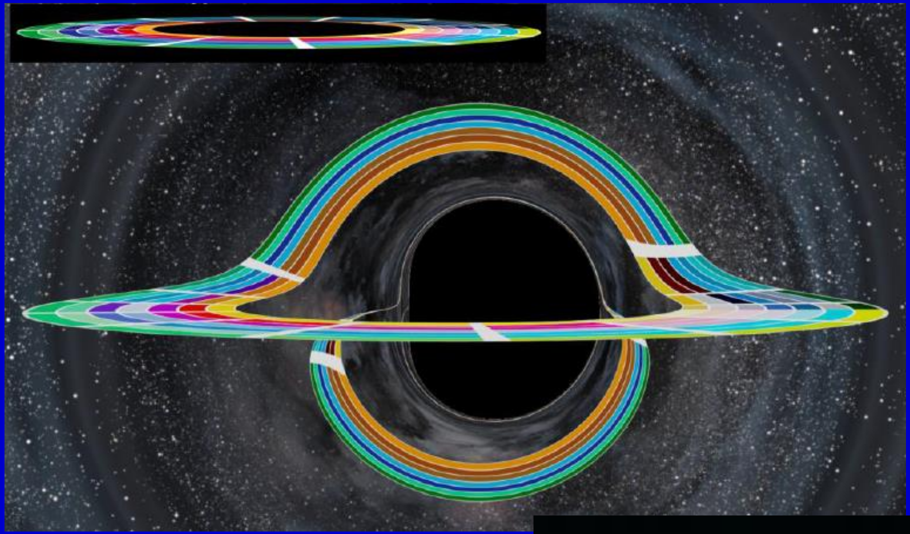

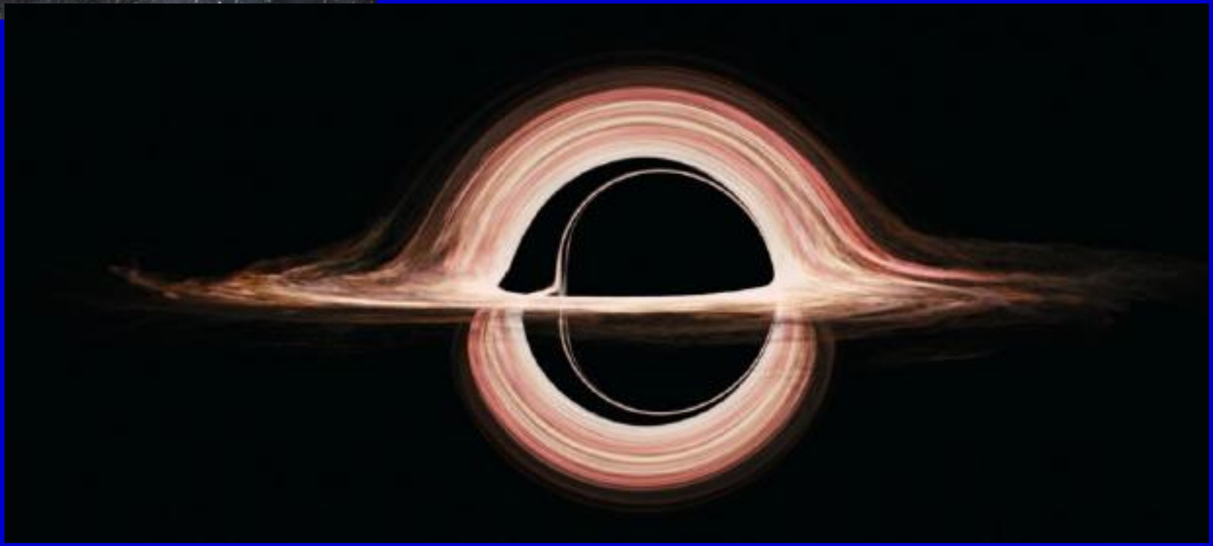

1502.03808

Different effects

$$r_+ = \frac{GM}{c^2} + \left[\left(\frac{GM}{c^2}\right)^2 - \left(\frac{J}{Mc}\right)^2\right]^{\frac{1}{2}}$$

For maximal rotation $r_{ISCO}=r_+$

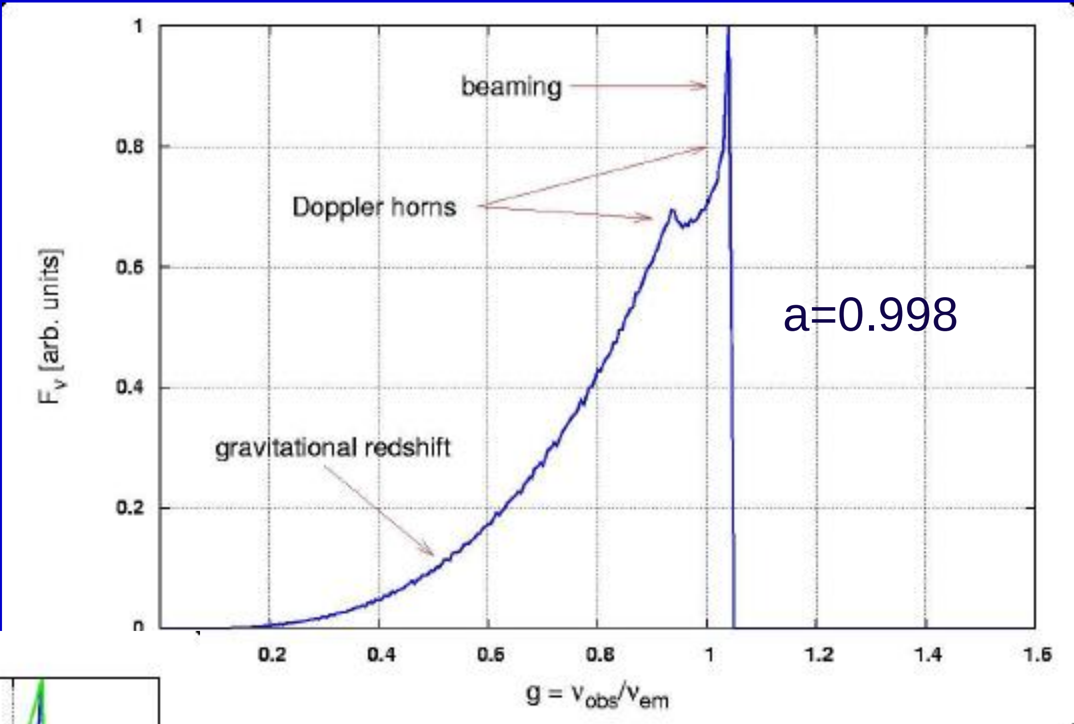

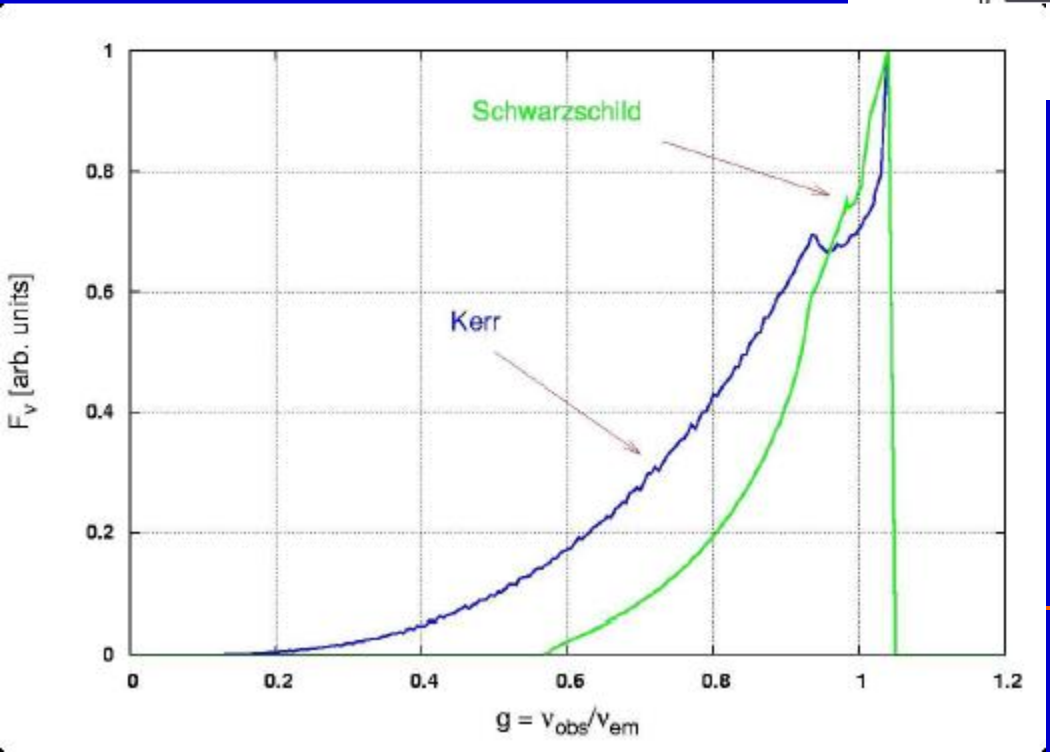

- Doppler effect
- Relativistic beaming
- GR light bending
- GR grav. redshift

arXiv: 0907.3602

Rotation direction

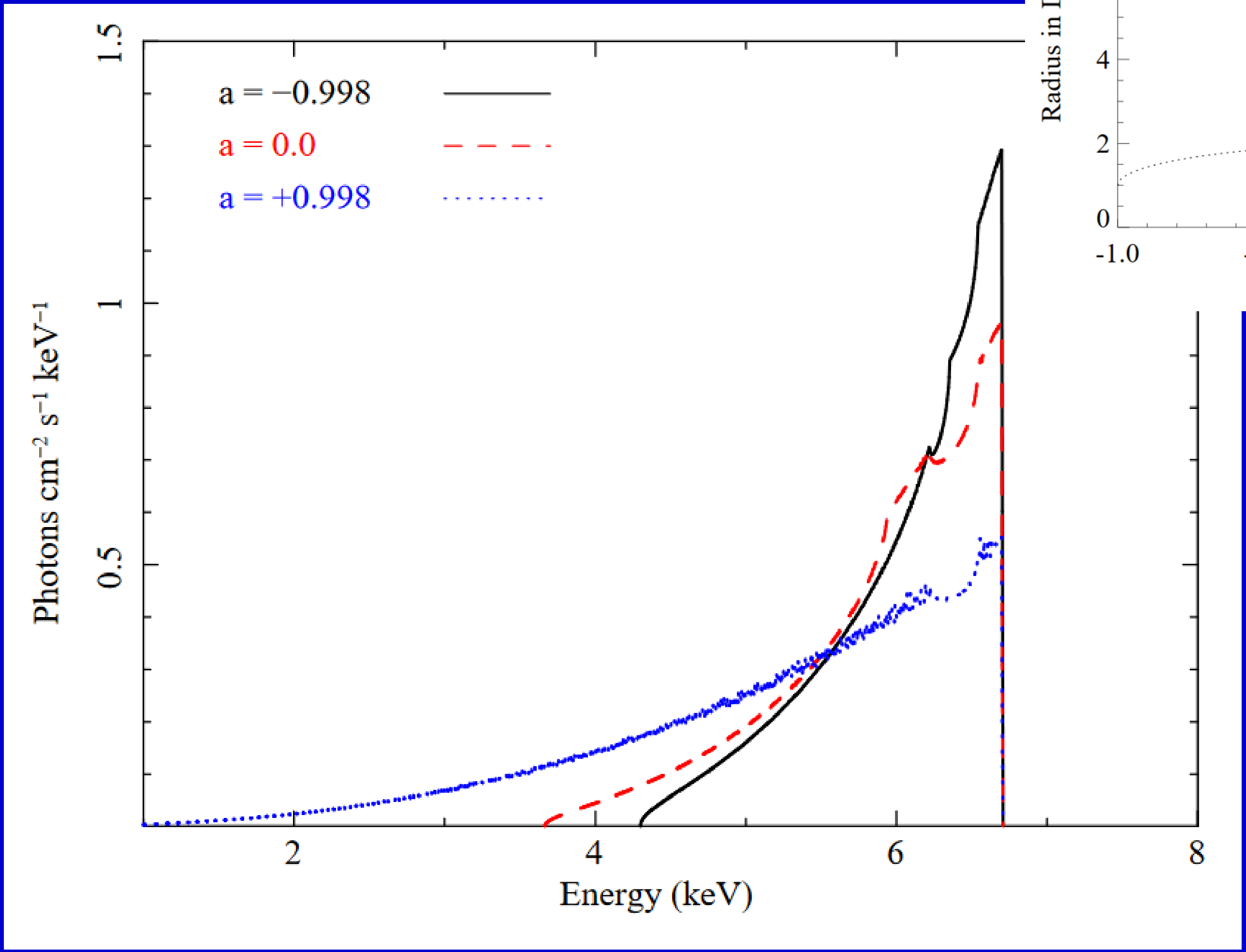

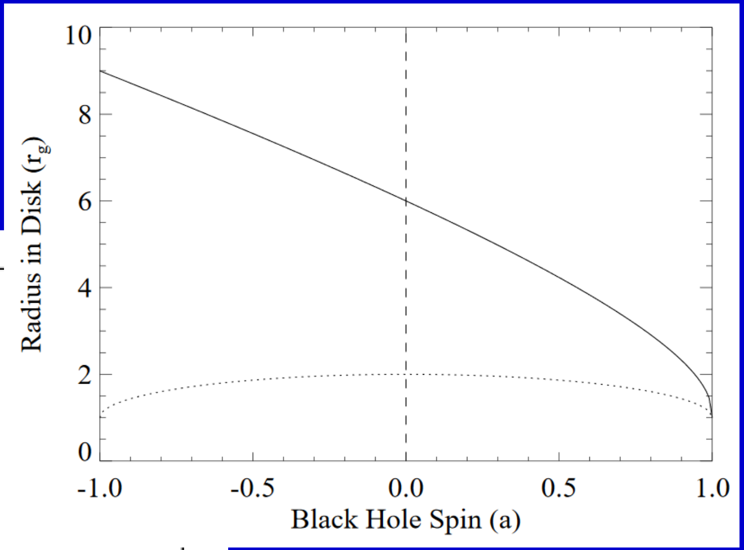

1309.6334

Fluorescent lines

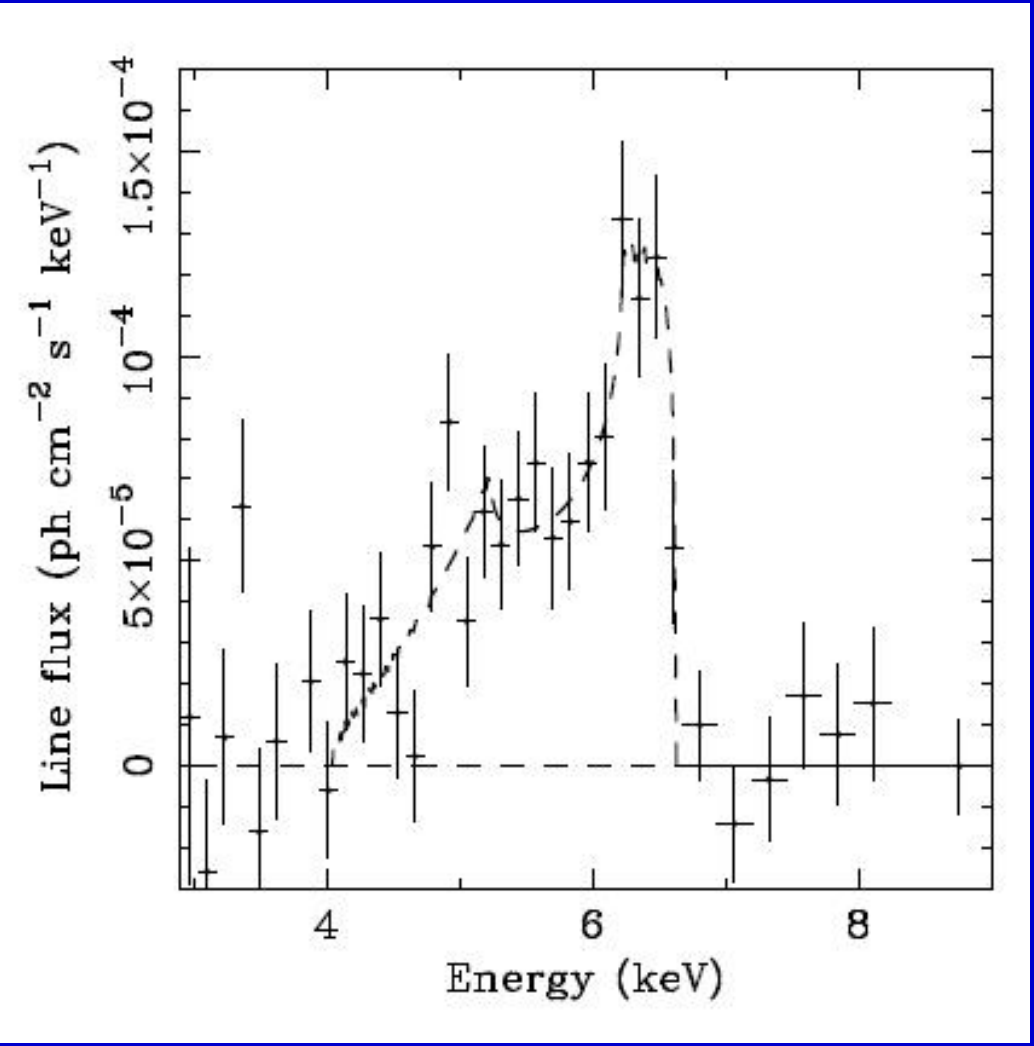

The Kα iron line observed by ASCA (1994 г.).
Seyfert galaxy MCG-6-30-15

Dashed line: the model with non-rotating BH,
disc inclination 30 degrees.

astro-ph/0212065

Lines and rotation of BHs

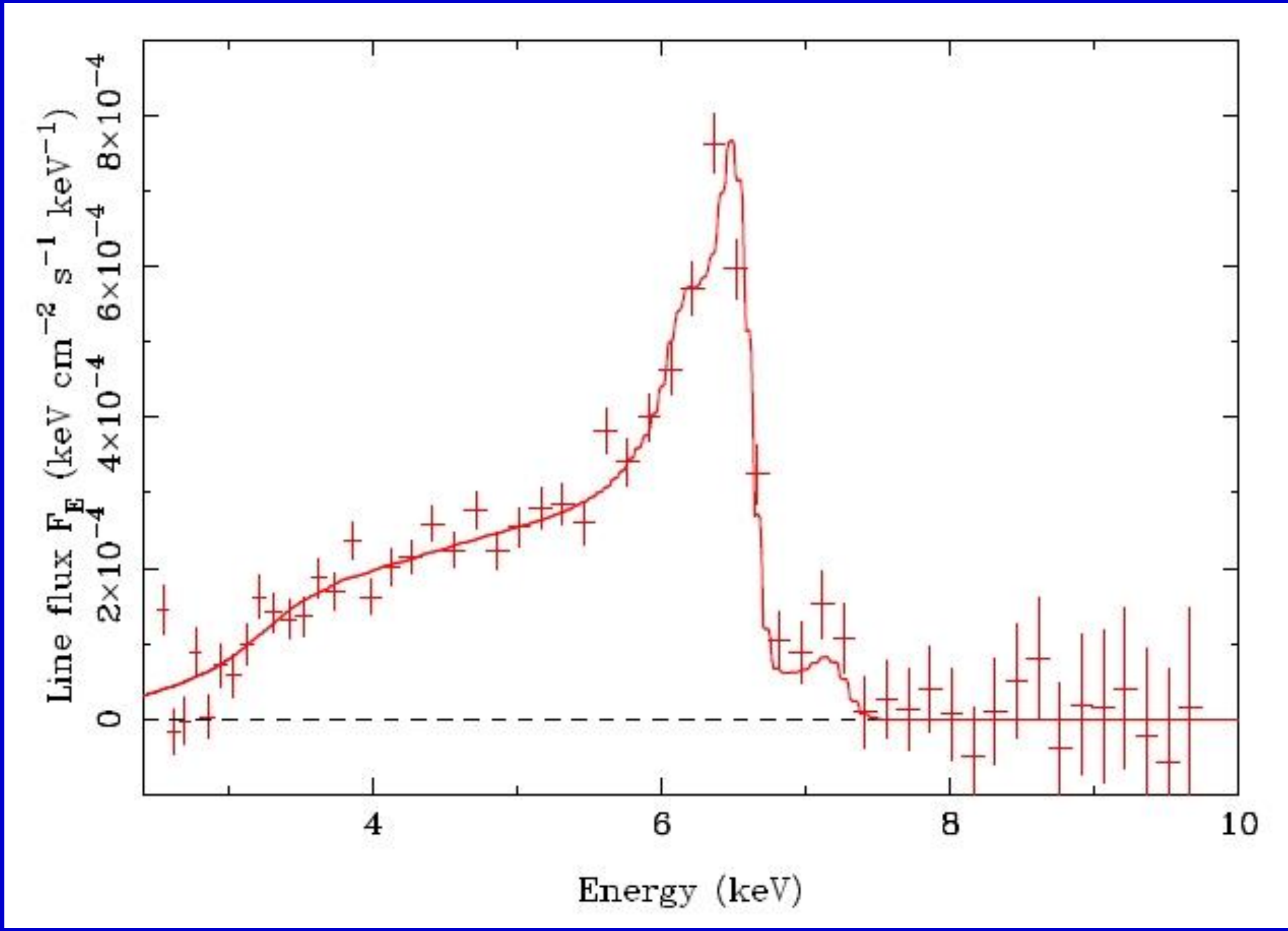

XMM-Newton data (astro-ph/0206095)

The fact that the line extends to the red side below 4 keV is interpreted as the sign of rapid rotation (the disc extends inside $3R_g$).

see astro-ph/0212065

Suzaku spin measurements program

NGC 3783 z = 0.00973

A very complicated model.
a > 0.93 (90% confidence)

AGN	a
MCG–6-30-15[a]	≥ 0.98
Fairall 9[b]	$0.65^{+0.05}_{-0.05}$
SWIFT J2127.4+5654[c]	$0.6^{+0.2}_{-0.2}$
1H0707–495[d]	≥ 0.98
Mrk 79[e]	$0.7^{+0.1}_{-0.1}$
Mrk 335[f]	$0.70^{+0.12}_{-0.01}$
NGC 7469[f]	$0.69^{+0.09}_{-0.09}$
NGC 3783[g]	≥ 0.98

A little bit more data
in 1307.3246
and a big review in 1309.6334

1104.1172

Relativistic reflection fitting of spectra

AGN	a	log M	L_{bol}/L_{Edd}	Host
MCG–6-30-15[a]	$\geq +0.98$	$6.65^{+0.17}_{-0.17}$	$0.40^{+0.13}_{-0.13}$	E/S0
Fairall 9[b]	$+0.52^{+0.19}_{-0.15}$	$8.41^{+0.11}_{-0.11}$	$0.05^{+0.01}_{-0.01}$	Sc
SWIFT J2127.4+5654[c]	$+0.6^{+0.2}_{-0.2}$	$7.18^{+0.07}_{-0.07}$	$0.18^{+0.03}_{-0.03}$	—
1 H0707–495[d]	$\geq +0.98$	$6.70^{+0.40}_{-0.40}$	$\sim 1.0_{-0.6}$	—
Mrk 79[e]	$+0.7^{+0.1}_{-0.1}$	$7.72^{+0.14}_{-0.14}$	$0.05^{+0.01}_{-0.01}$	SBb
Mrk 335[f]	$+0.70^{+0.12}_{-0.01}$	$7.15^{+0.13}_{-0.13}$	$0.25^{+0.07}_{-0.07}$	S0a
NGC 3783[g]	$\geq +0.98$	$7.47^{+0.08}_{-0.08}$	$0.06^{+0.01}_{-0.01}$	SB(r)ab
Ark 120[h]	$+0.94^{+0.1}_{-0.1}$	$8.18^{+0.05}_{-0.05}$	$0.04^{+0.01}_{-0.01}$	Sb/pec
3C 120[i]	≥ 0.95	$7.74^{+0.20}_{-0.22}$	$0.31^{+0.20}_{-0.19}$	S0
1 H0419–577[j]	$\geq +0.88$	$8.18^{+0.12}_{-0.12}$	$1.27^{+0.42}_{-0.42}$	—
Ark 564[j]	$+0.96^{+0.01}_{-0.06}$	≤ 6.90	≥ 0.11	SB
Mrk 110[j]	$\geq +0.99$	$7.40^{+0.09}_{-0.09}$	$0.16^{+0.04}_{-0.04}$	—
SWIFT J0501.9-3239[j]	$\geq +0.96$	—	—	SB0/a(s) pec
Ton S180[j]	$+0.91^{+0.02}_{-0.09}$	$7.30^{+0.60}_{-0.40}$	$2.15^{+3.21}_{-1.61}$	—
RBS 1124[j]	$\geq +0.98$	8.26	0.15	—
Mrk 359[j]	$+0.66^{+0.30}_{-0.54}$	6.04	0.25	pec
Mrk 841[j]	$\geq +0.52$	7.90	0.44	E
IRAS 13224-3809[j]	$\geq +0.995$	7.00	0.71	—
Mrk 1018[j]	$+0.58^{+0.36}_{-0.74}$	8.15	0.01	S0
IRAS 00521-7054[l]	$\geq +0.84$	—	—	—
NGC 4051[m]	$\geq +0.99$	6.28	0.03	SAB(rs)bc
NGC 1365[k]	$+0.97^{+0.01}_{-0.04}$	$6.60^{+1.40}_{-0.30}$	$0.06^{+0.06}_{-0.04}$	SB(s)b

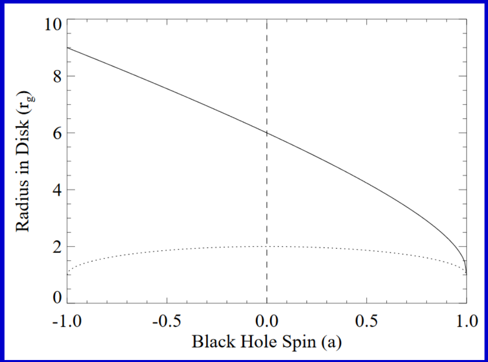

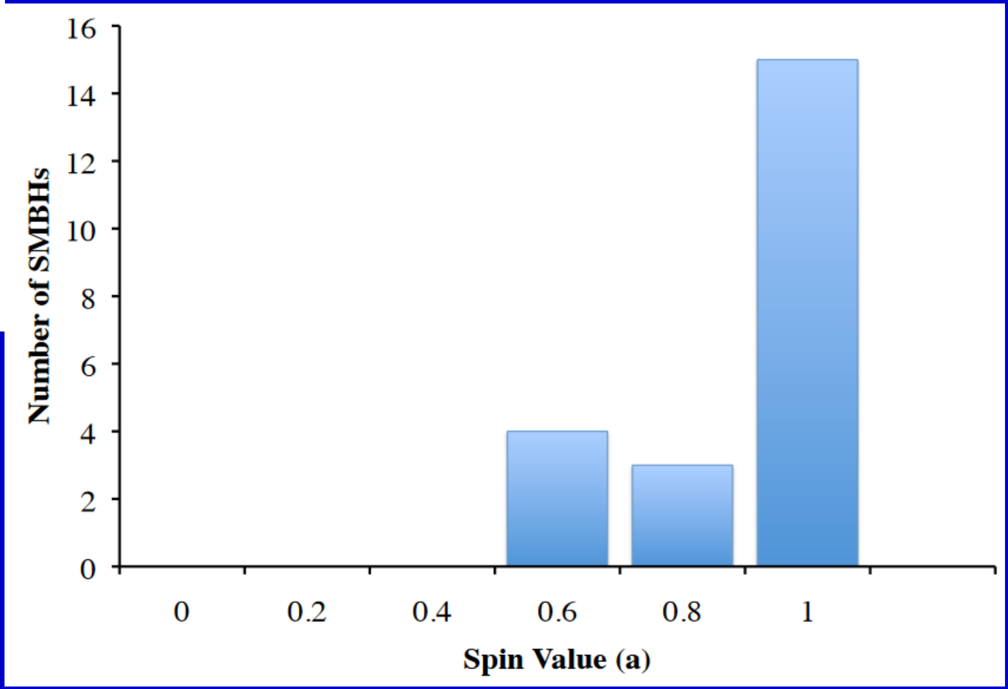

1309.6334

Gravitational redshift of the S2 star

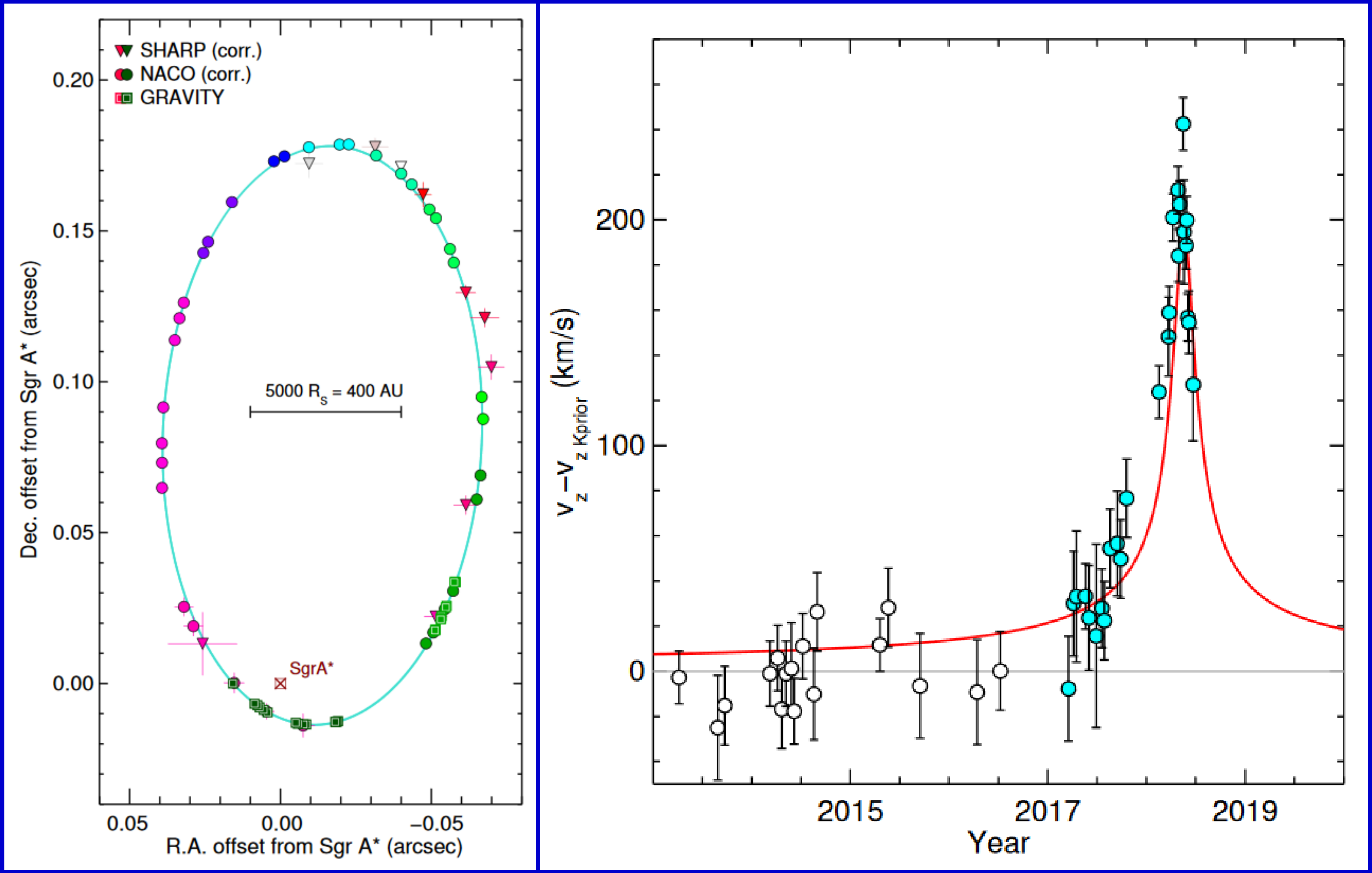

1807.09409

The inner edge

The place where the fluorescent line is formed is not necessarily the standard ISCO.

Especially for large accretion rates the situation is complicated.

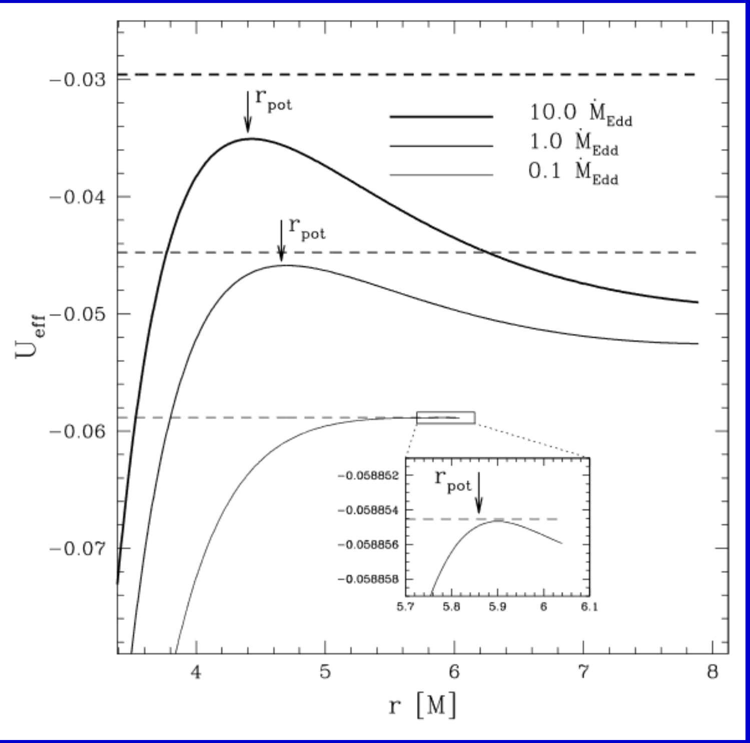

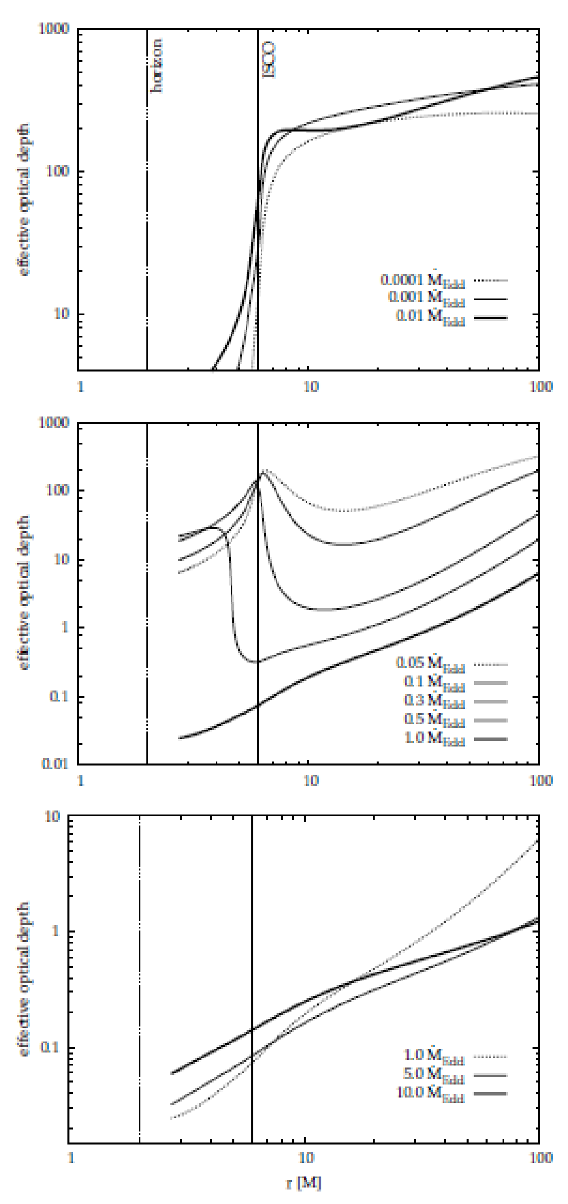

1003.3887

Inclination is important

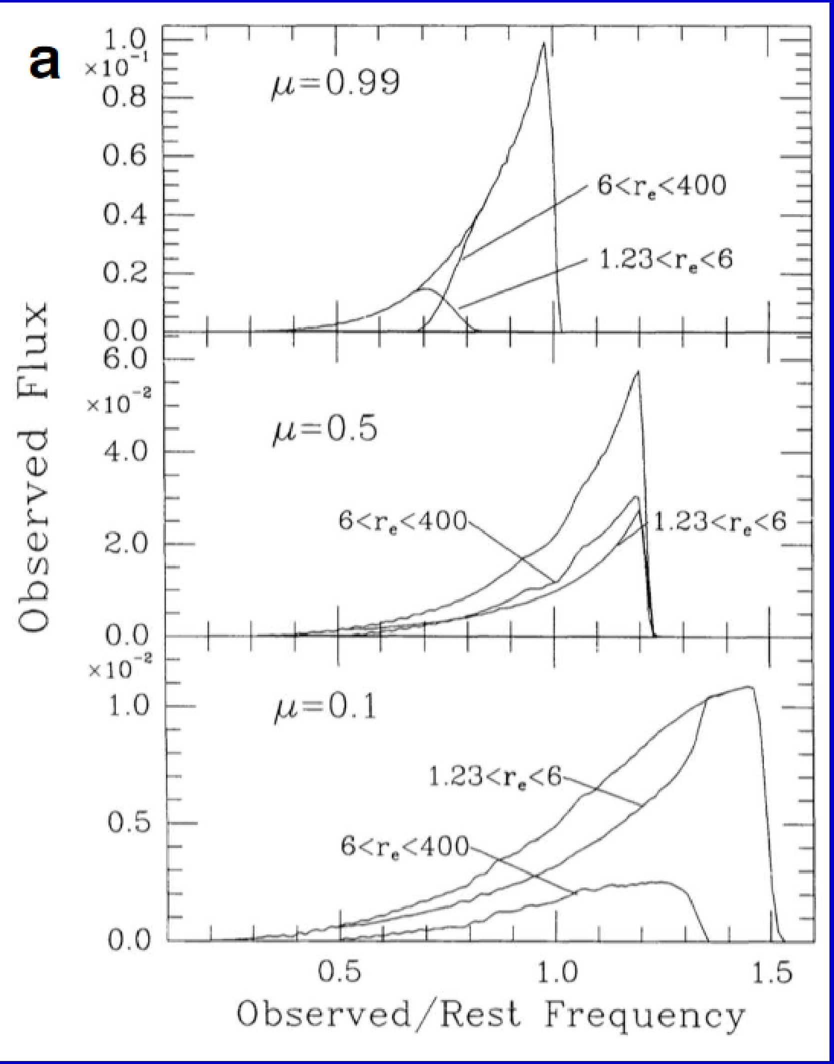

μ=cos θ
μ=1 – face-on

For inclined discs interplay between gravitational redshift and Doppler effect from inner and outer disc result in a profile with which it is difficult to put constraints on the inner boundary.

1903.09129

Measuring spins of stellar-mass BHs

Source	Spin a_*
GRS 1915+105	> 0.98
LMC X–1	$0.92^{+0.05}_{-0.07}$
M33 X–7	0.84 ± 0.05
4U 1543–47	0.80 ± 0.05
GRO J1655–40	0.70 ± 0.05
XTE J1550–564	$0.34^{+0.20}_{-0.28}$
LMC X–3	$< 0.3^{\mathrm{b}}$
A0620–00	0.12 ± 0.18

Different methods used
1101.0811

See a review on BH spin
(both XRB and AGN) in 1507.06153
and estimates of the spin parameter
with a model-depended method, but
for hundreds of sources in 1905.11319.

Twisted light

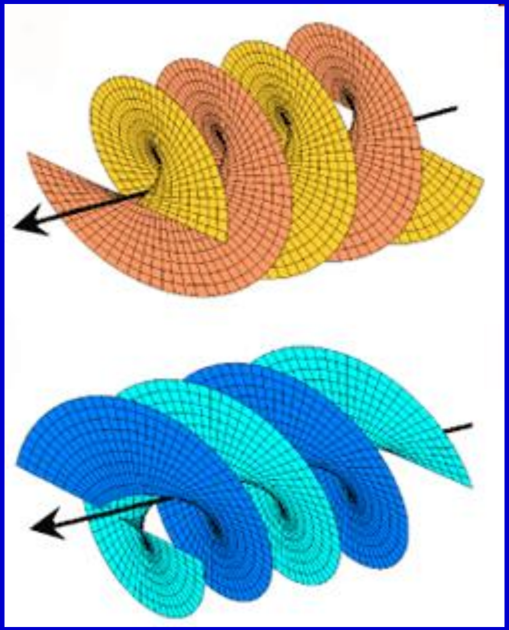

If the source of the gravitational field also rotates, it drags space-time with it. Because of the rotation of the central mass, each photon of a light beam propagating along a null geodesic will experience a well-defined phase variation.

This effect can be used to learn about spin of accreting BHs.

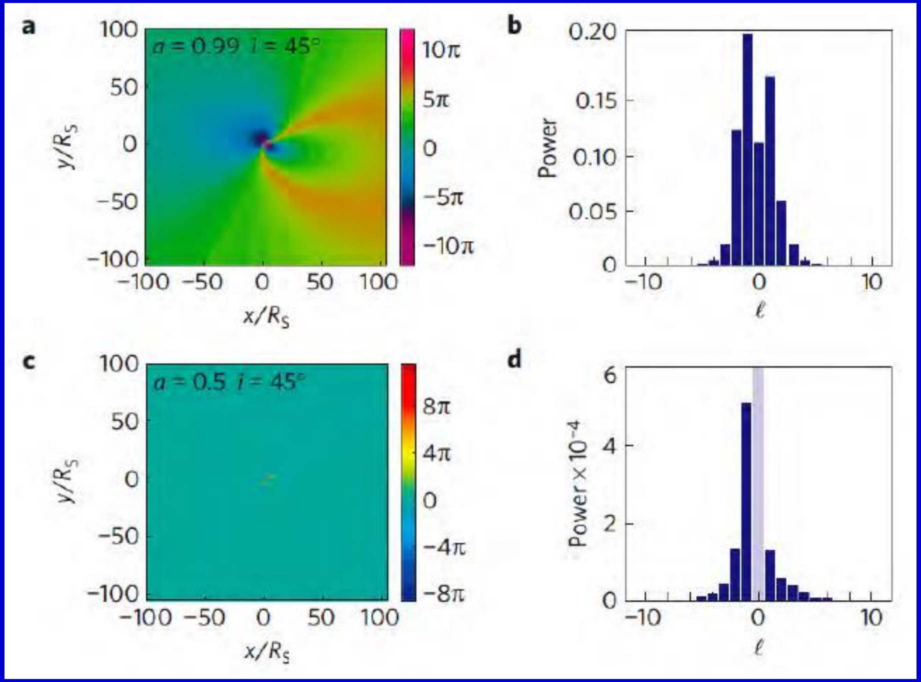

1104.3099

See http://www.physics.gla.ac.uk/Optics/play/photonOAM/
and astro-ph/0307430 about orbital angular momentum of photons